universität wien

MASTERARBEIT / MASTER'S THESIS

Titel der Masterarbeit / Title of the Master's Thesis

"Is there still dead ice in the Little Ice Age lateral moraine?"

verfasst von / submitted by

Sarah Maria Kamleitner, BSc

angestrebter akademischer Grad / in partial fulfilment of the requirements for the degree of

Master of Science (MSc)

Wien, 2017 / Vienna 2017

Studienkennzahl lt. Studienblatt / degree programme code as it appears on the student record sheet:	A 066 855
Studienrichtung lt. Studienblatt / degree programme as it appears on the student record sheet:	Masterstudium Geographie
Betreut von / Supervisor:	Univ.-Prof. Dr. Thomas Glade
Mitbetreut von / Co-Supervisor:	Dr. Sabine Kraushaar

Acknowledgements

Die vorliegende Arbeit ist am Institut für Geographie und Regionalforschung im Rahmen des Forschungsprojektes „Feasibility study for third party funded project 2016/2017" entstanden. Die Durchführung erfolgte in enger Zusammenarbeit mit der Arbeitsgruppe für Isotopenforschung und Kernphysik der Universität Wien und dem von der DFG (Deutsche Forschungsgemeinschaft) und den FWF (Fonds zur Förderung der wissenschaftlichen Forschung) geförderten PROSA-Projekts (High-resolution measurements of morphodynamics in rapidly changing PROglacial Systems of the Alps).

Zuallererst möchte ich mich bei meiner Betreuerin Sabine Kraushaar für die intensive fachliche Unterstützung während des gesamten Entstehungsprozesses der vorliegenden Arbeit bedanken. Danke für motivierende und inspirierende gemeinsame Geländekampagnen, Hinweise und Anmerkungen in zahlreichen Gesprächen und fachlichen Diskussionen, sowie Deiner persönlichen Unterstützung in meinem Bestreben weiterhin in der Wissenschaft tätig zu sein. Außerdem möchte ich Herrn Prof. Thomas Glade für die Übernahme der Erstbetreuung danken.

Johannes Lachner und Peter Steier, die mir im Rahmen dieser Arbeit die Welt der Physik näher gebracht haben, möchte ich für die Unterstützung während der Laborarbeit und über diese hinaus ein großes Dankeschön aussprechen.

Für die erfolgreiche Zusammenarbeit und Unterstützung im Gelände sowie anregende Diskussionen möchte ich mich besonders bei Verena Czarnowsky sowie Anne Schuchardt, Matthias Faust, und Kollegen und Kolleginnen aus dem PROSA Projekt bedanken. Für die wertvolle graphische Unterstützung danke ich außerdem meiner Cousine Veronika Kladnik.

Für die Bereitstellung von Daten, die im Rahmen des PROSA Projektes erhoben wurden, möchte ich allen Beteiligten und insbesondere Lukas Vehling und David Morche herzlich danken. Letzterem sei auch für die fachliche und logistische Unterstützung während der Geländekampagnen gedankt. Außerdem sei Jana Dusik für Ihre Unterstützung herzlich gedankt.

Des Weiteren gehört mein Dank den österreichischen und deutschen Steuerzahlern und Steuerzahlerinnen, deren finanzielle Unterstützung im Rahmen des Förderstipendiums nach dem StudFG SS 2016 sowie des DAAD-IAESTE Praktikumsplatzes (Ref. Nr.DE-2015-1321-1-A) wesentlich zur erfolgreichen Durchführung der Geländearbeiten beigetragen haben.

Für Motivation, Verständnis, Durchhaltevermögen und die nötige Ablenkung während des gesamten Masterstudiums sowie für hilfreiche Kommentare zur vorliegenden Arbeit möchte ich hiermit ganz besonders meinem Freund Alexander Sysel sowie Christina Hauck, Marie-Claire Schug, Kathrin Käppeler, Judith Spreitzer und Saskia Kamleitner danken, die mir stets mit Rat und Tat zur Seite gestanden haben.

Nicht zuletzt möchte ich meiner Familie und allen voran meinen Eltern für die großzügige Finanzierung meines Studiums, das diesem entgegengebrachte Interesse sowie Geduld und Nachsicht in den Prüfungszeiten und in der Fertigstellung der Masterarbeit danken.

Table of contents

List of figures

List of tables

List of abbreviations

ALS	Airborne Laser Scanning
AMS	Accelerator Mass Spectrometry
ELA	Equilibrium Line Altitude
GFI	Ground Freezing Index
GPS	Global Positioning System
GST	Ground Surface Temperature
IPA	International Permafrost Association
IC	Ion Chromatography
ICP-MS	Inductively Coupled Plasma Mass Spectrometry
IQR	Inter Quartile Range
LGM	Last Glacial Maximum
LIA	Little Ice Age
LiDAR	Light Detection And Ranging
LSC	Liquid Scintillation Counters
MAAT	Mean Annual Air Temperature
MIS	Marine Isotope Stage
NAO	North Atlantic Oscillation
NRF	Nuclear Reprocessing Facility
OSL	Optically Stimulated Luminescence
RNAA	Radiochemical Neutron Activation Analysis
SfM	Structure from Motion
TOF	Time-of-Flight

List of elemental formulas

AgCl	Silver Chloride
AgI	Silver Iodide
AgNO3	Silver Nitrate
$Ca(ClO_2)$	Calcium Hypochlorite
CH_3I	Methyl Iodine
HCl	Hydrochloric Acid
HNO_3	Nitric Acid
I^-	Iodide
IO_3^-	Iodate
^{127}I	Iodine 127
^{129}I	Iodine 129
KNO_3	Potassium Nitrate
$NaHSO_3$	Sodium Hydrogen Sulphite
NaOH	Sodium Hydroxide
NH_3	Ammonia
$NH_2OH \cdot HCl$	Hydroxylamine Hydrochloride
NO^{3-}	Nitrate
Xe	Xenon

Abstract

The ongoing retreat of Alpine glaciers since the end of the Little Ice Age (LIA) in 1850 AD, exposes large quantities of unconsolidated and unvegetated glacial sediments prone to geomorphic processes. In the face of intense morphodynamics of proglacial areas, the present study aims to clarify the origin of springs evolving from LIA lateral moraines of the Geptaschferner glacier in Upper Kaunertal Valley (Tyrol, Austria) that have been found to be fed by ice (Czarnowsky, 2016). If old dead ice, which remains buried inside of the lateral moraines from former glacier extents, is present in the study area is thereby assessed. The origin of evolving springs is clarified by relative age dating of glacial waters, spring waters and precipitation using iodine 129 (^{129}I) concentration measures. At the same time, the applicability of the anthropogenic radionuclide for dating is verified. Based upon the spatial distribution of old, ice-fed springs, the study further aims to statistically assess if indicated dead ice areas can be explained by topographic characteristics and/or are indicated by hydro-chemical characteristics (temperature and electrical conductivity) of spring waters. On the basis of ground surface temperature (GST) measurements, a further exploration is made as to whether seasonal ice growth is generally possible given the local thermal conditions.

Results show that ice-fed springs in Upper Kaunertal Valley originate from modern waters as well as from waters that have probably been formed prior to 1950. While the former are associated with melt waters of seasonal ice growth, the latter are ascribed to the presence of dead ice within the moraine matrix and its degradation, provided that infiltration from upstream areas is improbable. Spring signatures indicate remaining dead ice throughout the study area. Yet, no valid conclusion on the topographic parameters controlling their spatial distribution could be made given the present data set. Nor were meaningful correlations to any hydro-chemical characteristics found. Further, local ground temperatures do not suggest that the formation of extensive seasonal ice at the specific site has been possible. The present study shows that ^{129}I can be successfully applied for relative age determination of waters, though further investigations, including validation of the method are essential. Presented results further specify geomorphological processes in a recently deglaciated area and indicate that dead ice degradation is affecting present (sub)surface dynamics. This has basic implications for the interpretation of volume losses detected by surface elevation measures and sediment budgets. Besides, results may be of interest for the assessment of the hydrological situation on site, water resource management and natural hazard assessment.

Kurzfassung

Durch den fortlaufenden und seit dem Ende der Kleinen Eiszeit (1850 AD) anhaltenden Gletscherrückgang werden in den Vorfeldern der Alpengletscher bedeutende Mengen an unverfestigten, glazialen Lockersedimenten freigelegt. Da die Lockersedimente kaum bewachsen sind, sind sie anfällig gegenüber geomorphologischen Prozessen. Vor dem Hintergrund hoher morphologischer Aktivität proglazialer Gebiete, ist es Ziel der vorliegenden Arbeit, den Ursprung von auf den Seitenmoränen des Gepatschferners (Kaunertal, Tirol) entspringenden Quellen zu klären. Vorrangegangene Studien konnten zeigen, dass ein Teil dieser Quellen von Eis gespeist wird (Czarnowsky, 2016). Ob diese auf alte Toteisvorkommen und damit auf deren bisher unbemerkte Existenz im Inneren der Moränen zurückzuführen sind, soll im Rahmen dieser Arbeit evaluiert werden. Die Herkunft der beobachteten Quellen wird dabei durch relative Altersdatierung anhand von Iod 129 (^{129}I) Konzentrationsmessungen in Gletscher- und Quellwässern sowie Niederschlägen bestimmt. Damit soll gleichzeitig die Eignung des anthropogenen Radionuklids für relative Altersdatierungen validiert werden. Basierend auf der räumlichen Verteilung von Quellen die durch altes Eis gespeist werden ist es weiter Ziel der Arbeit, mittels statistischer Methoden zu beurteilen, ob ein Zusammenhang zwischen vermuteten Toteisvorkommen und den jeweiligen topographischen Gegebenheiten besteht. Außerdem wird untersucht, ob hydrochemische Charakteristika der Quellwässer bereits auf Toteis hinweisen können. Des Weiteren wird anhand von Bodentemperaturmessungen an einem ausgewählten Standort im Gletschervorfeld untersucht, ob die lokalen thermalen Gegebenheiten die Ausbildung von saisonalem Eis erlauben.

Ergebnisse der Altersdatierung zeigen, dass eisgespeiste Quellen im Proglazial sowohl auf moderne Wässer als auch auf Wässer zurückgeführt werden können, die mit großer Wahrscheinlichkeit vor 1950 gebildet worden sind. Erstere können mit Schmelzwässern von saisonalem Eisaufbau in Zusammenhang gebracht werden. Letztere werden der Existenz von degradierendem Toteis im Inneren der Moränen zugeschrieben, sofern Infiltration von höherliegenden Bereichen ausgeschlossen werden kann. Spezifische Quellsignaturen legen die Existenz von Toteis in mehreren Bereichen des Untersuchungsgebietes nahe. Jedoch erlauben die vorhandenen Daten keine validen Rückschlüsse auf einen Zusammenhang mit topographischen oder hydro-chemischen Parametern. Lokale Bodentemperaturmessungen lassen vermuten, dass die Bildung von saisonalem Eis nicht überall im Untersuchungsgebiet in relevanten Mengen möglich war. Die vorliegende Arbeit belegt, dass Iod 129 zur relativen Altersdatierung verwendet werden kann. Weitere Untersuchungen, welche Validierungen beinhalten, sind jedoch unerlässlich. Die präsentierten Ergebnisse spezifizieren zudem lokal wirksame geomorphologische Prozesse in proglazialen Gebieten und zeigen, dass mit der Degradation von Toteis bedeutende Änderungen im morphologischen Geschehen an der Erdoberfläche verbunden sind. Damit sind wesentliche Implikationen für die Interpretation von mittels differenziellen Höhenmodellen beobachteten Volumenverlusten, sowie auf diesen basierenden Sedimentbudgets verbunden. Zudem sind die erzielten Ergebnisse für die Beurteilung der lokalen hydrologischen Gegebenheiten, Wasserressourcenmanagement sowie die Bewertung des Naturgefahrenpotentials von Interesse.

1 Introduction & background

The increase in mean annual air temperature in Austria of ~ 2 °C since the 1880s means that Austria and more generally the European Alps have experienced a temperature increase twice as high as the global average. An additional rise in temperature is expected and a warming of another 1.4 °C is estimated for the first half of the 21st century (APCC, 2014). Present alpine glacial and periglacial environments are particularly sensitive to climate change (Chiarle and Mortara, 2008). Mountain glaciers and permafrost are close to melting conditions and are key indicators in monitoring climate change and its impact on cold mountain areas (Kääb et al., 2007). As a consequence of global warming, glaciers are melting and permafrost is thawing (Heckmann et al., 2016). The Little Ice Age (LIA) was the Holocene's last cold period, during which global climatic deterioration did allow for maximum postglacial ice advances (Zasadni, 2007) between the 14th century and 1850 (Ivy-Ochs et al., 2009). However, since the end of the LIA, the net balance of Alpine glaciers is negative (Baewert and Morche, 2014). Glacial retreat up to the year 2005 resulted in a loss of total glacier volume of 85 to 90 % over the entire European Alps (Haeberli et al., 2007). The remaining ice volumes are expected to further decrease by 70 % by the end of the 21st century (Frezzotti and Orombelli, 2014). The ongoing retreat of Alpine glaciers exposes large quantities of glacial sediments in expanding proglacial areas. Tills and glacio-fluvial deposits are unconsolidated and non-vegetated and hence prone to geomorphological processes (Baewert and Morche, 2014). Besides intense geomorphic activity, the ongoing transition in proglacial systems also involves hydrological and ecological dynamics (Heckmann et al., 2016). Knight and Harrison (2014, p. 245) further predict that *"future changes in glacial and paraglacial environments (…) will have downstream implication for the biosphere (…), the human environment (…) and for policy and planning"*.

Austria's second largest glacier, Gepatschferner glacier, situated in Upper Kaunertal Valley (Tyrol) is no exception to the overall glacier trend of the European Alps. From the LIA maximum up to 2006 Gepatschferner glacier has lost 36 % of its ice volume and 32 % of its areal extent (Hartl, 2010). The present glacier front reclines more than 2.5 km upstream of the 1855 maximum position (Vehling et al., 2016). Glacial retreat of Gepatschferner has left behind steep lateral moraines of up to 200 m height. The moraines crestline marks the maximum thickness of the ice during the LIA advance ~ 1850 (Schomacker, 2011). The unconsolidated and bare till material within the proglacial is subject to intense sediment dynamics and is frequently remodelled by gravitational and fluvial processes (Dusik et al., 2014, 2015a; Mortara and Chiarle, 2005).

1.1 Sediment dynamics in high-mountain proglacial areas

A proglacial area is a landscape transitioning from a glacial to a non-glacial state (Heckmann et al., 2016). The definition by Penck and Brückner (1909) is commonly used and defines proglacial environments as "*those which are located close to the ice front of a glacier, ice cap or ice sheet"* (Slaymaker, 2011, p. 85). From today's perspective the proglacial is sometimes referred to the area within LIA moraines (Heckmann et al., 2016). The term proglacial is a function of spatial location (Slaymaker, 2011) and is in the following used synonymously with the term glacier forefield.

Proglacial systems are characterized by a high geomorphic activity of paraglacial processes (Baewert and Morche, 2014). After Church and Ryder 1972 (Iturrizaga, 2011), paraglacial processes involve all *"non-glacial processes, which are directly conditioned by glaciation"* (Iturrizaga, 2011, p. 817). Frequently available, unconsolidated glacial sediments and instable de-glaciated rockwalls condition intense morphodynamics (Heckmann et al., 2016). The rate of surface change is generally high (Heckmann et al., 2016). Maximum rates occur shortly after the initial deglaciation and decline as slopes stabilise (Knight and Harrison, 2009). Furthermore, it is argued that "*because of global warming and ice loss, paraglaciation will become the most significant process controlling sediment supply and landscape change in the mid- to high-latitudes over the next few hundred years"* (Knight and Harrison, 2009, p. 230). In doing so, it has also been recognized that increased sediment supply is a critical factor when considering potentially hazardous events (e.g. floodings, landslides) originating from proglacial areas (Heckmann et al., 2016; Knight and Harrison, 2009).

Sediment transport and (re)deposition into, within and beyond the proglacial area is highly connected to the natural dynamics of these landscapes (Heckmann et al., 2016). The sediment budget approach provides a theoretical framework to link sediment sources and sinks in a quantitative manner. It is based on the principle of mass conservation, where sediment input equals the change in sediment storage plus sediment output, and is key to understanding ongoing sediment dynamics (Hinderer, 2012). When addressing a sediment budget, the components of sediment sources, fluxes and deposits have to be identified and quantified. The range of tools used to determine sediment fluxes and stores is exceptionally wide due to the variety of spatial and temporal scales. Among others, the toolbox of common methods also includes surveys of movements (Hinderer, 2012). Multi-temporal topographical surveys of the earth surface can be achieved by airborne or terrestrial LiDAR (light detection and ranging) scans (Müller et al., 2014; Vosselman and Maas, 2010) or from structure from motion (SfM) (Smith et al., 2014). Based upon surface elevation differences of two temporally divergent digital elevation models (DEM) a DEM of difference (DoD) can be derived, which allows for direct geomorphic and volumetric change detection (Heckmann et al., 2016; Williams et al., 2011). Additionally, observed surface changes may be supported by sub-surface information gained by the application of geophysical methods (Heckmann et al., 2016) (e.g. ground-penetrating radar, seismic reflection methods, electrical resistivity surveys) or borehole networks (Hinderer, 2012).

Sediment dynamics in Upper Kaunertal Valley have been intensely studied between 2012 and 2015 in the frame of the PROSA joint project (High-resolution measurements of morphodynamics in rapidly changing PROglacial Systems of the Alps). Sediment erosion, re(mobilisation) and deposition have been mapped and quantified to set up a proglacial sediment budget. In order to do so, a combination of field methods and multi-temporal airborne and terrestrial LiDAR surveys have been applied (Heckmann et al., 2012). In this context, surface change detection analysis revealed that the prominent LIA lateral moraine on the right valley side is subject to erosion (Dusik et al., 2015a). A net erosion of -1357.2 m³ and -926.2 m³ has been

quantified for a section of 0.04 km² in size, between July 2010 and September 2011 and July 2012 and July 2013 respectively (Dusik et al., 2014). The majority of the erosion takes place early on in the year and measured net volume losses have been attributed to debris flows, fluvial erosion, slope wash, gullying and other mass movements (Dusik et al., 2014; Hilger et al., 2014). However, doubts about the origin of detected volume losses have been raised and the exclusive role of surface processes being active on site is questioned.

In summer, several episodic and perennial springs evolve out of the lateral moraine deposits in the forefield of Gepatschferner glacier. The origin of these springs is not clear and first assumptions of them being sourced from ice within the moraine deposit have been raised (Kraushaar et al., 2014). Subsequently, stable isotope measures of spring waters were applied in September 2013 and July 2014. The results derived showed that waters in the proglacial area are potentially influenced by melting ice (Kraushaar et al., 2014). Pursuant, a monitoring of isotopic and hydro-chemical characteristics ($\delta^{18}O$, $\delta^{2}H$, water temperature and electrical conductivity) of springs in Upper Kaunertal Valley was conducted between June and October 2015 (Czarnowsky, 2016). Results confirm former findings and prove that springs emerging from north and northeast exposed lateral moraines are fed by ice, which is likely originating from ice lenses within the moraine. Additionally, particular springs evolving from the west exposed LIA moraine are also influenced by melting ice (Czarnowsky, 2016).

While it has been proven that springs evolving from the lateral moraines are fed by ice, previous studies have not specified the source of the ice within the moraine. Generally ice found within a moraine deposit may be of two different origins, seasonal ice formation (A) or buried dead ice deposits, which remain from a former glacial extent (B).

(A) Sub-zero ground temperatures allow for the development of a freezing front near-surface (Woo, 2012). *"However, water in the ground usually freezes at temperatures of a fraction of a degree or even several degrees below 0 °C"* (Woo, 2012, p. 2). Gravitational waters farthest from the soil particles freeze first, followed by capillary water and adsorbed water closer to the grain's surface. If sudden ground cooling takes place, the downward movement of the freezing front is rapid. Soil water freezes in situ and pore ice will form. As cooling is continued, the freezing front advances. Where moisture is available and sediment texture allows for the sucking up of moisture to the freezing front, moisture will be able to migrate to the freezing front. If so, segregation ice will form, e.g. in form of segregated ice lenses (Woo, 2012). The vapour pressure over ice is lower than those over liquid water and a gradient of vapour pressure develops. Water vapour is migrating towards the ice surface, re-sublimates and adds up to the existing segregation ice lenses. In order to counterbalance water vapour loss, water movement within the pore system is initiated (Zepp, 2014). Moisture for ice lenses formation and growth may originate from waters present within the frozen fringe (the area between the frost front at 0 °C and the actual freezing front), from waters of adjacent unfrozen sediments that are subject to suction or from waters entering from surrounding areas.

If moisture availability is not a limiting factor, growth of segregated ice lenses may be possible as long as the freezing front is sustained. However, as implied by the term itself seasonal ice formation is restricted to the winter season and developed ice is not preserved over more than one year (Woo, 2012).

(B) Dead ice or stagnant ice is glacier ice which has been isolated from the active glacier (Dobhal, 2011). Any movement due to glacier flow has ended and the ice becomes stagnant (Schomacker, 2008). Dead ice may be of various size, ranging from small dead ice bodies up to enormous ice masses (Zepp, 2014). Whenever a glacier is retreating and a sediment or debris cover of sufficient thickness is established at a glacier's margins, dead ice may form (Schomacker, 2008). The sufficient thickness of sediments may thereby vary between several decimetres up to metres depending on the local situation (Lukas, 2011). Covering material may be derived from different sediment sources and various processes, e.g. from supraglacially transported till, from englacial till melting out in the ablation area, aeolian deposits, or debris from adjacent slopes (Lukas, 2011; Schomacker, 2008) or moraines (Ackert, 1984). The covering material insulates the underlain ice and shields it from melting. This differentiates the melting of clean, debris-free glacier ice and that of debris-covered glacier ice. The latter is cut off eventually and dead ice is formed (Lukas, 2011). "*From this point onwards (…) the body of sediment covered ice, especially if ridge- or mound-like in appearance and occurring along the ice margin, can be regarded as ice-cored moraine…*" (Lukas, 2011, p. 617). Ice-cored moraines are important transitional ice-marginal features, which are widespread in many proglacial areas (Lukas, 2011). Ice-cored frontal moraines have thereby received greater attention, while fewer studies focus on dead ice within lateral moraines (Lyså and Lønne, 2001). Nonetheless, modern glacial environments can be characterized by the presence of ice-cored lateral moraines (Schomacker, 2011). Ice cores within lateral moraines have generally been reported from Scandinavia by Østrem (1971), while others found ice-cored lateral moraines adjacent to glaciers in northern Sweden and Svalbard (Ackert, 1984; Schomacker and Kjær, 2008). Studying large moraines of an Alpine valley glacier in Switzerland, Lukas et al. (2012) further report the presence of dead ice at the base of a lateral moraine, reaching up to thirty metres above the valley floor. Similar observations have been made at Gepatschferner glacier in Upper Kaunertal Valley, where great dead ice deposits are visibly incorporated in moraines that have been deposited within recent decades (Vehling, 2016).

Both, melt waters of seasonal ice and buried dead ice are able to feed springs on the moraines. Likewise, melt waters of both types would be characterized by a low isotopic signatures as found by Czarnowsky (2016). Yet, the age of evolving melt waters would differ depending on their source. Relative age dating of ice-fed waters would hence allow their ascription to either

modern seasonal ice or old dead ice. Which type of ice is present on site has essential implications for applied sediment studies based on multi-temporal surface elevation measures and the interpretation of processes active on site. Further, it may be of interest for the local hydrological situation, water resource management and natural hazard assessment.

1.2 Relevance of the present type of ice for the application of DEMs of differences in sediment budget studies

A moraine's surface responds differently to the development of seasonal ice than it does to the presence of buried dead ice under climate warming. This difference has essential implications for applied surface elevation measurements. In order to understand how the presence of different types of ice alters ongoing surface dynamics on site, a conceptual model has been set up. Figure 1 compares the evolution of a moraine deposit facing seasonal formation and degradation of ice (A) over time with those of an continuously degrading ice-cored moraine (B). Confronting the surface elevation changes between the initial and the final situation of both series, the graphic shows why the present type of ice is of relevance for erosion quantification based on any surface elevation measure.

The first picture of scenario A represents an ice-free lateral moraine deposit. When temperatures fall at the end of summer, the ground cools and freezing processes start to occur. Ground ice may develop (Woo, 2012). The phase transition from water to ice then conditions an increase in volume of about 10 % (Ahnert, 2009) of the original (unfrozen) water content (Woo, 2012). As a consequence of the volume increase, the surface of the moraine deposit lifts up. However, the frost heave associated with pore ice is minor in comparison with the formation of segregated ice lenses (Woo, 2012). Primary frost heaving and therewith the largest moraine surface lifting may be associated with segregated growth of ice lenses. Certainly, surface lifting may, as consequence of the sediments heterogeneity, not be as uniform as shown in the conceptual model (Woo, 2012). If ground temperatures rise again, the freezing front disperses. Ice built up over winter time is then expected to melt out completely as the mean annual air temperature (MAAT) of the study area is assumed to be above 0 °C (c.f. section 2.2) (Ahnert, 2009). Multi-year ice is restricted to permafrost areas (Woo, 2012) and concerned areas have been modelled to be free of permafrost (Vehling, 2016). The phase transition from ice to water goes along with a volume reduction analogously to the increase prior. Excessive waters from the melting of segregated ice lenses are consequently flowing off in the subsurface or as overland flow. As the winter ice melts, the moraine surface settles and the original elevation is restored. In total, the seasonal development and degradation of ground ice results in an up and down movement of the moraine surface. However, comparing the initial and the final situation of the moraine in picture series A, neither a net volume loss nor a net volume gain has occurred, meaning that net volume changes are zero. The formation of seasonal ice may hence only introduce minor uncertainties into surface elevation measurements, calculations of DoDs and conducted sediment budgets. Corresponding errors may be excluded if DEMs are computed after seasonal ice has been melted completely and before new ice could have been developed, e.g. in late summer.

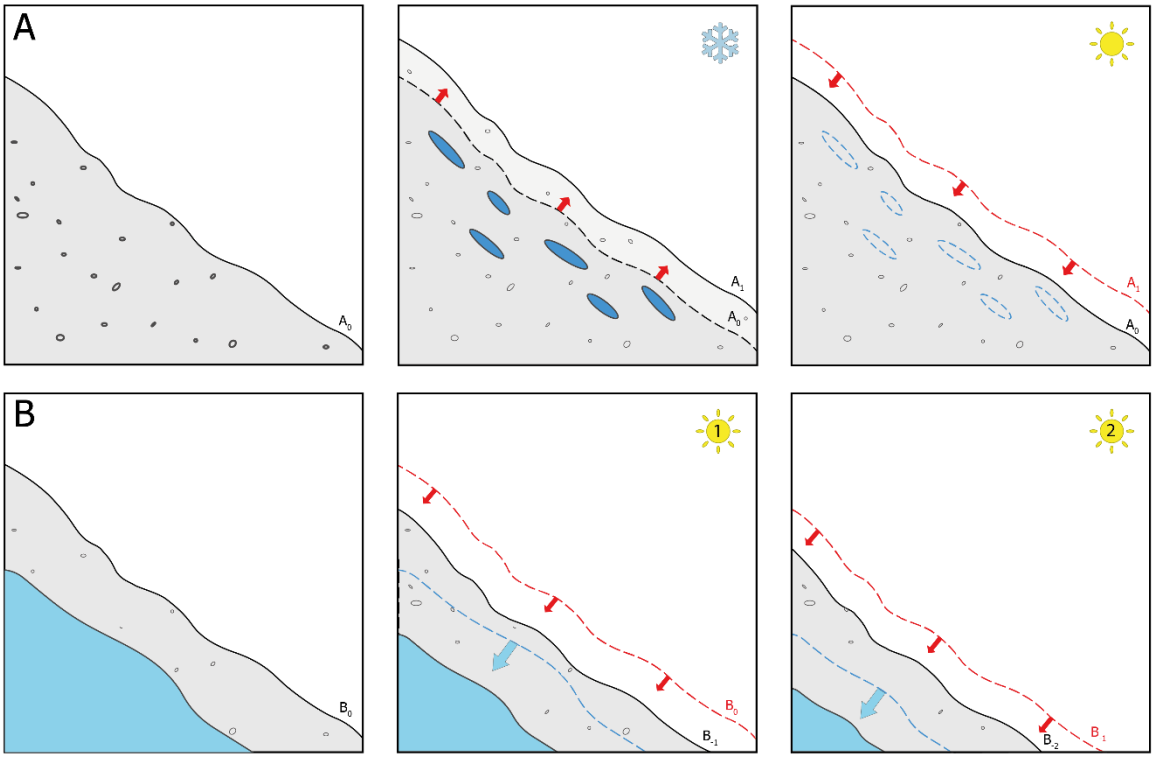

Figure 1: Response of moraine surface to A, formation and degradation of seasonal ground ice and to B, continuous degradation of remaining dead ice cores

The situation is different, if massive ice, which remains from a former glacier position is buried within the moraine matrix (Figure 1, scenario B). As soon as the active layer depth is greater than the thickness of overlaying sediments, the moraines dead ice core will start to degrade. Admittedly, the first season of degradation does not necessarily correspond to the formation of the ice-cored moraine. If permafrost or near permafrost conditions exist (Etzelmüller and Frauenfelder, 2009), buried dead ice may be preserved over long-time if the thickness of covering tills is greater than those of the active layer (Harris and Murton, 2005; Tonkin et al., 2016; Waller et al., 2012). Nevertheless, if positive temperatures reach down through the superimposed tills, present dead ice will degrade. Excessive melt waters are flowing off and eventually appear as springs on the moraine surface. Volume losses due to dead ice degradation then trigger the settling of overlain tills (Ahnert, 2009). Consequently, the moraines surface elevation decreases. In winter, ice volume losses are unlikely to be fully restored. The moraine surface remains lowered. If positive temperatures again penetrate down to the ice front in the following ablation season, described processes repeat themselves. In summation, the degradation of massive dead ice inside a moraine deposit causes the lowering of the moraine's surface elevation. Comparing, the initial and the final situation of the moraine in picture series B, a net volume loss is evident. This net volume loss may also be detected in applied DoD analyses. However, if the presence of dead ice in the subsurface is not known, observed volume losses may be solely ascribed to present surface processes e.g. debris flows, slope wash, fluvial erosion. Erosive processes of differential ice melt (thermal erosion) (Etzelmüller, 2000) taking place in the subsurface may remain unnoticed. Ignoring the possibility of thermal erosion in proglacial areas can therewith introduce uncertainties into calculated sediment delivery ratios and sediment budgets.

The pictures series shown in Figure 1 considers the implications of seasonal ice formation and degradation and the degradation of buried dead ice for the moraine's surface elevation as two separate processes. Unquestionably both processes may also be active at the same time. Seasonal segregation ice thereby could appear as single ice lenses independent of the dead ice body or as ice layers building up upon already existing massive dead ice. Overlapping each other, the combination of both processes may result in a more complex pattern of surface elevation changes on site.

Summing up, the formation of seasonal ice is unlikely to significantly affect applied surface elevation measures. Contrarily, the undetected degradation of buried dead ice would result in an overestimation of sediment erosion via surface processes.

Recent studies show the dimensions of uncertainties that may be introduced into DoDs due to thermal erosion of buried dead ice. In high-arctic Svalbard surface lowering due to ice-cored moraine wastage has been quantified as to be in the range of -0.3 to -1.8 m a^{-1} (Ewertowski and Tomczyk, 2015; Schomacker and Kjær, 2008; Tonkin et al., 2016). Measurements from a humid and subpolar area of Iceland reveal similar rates of -0.3 to -1.4 m a^{-1} (Krüger and Kjær, 2000). Existing studies mainly focus on proglacial areas at higher latitudes rather than on alpine environments. Assuming higher mean annual air temperatures in proglacial areas of the European Alps, ice core degradation is likely proceeding at higher speed with greater rates of surface lowering. The net volume loss caused by thermal erosion is further enhanced by the release of fine sediments through melt waters. The extent of annual material mobilisation due to thermal erosion can thereby be similar to those of annual suspended sediments (Etzelmüller, 2000). Therefore, the issue of dead ice presence and ongoing thermal erosion needs to be addressed when working on sediment dynamics in recently deglaciated areas and research to that effect is needed especially in alpine areas.

Ice-cored moraines are transitional landforms, as final surface stabilisation will not take place until all dead ice has degraded (Lukas, 2011). By definition, the existence of ice-cored moraines demonstrates that the deglaciation of a present landscape has not yet been completed (Lukas, 2011). It is understood that ice-cored moraine wastage is driven by topography and surface processes, rather than climate parameters (Schomacker, 2008; Schomacker and Kjær, 2008; Tonkin et al., 2016). But at present the preservation potential of ice-cored moraines is unclear (Tonkin et al., 2016), especially in alpine environments. Nonetheless, it has been generally suggested that dead ice may survive over a time range of decades to millennia (Everest and Bradwell, 2003). This means that even though a "*glacier may have visibly retreated from a zone of apparently stable moraines, it needs to be considered that dead ice may still be present*" (Lukas, 2011, p. 618). Applied surface elevation measurements may therefore be affected long-term.

1.3 Objectives and limitations of the study

The previous sections demonstrate the problem with calculating erosion volumes and sediment budgets based on remotely sensed elevation models in alpine proglacial areas. Notably, the presence of buried dead ice cores and any uncertainties for surface elevation changes associated with them are not addressed. The present study aims to clarify the existence of dead ice in the lateral moraines of Gepatschferner glacier based on the relative age assessment of evolving spring waters using iodine 129 (^{129}I). For this purpose, the following hypothesis is to be verified:

H_1 *Melt waters of ice-fed springs, that evolve from the LIA lateral moraines can be ascribed to modern seasonal ice and old dead ice, which has remained from former glacial extents, based on ^{129}I concentrations.*

Thereof, several research questions arise:

Can ^{129}I concentrations prove that ice-fed springs on site are of older origin (older than 1950) and hence indicate dead ice in LIA lateral moraines of Gepatschferner glacier?

In which range do ^{129}I concentrations of modern precipitation at the location of the study area operate?

Furthermore, a second hypothesis concerning the spatial distribution of dead ice within the glacier forefield is raised:

H_2 *The spatial pattern of ice-fed springs low in ^{129}I, as surrogates for present dead ice, is explained by topographic characteristics and/or is indicated by hydro-chemical spring characteristics.*

The following research questions are pursued:

How are springs, which are likely fed by degrading dead ice, spatially distributed within the proglacial area of Gepatschferner glacier?

Can plausible and statistically significant correlations between the ^{129}I concentrations of waters from Upper Kaunertal Valley and associated topographic and hydro-chemical characteristics be found?

It is further assessed whether local thermal conditions within the LIA lateral moraines on the right valley side of Upper Kaunertal Valley allow for the formation of seasonal ice:

H_3 *Local ground temperatures within the LIA lateral moraine allow for seasonal ice growth.*

On that basis, the following two research questions are raised:

How distinct are annual fluctuations of local ground temperature at different depths?

Do ground temperatures within the LIA lateral moraine fall below zero degrees?

The proglacial area of Gepatschferner glacier is well suited for any research regarding surface dynamics in proglacial areas, not only due to high rates of glacial retreat and intense morphodynamics present, but also as it has been well studied in recent years. Furthermore, the accessibility of the proglacial area is comparatively easy.

The present study aims to clarify the origin of ice-fed springs on the lateral moraines in Upper Kaunertal Valley. Active processes in local sediment dynamics are assessed. Applied surface elevation change analyses in proglacial areas as well as sediment budgets are further validated. Gained results will also provide new insights into the hydrological situation on site.

1.4 Organisation of the study

In order to respond to the primary research question, age determination of the spring waters must be realised. Given the demands of the study, the selected dating method either has to be absolute or has to be efficient in distinguishing between modern waters and old waters formed prior to 1850. As such tritium (^3H) or tritium/ helium-3 ($^3H/^3He$) could be considered established options (Mook, 2000). Nonetheless, the level of several global fallout isotopes (e.g. ^3H) has almost dropped back to pre-anthropogenic values by now (Snyder et al., 2010). When being short-lived (c.f. half-life of tritium: 12.32 years (Krieger, 2012)), their applicability for relative age dating lessens. The long-lived and continuously emitted isotope ^{129}I (Fan et al., 2013) represents an alternative radionuclide (Povinec et al., 2013) and the present study intends to test its applicability for relative age dating in the setting of Upper Kaunertal Valley. The general environmental interest in ^{129}I makes it an object of research of a growing scientific community (López-Gutiérrez et al., 2000b).

In trying to address the spatial patterns of potential dead ice locations (H_2), present relationships between the ^{129}I concentration of evolving spring waters and topographic or hydro-chemical parameters are statistically assessed. Additionally, ground temperature measurements at different depths are taken to address the question on local thermal regimes and the formation of seasonal ground ice (H_3).

In the following (section 2), the study area of Upper Kaunertal Valley is introduced in detail with regard to location, climate, geology, geomorphology, pedology and vegetation, as well as other characteristics of relevance. With regards to the unestablished character of ^{129}I, extensive understanding of general information, natural production, anthropogenic releases, and its global transport cycle is given in section 3. Based on the aforementioned, the use of ^{129}I for age determination in general and in context of the study area is clarified. Section 4 focusses on the methods and analyses used to answer previously raised research questions and demonstrates the applied workflow. Results gained are described and presented in section 5. The discussion of results follows focussing on raised research questions, the assessment and integration of results from Kaunertal Valley into published research and their implications. Closing, the present work is summarised (section 7) and future research needs and suggestions are outlined (section 8).

2 Study area

The present investigations defined in the previous section are set in the study area of Upper Kaunertal Valley in Tyrol, Austria. Its location north of the main Alpine divide (Abermann et al., 2009) is forthwith addressed in more detail. As the climatic, geologic, hydrologic and geomorphic setting as well as the glacial history of the study area are of particular importance given the present study aim, they are discussed in detail. The catchments pedology and vegetation are of minor concern within the studies limitation and are outlined briefly, before the moraines of the study area, as objects of actual interest, are described in section 2.8.

2.1 Location

Kaunertal Valley is a north-south trending valley in the central part of the Eastern European Alps (c.f. Figure 2). Located southwest of Innsbruck at around 47° N and 11° E Kaunertal Valley is associated with the Ötztal Alps (Abermann et al., 2009). The study area itself lies within the upper reaches of Kaunertal Valley and is, in accordence with the framing of the PROSA project, defined as the surface catchment area of the draining Fagge River (Fagge) at its mouth into the Gepatsch reservoir at 1750 m a.sl. (Baewert and Morche, 2014). The study area reaches down to the LIA maximum extent of Gepatschferner glacier and covers an area of 62.54 km² (Heckmann et al., 2016). The catchment is characterised by high relief energy (Vehling, 2016) as the highest peaks are found above 3500 m (e.g. Hochvernagtspitze 3535 m; Glockturm 3353 m; Weißseespitze 3518 m) (Baewert and Morche, 2014). With the prominent plateau glacier Gepatschferner, the adjacent Weißseeferner, two main glaciers located at the head of the valley, and some smaller cirque glaciers around 30 % of the study area is currently glaciated (Vehling, 2016). The term *Ferner* is regionally used as synonym for glacier (Murawski and Meyer, 2010). Figure 3 gives an overview on the study area.

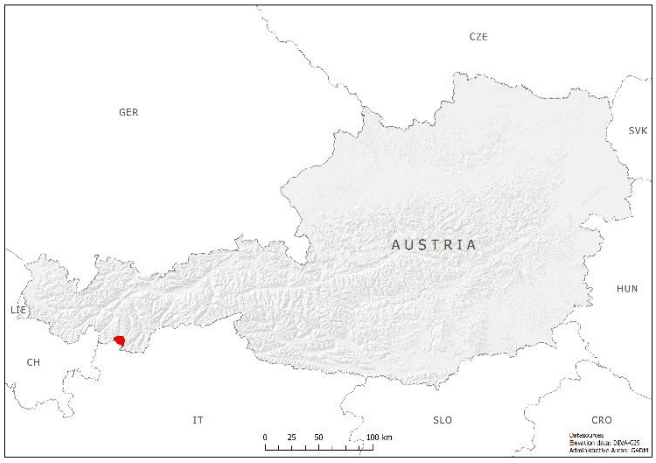

Figure 2: Location of the study area of Upper Kaunertal Valley in Austria

Upper Kaunertal Valley is accessible by the "Kaunertaler Gletscherstraße", a toll road which was built for the construction of the Gepatsch-Hydropower-Reservoir (Umweltbundesamt, 1993) in the early 1960s (Baewert and Morche, 2014) and has been extended to the glacier ski area of Weißseeferner at 2750 m a.s.l. in 1980 (Egger and Hesse, 2014). It attracts about 150,000 tourists throughout the year, especially in the winter season for ski touring and the glacier ski area (Egger and Hesse, 2014). In summer, many hiking trails, the climbing garden "Fernergries", glacier navigational trainings, mountain pastures or the high alpine road and the easy access of Weißseeferner glacier itself provide tourist destinations in the Upper Kaunertal Valley. Next to tourism, the pastures of Upper Kaunertal Valley are used for summer grazing.

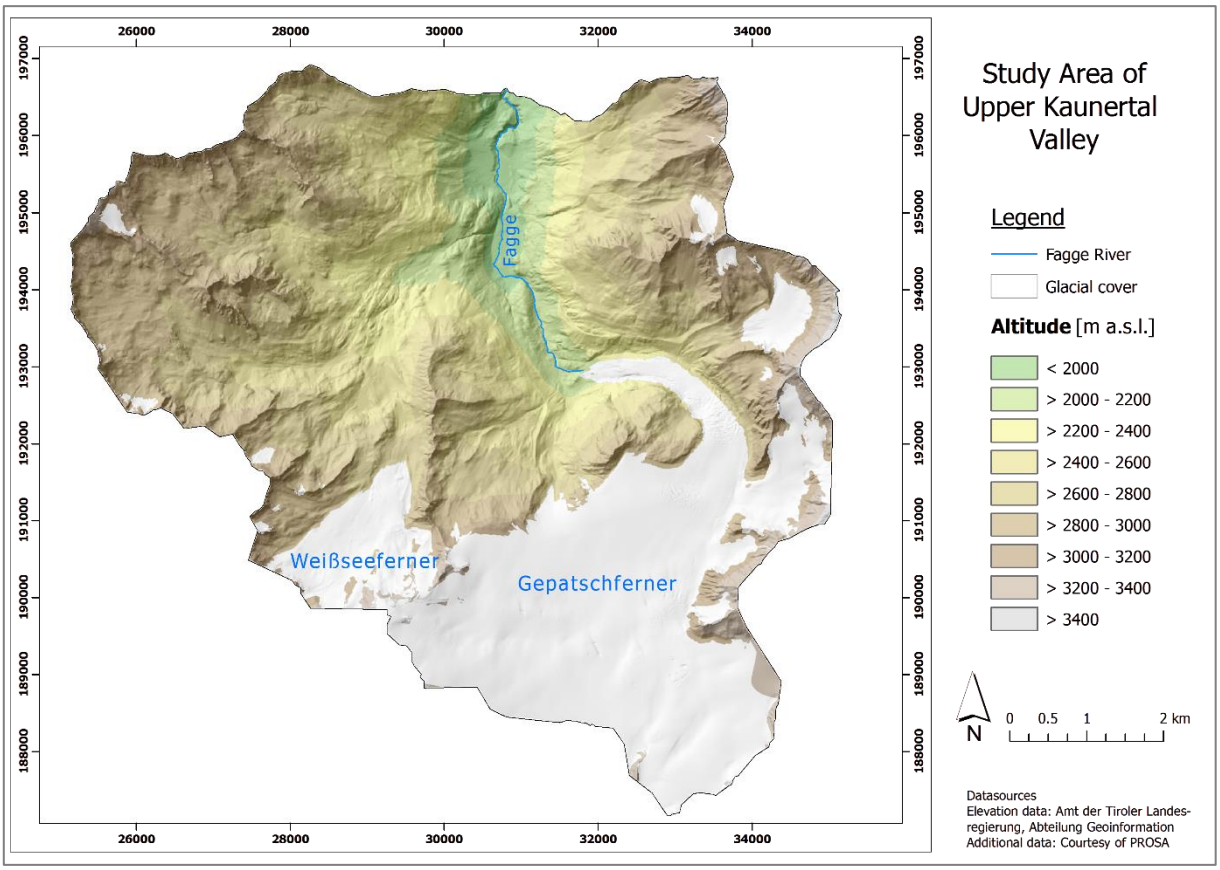

Figure 3: Study Area of Upper Kaunertal Valley

2.2 Climate

Caused by its central location within the Central Eastern European Alps, Kaunertal Valley is termed an inner Alpine dry valley. On a large scale, the Central Alps receive increased solar radiation, compared to the northern and southern fringe. This is conditioned by topographic barriers and consequent lower cloudiness and less precipitation. Isotherms are found higher within the Central Alps. However, radiation is highly variable on a local scale (exposition, relief, snow cover, vegetation) (Veit, 2002) and climate variability, due to great differences in elevation, is substantial (Heckmann et al., 2016).

In contrast to other high-alpine regions (Veit, 2002), detailed climate data exist for several locations in (Upper) Kaunertal Valley, due to climate stations and totalisators operated by TIWAG (Tyrolean Hydropower company). Thankworthy, precipitation and air temperature data from Gepatschalm, at the base of the study area, have been made available to the PROSA project and the present study.

Mean annual air temperature at the locality of Feichten (1280 m a.s.l.) is 4.6 °C (1961 to 1990, c.f. Figure 4) (Tirol Atlas, 2013), while it is only -0.4 °C within the study area at the climate station Weißsee (2540 m) (Vehling et al., 2016). At the climate station of Gepatschalm, located closest to the actual study sites and with roughly the same elevation (1980 m a.s.l.), a mean annual air temperature of 3.3 °C was recorded in 2015 (c.f. Figure 5).

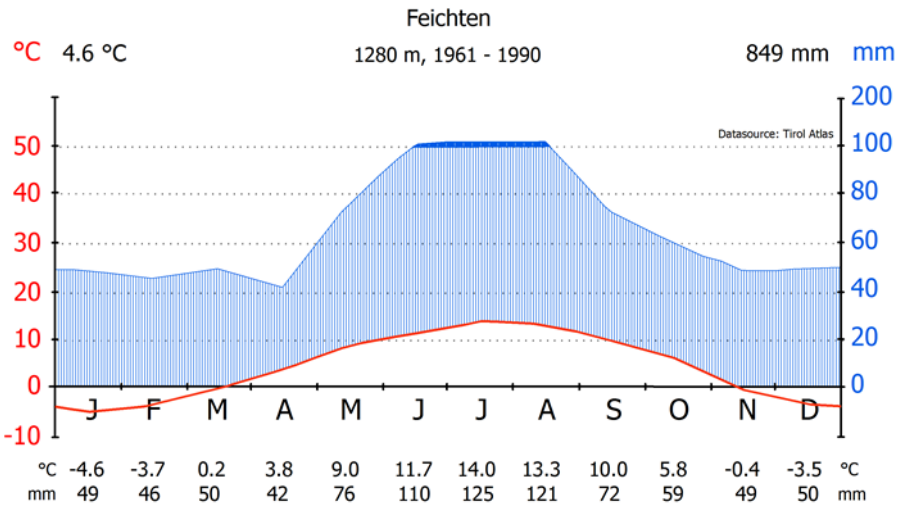

Figure 4: Climate graph of Feichten (1961 – 1990)

Compared to the humid Northern and Southern Alps, the central (eastern) parts of the Alps, including Kaunertal Valley, are rather dry. Dryness of the inner alpine valleys is thereby mainly induced by Luv-Lee effects. Mean precipitation minima in winter (Feichten: 49 mm in January) and mean precipitation maxima in summer (Feichten: 125 mm in July) are characteristic (c.f. Figure 4). The amount of precipitation increases as single rain events become more abundant with higher altitude and the prevailing relief forces. Up to elevations around 2000 m precipitation gain within inner Alpine dry valleys is minor and usually below 60 mm per 100 m altitude difference. However, precipitation is highly variable on a regional scale and may also be provided by fog (Veit, 2002). Dependent on altitude and aspect, annual precipitation within the study area ranges between 1000 and 1300 mm (Vehling et al., 2016) but shows great monthly variability (Vehling, 2016). Precipitation at Gepatschalm in 2015 (978 mm) ranks just below the annual average of the study area, while mean annual precipitation at the lower elevated station of Feichten is only 849 mm (Tirol Atlas, 2013).

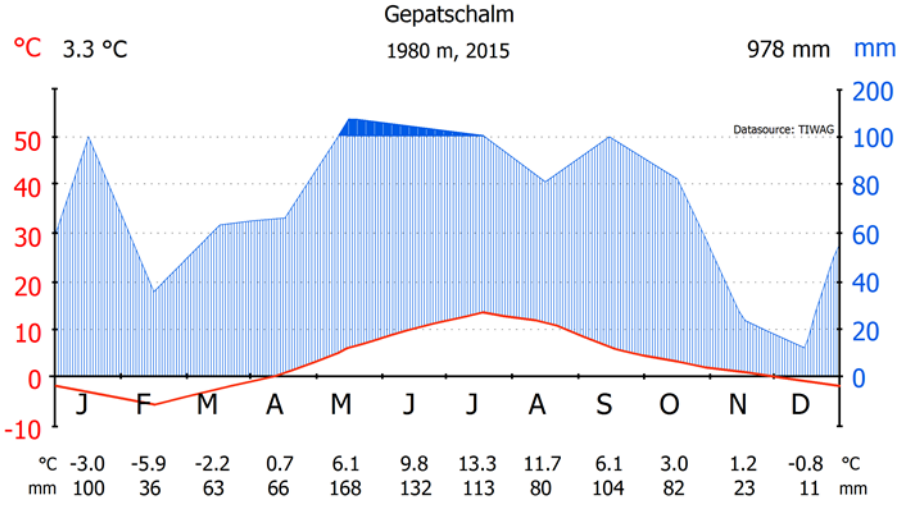

Figure 5: Climate graph of Gepatschalm (2015)

As to screening effects, the period of snow cover is decreasing from the margins towards the central part of the Alps (Veit, 2002). Still, the study area is covered in snow for several months per year (Vehling, 2016). Annual snow depth may vary considerably between years and even annual conditions of snow cover are highly variable on a regional scale. Prevailing winds cause scattered snow cover and are subsequently lead to ablation variability in area and time, but with annual similarity (Veit, 2002).

If large-scale synoptic circulations are weakened, local wind systems may develop due to the great topographic relief. As such mountain valley breezes, mountain slope winds or firn (glacier) winds are to be expected (Veit, 2002).

2.3 Hydrological system

Kaunertal Valley drains northbound as a tributary to the Upper Inn river system (Heckmann et al., 2016). It is part of the Danube drainage basin. The southern margin of the drainage divide further correlates with the Austrian-Italian border. Geologic lineaments and foliation present in Upper Kaunertal Valley (c.f. section 2.4) determine the orientation of waters and glaciers within the study area on a large-scale (Vehling, 2016).

Figure 6: Gepatschferner glacier from WNW, (Abermann J. 2008)

Gepatschferner glacier is, after Pasterze glacier, Austria's second largest glacier. Emanating from a large plateau position (Heckmann et al., 2016), the north draining part of the glacier covers an area of 17 km² (Abermann et al., 2013). The accumulation zone of Gepatschferner glacier can be found above 3200 m a.s.l. and covers the upper parts of the plateau up to elevations of 3526 m a.sl. Below, the glacier narrows down to a width of ~ 500 m and flows off to the northeast of the vast plateau by dropping 600 m in an icefall towards the bottom of the valley at 2600 m. At the base of the deeply serrated ice fall, the glacier tongue takes a sharp northwest turn and flows relatively levelled towards the glacier front (c.f. Figure 6) (Keutterling and Thomas, 2006).

Fagge River originates from Gepatschferner glacier mouth at 2206 m a.s.l. and further drains the catchment (Baewert and Morche, 2014). Downstream of the glacier snout, several episodic and perennial tributaries of both valley sides with varying discharge coalesce into the recipient Fagge. The outlet of the study area is marked as the mouth of Fagge River into the Gepatsch reservoir, a hydropower reservoir that has filled the valley floor since 1964 with a maximum water surface level at 1767 m a.s.l. (Strauhal et al., 2016), operated by the TIWAG (Baewert and Morche, 2014). Subsequent, the Fagge River is mouthing into the Inn river at the municipality of Prutz (Vehling, 2016).

The Fagge River is characterised as proglacial fluvial system with high sediment load (Baewert and Morche, 2014) and great seasonal and daily fluctuations. Peak discharges are to be expected during maximum ablation in July and August (Veit, 2002). Mean annual discharge at the *Gepatschalm* gauging station has been measured by TIWAG as 3.42 $m^3 s^{-1}$, but short-term glacial dynamics can have significant impacts on its discharge (Vehling, 2016). The potential rupture of a (sub-) glacial water pocket during a heavy rainfall event in August 2012, described by Baewert and Morche (2014), caused a maximum discharge of 47.3 $m^3 s^{-1}$. Estimations of fluvial sediment transport in the Fagge over a period of 25 years by Tschada and Hofer (1990) revealed a mean annual bed load yield of 12,410 $m^3 a^{-1}$ and a mean annual suspended load yield of 45,930 $m^3 a^{-1}$ leaving the study area. However, latest measurements support the transport of much higher amounts of sediments, also when being compared to other proglacial and alpine areas (Baewert and Morche, 2014). Mouthing into the Gepatsch reservoir, the transported material is accumulated as alluvial fan (Vehling, 2016).

Ground water studies just below the study area and in the slopes surrounding the Gepatsch reservoir have been conducted by Strauhal et al. (2016). The vadose zone residing below the mountain crests can be expected to be of some hundred metres thickness. Beneath, "*groundwater flows preferentially within zones of highly weathered bedrock (…), brittle fault and fracture zones, deep-seated rockslides, and conductive Quaternary deposits, i.e. alluvial, debris flows, talus and colluvial deposits"* (Strauhal et al., 2016, p. 12). Groundwater circulation within fractured bedrock is believed to be restricted to a few hydrologically well connected faults and joints. Results further indicated short residence times below five years and meteoric origin of ground water without signs of evaporative processes taking place (Strauhal et al., 2016).

2.4 Geology

Upper Kaunertal Valley is underlain by the Ötztal crystalline (Heckmann et al., 2016), a geological unit of the superimposed metamorphic Eastern Alpine crystalline zone. The Palaeozoic rock series have been shaped by metamorphic episodes multiple times during Caledonian and Variscan orogenesis. Metamorphosis during Alpine orogenesis was comparatively less intense. Nevertheless, the overthrust of the Ötztal crystalline to the Pennine nappes during Alpine orogenesis exerts tectonic loading to this day. This is expressed by rates of tectonic uplifting > 1 mm a^{-1} in the Central Alps (Vehling, 2016). Large scale tectonic structures within the study area are characterised by mainly E-W trending, steeply dipping foliation (Heckmann et al., 2016). Additionally, NE to SW and NW to SE striking lineaments are crossing (Vehling et al., 2016).

High- to medium-grade metamorphic orthogneiss and paragneiss are the dominating rock types in Upper Kaunertal Valley. Present orthogneiss may be differentiated in granite gneiss and augen gneiss, the latter being characterised by large feldspar inclusion. Foliated gneiss, however, is the main variation of paragneiss within the study area. Its rusty weathering easily uncovers this rock type in the field. Intermittent, green coloured amphibolite, intruded in tectonically stressed paragneiss, exists as ten metre wide belts with a banded structure and high

resistances. Alternate bedding of paragneiss and amphibolite is primarily found in the proglacial area of Gepatschferner glacier. Outcropping gneiss within the glacier forefield has been migmatised and is consequently marked by light and several centimetre wide quartzose streaks. Mica schist, phyllite, granite porphyry, diabase or basalt rock types are of minor spatial importance or occur as dyke rocks (Vehling, 2016).

The geological over-view map of Upper Kaunertal Valley by Vehling summarises dominating rock types and tectonic structures in Figure 7. Extensive geologic details of the study area can further be found in (Vehling, 2016).

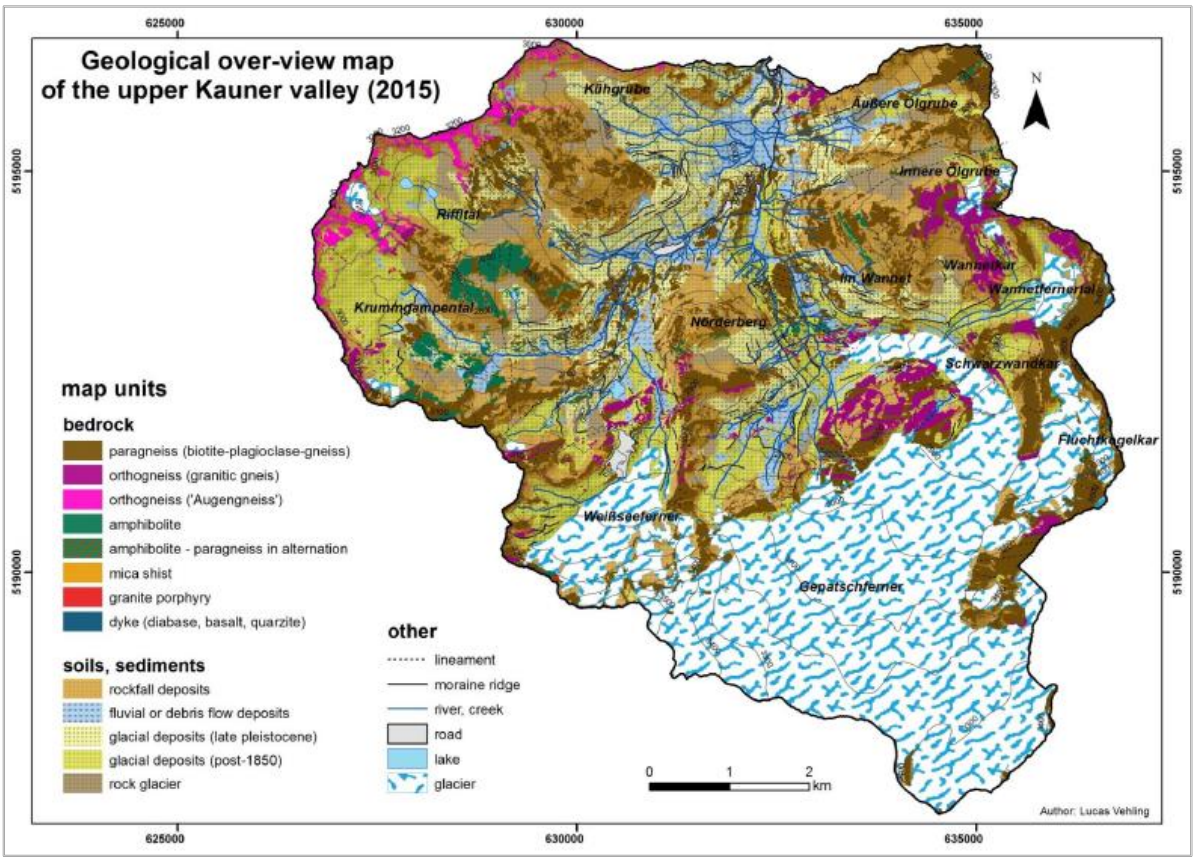

Figure 7: Geological map of Upper Kaunertal Valley (courtesy of Lucas Vehling)

2.5 Geomorphology

From a geomorphologic point of view, Upper Kaunertal Valley does not represent a typical glacial-carved, trough-shaped valley. It branches off to several small lateral valleys, due to the extensive and ramified ancient plateau glacier draining into each direction. The study areas relief in general, is highly influenced by Pleistocene glacial dynamics and their morphological impact. As a consequence, Upper Kaunertal Valley can be divided into the topographical units of two main valleys (*Gepatschfernertal* & *Weißseefernertal*), where the main glacier lobes have been draining north, and several tributary valleys with (e.g. *Fluchtkogelkar, Innere Ölgrube, Krummgampental, Riffltal*, *Schwarzwandkar, Wannetfernertal*, *Weißseejochtal*) or without existing (or former) cirque glacier (e.g. *Äußere Ölgrube*, *Kühgrube*, *Wannetkar*). The small

cirques glaciers of the latter were missing erosive forces of the main glacier tongues. By developing large altitude differences and/or escarpments towards the main valleys, those valleys can be specified as typical hanging valleys (Vehling, 2016).

The morphology of present scarp slopes is stepped but varies on a small scale. Large, perpendicular cliffs are absent. Mean slope within the main valleys is given as 22° (c.f. lateral valleys: 29°). Middle slopes and footslopes of the main valley have been glacially eroded and have locally been left behind oversteepened after glacial retreat. One half of all rock slopes is directly affected by modern ice recession. One third of the slopes is free of ice since ~ 1850 and can be defined as proglacial (Vehling, 2016). Besides steep cliffs and cirques, Pleistocene and Holocene glaciation in combination with the cold alpine climate did lead to the formation of other typical glacial and periglacial landforms. Prominent talus slopes at the foot of the steep rock walls, moraine bodies of different age, massive roche mountonnées in the glacier forefield (Vehling et al., 2016) or rock glaciers in the tributary valleys (Dusik et al., 2015b) are characteristics of Upper Kaunertal Valley. Unconsolidated material covers roughly 40 % of the study area (Vehling, 2016) and is derived by gravitational, fluvial, glacial or glacio-fluvial processes (Baewert and Morche, 2014; Vehling, 2016). Deposits of multiple types of mass movements (e.g. debris flow, rockfall, deeply-seated landslides, rockslides,…) (Strauhal et al., 2016), fluvial and glacio-fluvial sediments, alluvial fans, wide alluvial planes (so-called *Griese*) or glacial till, exemplify those processes. Their areal extent is also mapped in Figure 7. To some extent, those deposits may function as temporary sinks or sediment barriers (Heckmann et al., 2016; Vehling, 2016). However, parts of them may easily be mobilized and act as potential sediment sources for other geomorphological processes (Baewert and Morche, 2014; Vehling, 2016).

2.6 Pedology & vegetation

Soil development within the study area has been intensively investigated by Temme et al., (2016) and has been proven to strongly depend on soil age and the time since last glaciation. As such, Upper Kaunertal Valley is comparable to other well investigated Alpine valleys. Processes of erosion and deposition gain importance in such highly active environments. Within the proglacial area, A-horizons were observed on approximately 40 years old soils only. Nonetheless, pioneer vegetation has been reported on soils younger than ten years old. Parent material in the glacier forefield usually exceeds a depth of 25 cm to bedrock, hence only a few Leptosols have been reported. Cambisols have been identified as the most typical soils in areas that have been exposed by the retreating glacier for longer. While (Skeletic) Regosols dominate in locations of more recent exposure. With increasing time since last glacial coverage podsolization is taking place. The most developed soil profile found within the proglacial area was a weakly developed Skeletic Podsol, which has been dated to be ~ 160 years old. Under current climatic conditions, Haplic Podsols can be seen as the climax soil and has been reported from outside of the LIA glacial extent (Temme et al., 2016).

In analogy to prevailing soils, vegetation found in the study area is likewise characteristic for high alpine regions (Vehling, 2016), with high vegetal variability due to great altitudinal differences (Heckmann et al., 2016). The montane zone of the Central Alps is characterised by spruce (*Picea abies*)-, scots pine (*Pinus sylvestris*) - or mountain pine (*Pinus uncinata*) forests. Certainly, species such as stone pines (*Pinus cembra*) or larch (*Larix decidua*) dominate with increasing altitude (Veit, 2002). Coniferous forests in Kaunertal Valley exist up to 2150 m a.s.l. (Heckmann et al., 2016) and comprise stone pine, larch and spruce. Forests in the Subalpine Zone are less dense with increasing altitude. Krummholz (e.g. green alder (*Alnus viridis)* or knee pine (*Pinus mugo*)) is found within the Subalpine zone (Veit, 2002). Nicolussi et al. (2005) defines the present-day tree-species line for *Pinus cembra* in Upper Kaunertal Valley at ~ 2370 m above sea level. Above, a transition into dwarf shrub heath is taking place while alpine meadow communities (e.g. *Curvuletum, Seslerio-Semperviretum, Firmetum*) dominate the main parts of the alpine zone (Veit, 2002). Pastures within the alpine zone are intensely used for cattle grazing during summer months. At ~ 2800 to 3000 m a largely vegetation-free zone begins (Heckmann et al., 2016). However, individual cushion or rosette plants, single phanerogams and lichen do exist within Subnival- and Nival Zone (Veit, 2002).

Concerning the proglacial area, pioneer plants have established themselves in areas that are free of ice for a few decades, while recently exposed areas still remain free of vegetation (Vehling, 2016). But a notable difference between the two valley sides must be mentioned here. While the east facing left side of the valley is fairly covered, the west-exposed right valley side and specifically the prominent LIA lateral moraines are mostly lacking any vegetation.

2.7 Quaternary glaciation

The European Alps have witnessed vast shaping and remodelling by repeated glaciations. Sediments were carved out, transported downstream and accumulated onto alpine forelands by glacial action (Ivy-Ochs et al., 2008). This also applies for Kaunertal Valley, where Late Pleistocene maximum glaciation has completely covered (c.f. Figure 8) and highly altered the study areas topography (Heckmann et al., 2016; Vehling, 2016).

Variations in the suns orbit and a consequently reduced receipt of solar energy allowed for a global build-up of large ice masses (Ehlers and Gibbard, 2011) at the end of the last glacial cycle (Würm glacial). Climate cooling led to a significant lowering of the glaciers equilibrium line altitude (ELA) and local glaciers started to advance from tributary valleys into longitudinal valleys. The following ELA lowering was small but sufficient to create large valley and piedmont glaciers (van Husen, 1997). Total ELA depressions associated with the Late Würmian maximum glaciation are given as 1200 to 1500 m based on LIA ELA (Ivy-Ochs et al., 2008). Advancing from their accumulation areas, large valley glaciers overflowed smaller passes of the limestone Alps and spread tens of kilometres into the alpine forelands, forming (confluenced) piedmont lobes (c.f. Figure 8) (Ivy-Ochs et al., 2008; van Husen, 1997). Glaciers of Kaunertal Valley and other tributaries could have reached the Inn valley around 25 to 24 ka BP as suggested by van

Husen (1997). Most extensive glacial extents between 30 to 18 ka BP occured during MIS (Marine Isotope Stage) 2 (Ivy-Ochs et al., 2008) and probably culminated around 21 ka BP (van Husen, 1997). This final ice advance is termed the Last Glacial Maximum (LGM). Given the estimated preservation of the glaciers at their maximum position for a period of 3,000 to 4,000 years (van Husen, 1997), the LGM roughly correlates with the maximum global ice volume during the Würmian glacial, dated as 18 ka BP (Ehlers and Gibbard, 2011). During maximum glaciation the Inn glacier also spread out into the lowlands, developing a prominent piedmont lobe and coalescing to the Inn-Chiemsee glacier. Peak level of Würmian ice advance is illustrated in Figure 8 after Ivy-Ochs (2015) and shows, upon others, the labelled Inn glacier piedmont lobes and the location of Kaunertal Valley within the Central Alpine icecap.

Gradual climate warming following the Würmian maximum glaciation (Hippe et al., 2014), conditioned rapid downwasting of the piedmont glacier in the forelands and initialised the final ice decay (Kerschner and Ivy-Ochs, 2008). The disintegration of the Central Alpine ice cap followed (Hippe et al., 2014) and may not have taken longer than a few centuries (Ivy-Ochs et al., 2008). Deglaciation of the inner alpine valleys has most likely been completed by 19 to 18 ka BP. Notably, 80 % of the LGM ice volume had vanished by then (Ivy-Ochs et al., 2008). These dates are supported by radiocarbon and OSL (optically stimulated luminescence) dating and mark the beginning of the Alpine Lateglacial (Hippe et al., 2014; Ivy-Ochs et al., 2008). However, the trend of climate warming and consequent ice decay was interrupted by several climatic fluctuations (Hippe et al., 2014), which were mainly caused by variation in the North Atlantic Oscillation (NAO) and consequent weakened oceanic heat transport (Kerschner and Ivy-Ochs, 2008). Multiple Lateglacial stadials (Gschnitz, Senders/Clavadell, Daun, Egesen (Kerschner, 2009)) are associated with these short stagnations and re-advances prior to the Holocene warming (Hippe et al., 2014; Ivy-Ochs et al., 2008). Among them, Gschnitz and Egesen stadial moraines, have been reported from Kaunertal Valley. During the Gschnitz stadial, Kaunertal Valley was intensely glaciated as indicated by moraines in lower parts of Kaunertal Valley (Vehling, 2016). Egesen stadial, which correlates to the Younger Dryas (Ivy-Ochs et al., 2009) can be determined in the upper parts of the valley outside the study area. Position of well-preserved moraines allow for the reconstruction of a glacial area of approximately 60 km². Broad parts of the tributary valleys, among them Riffltal and Krummgampental, still had a connection to the main

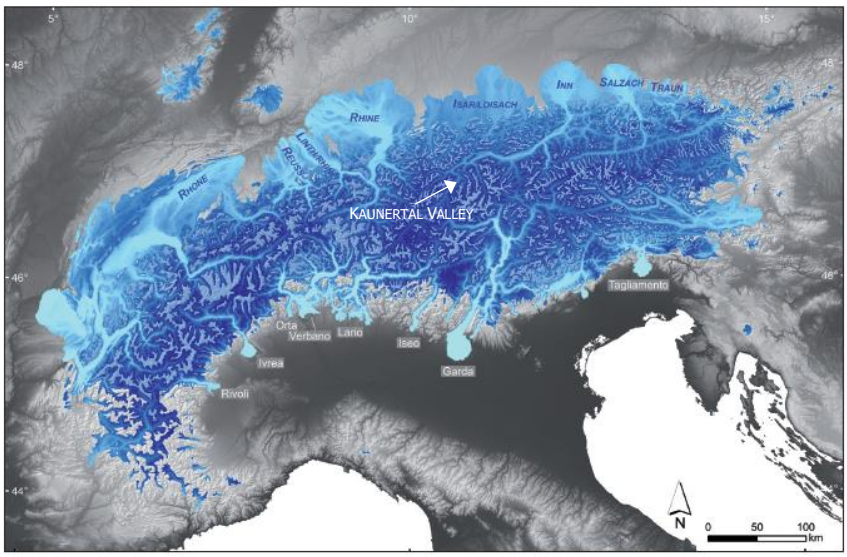

Figure 8: Alps during Last Glacial Maximum (Würmian) (Ivy-Ochs, 2015), location of Kaunertal Valley has been labelled

glacier during Egesen stadial (Vehling, 2016). Information on glacial stadials between Lateglacial and Early Holocene is available for other Alpine valleys and is given in e.g. Ivy-Ochs et al. (2008, 2009), Kerschner (2009) and Kerschner and Ivy-Ochs (2008).

From the beginning of the Holocene (11,000 a BP (Ehlers and Gibbard, 2011)) and up to ~ 3.3 ka BP climate shifted to prolonged warmer and drier conditions. Given this glacier-hostile climate, documented for multiple large Alp glaciers, glacial expansion usually lagged behind today's extent (Ivy-Ochs et al., 2009). Nonetheless, dendrochronological dating successfully documented several short re-advances of Gepatschferner glacier up to and above its 1950/60 position, between 7000 to 2000 a BP (Nicolussi and Patzelt, 2001).

After 3300 ka BP, climate cooling started once more. Tree lines descended to lower altitudes. Glacial advances and their duration increased, while glacial recessions shortened. These evolutions found their climax in prominent advances during LIA (Ivy-Ochs et al., 2009). Climate cooling and glacial advances during LIA have been associated with periods of reduced solar activity (Maunder and Dauner minima), negative NAO index, and humid conditions with enhanced winter precipitation. Additionally, the contribution of increased volcanic activity has also been considered. These climatic changes led to glacier fluctuations from several hundred metres up to three kilometres, based on glacier size. In the Alps, LIA glacial advances occurred in three principal stages roughly around 1350, 1650 and 1850 AD. Throughout most locations, the final advance of the 19th century represents the most extensive LIA advance (Zasadni, 2007). Furthermore, the 1850 advance depicts the Holocene glacial maximum in most Alpine catchments (Ivy-Ochs et al., 2008). During the LIA maximum, an ELA lowering in the Eastern Alps down to 2600 to 3100 m a.s.l. was suggested (Zasadni, 2007).

At Upper Kaunertal Valley, dendrochronological studies by Nicolussi and Patzelt (2001) combined with early observations, drawings and writings allow for detailed reconstruction of LIA advances. Modern glacial maxima of Gepatschferner glacier have been dated to 1630/1635, 1679 and 1855 AD. The maximum of 1630 remains close to the advance of 1679, and glacial maxima of 1679 and 1855 have basically been identical - as indicated by partially merging moraines (Nicolussi and Patzelt, 2001). Whilst the LIA maxima, the glacier advanced as far as the locality of Gepatschalm (c.f. Figure 9). In the period between the proven maximum advances, it is accepted that today's proglacial area was heavily covered by ice over long episodes during LIA (Vehling, 2016).

Based on the Holocene glacial maxima in the mid-19th century, glaciers of the European Alps have decreased considerably (Keutterling and Thomas, 2006). Within the last decades, particularly since increased climatic warming around 1985 AD, glacial shrinkage has happened rapidly and notably faster than the long-term average retreat (Ivy-Ochs et al., 2009; Zasadni, 2007). Overall, glacial coverage within the European Alps has halved between 1850 - 2000 (Zemp et al., 2008). Gepatschferner glacier in Upper Kaunertal Valley is no exception. Figure 9 shows progressive glacial retreat in several time steps. Retreat since 1856 started slowly and has been well documented in drawings, photographs, length measurements and earliest examples of exact topographic maps (Brunner, 2006; Nicolussi and Patzelt, 2001). In 1870/71

Gepatschferner glacier had retreated 110 to 115 m behind its 1855 maximum position, as documented by the *Dritten Landesaufnahme* on behalf of the Austro-Hungarian monarchy. Tachymetric records compiled by Finsterwalder & Schunk in 1888 reveal an increased retreat of overall ~ 460 m based on the 1855 end moraine (Nicolussi and Patzelt, 2001). The evolution of Gepatschferner glacier has been dominated by almost uninterrupted recession since then. Except for a phase of stagnation (1900 to 1920) (Hartl, 2010) and minor re-advances from 1971 to 1979 (Keutterling and Thomas, 2006). Since LIA maximum, 36 % of its ice volume and 32 % of its areal extent (~ 7.8 km²) has disappeared (status 2006). The distributary glacier *Östlicher Wannetferner* had been disconnected from the main glacier by 1922 (c.f. Figure 9). The second glacier tongue evolving from the Gepatschferner glacier plateau, at the so-called *Münchner Abfahrt,* had also lost its connection by that same year (Hartl, 2010). Annual length and volume changes between 1850 and 2006 are accurately described in five time slices by Hartl (2010). However, retreat has been accelerating. Between 2006/07 and 2015/16 a length decline of 623 m (Ø 62 m a^{-1}) can be calculated based on glacial measurements of the Austrian Alpine Club (ÖAV). In recent years Gepatschferner's glacier tongue shows signs of disintegration and highest retreat values among Austrian glaciers (-114 m (2012/13), -91 m (2013/14), -121,5 m (2014/15), -40.5 m (2015/16) (Fischer, 2017, 2016, 2015, 2014, 2013, 2012, 2011, 2010, Patzelt, 2009, 2008, 2007). Considering recent losses in length, the current glacier front of Gepatschferner glacier resides more than 2.5 km upstream of the 1855 maximum position (Vehling et al., 2016).

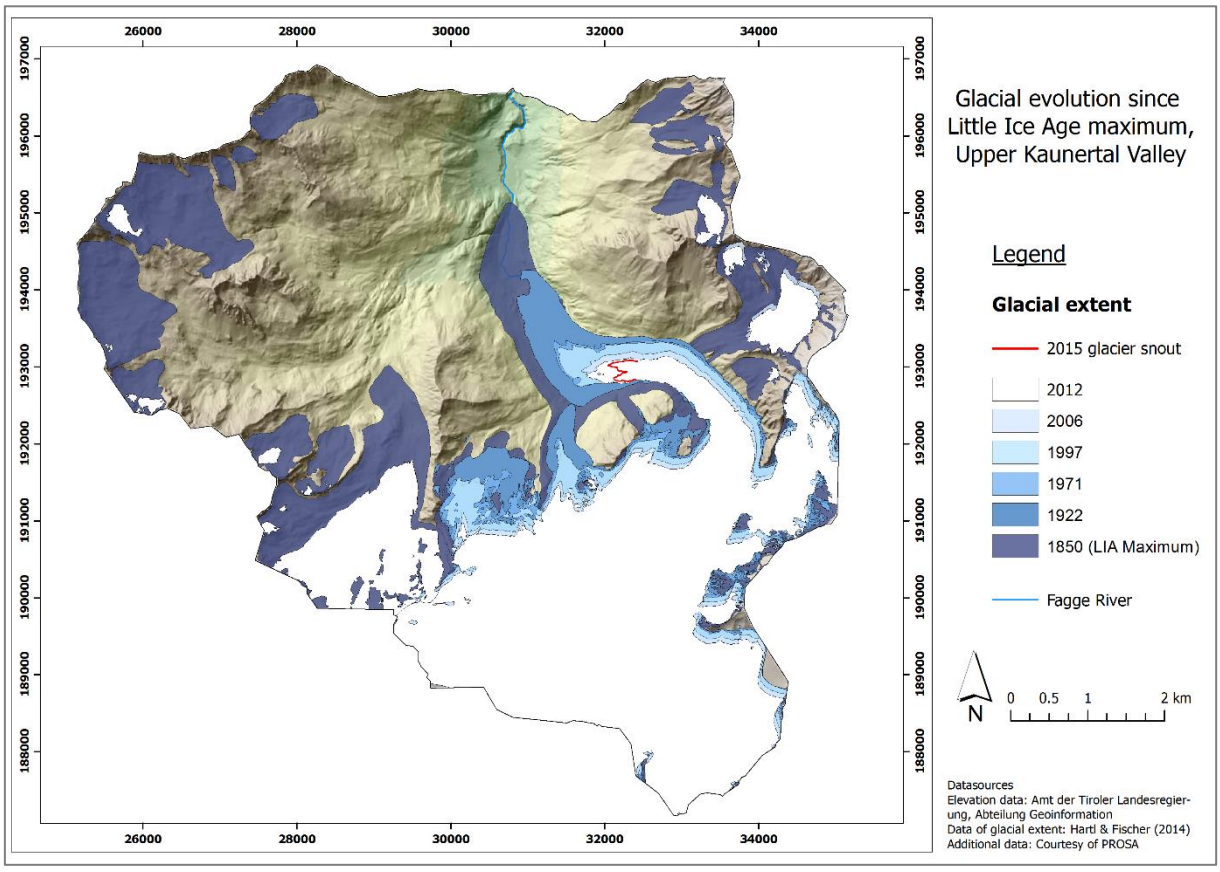

Figure 9: Time series on the glacial evolution of Gepatschferner glacier in Upper Kaunertal Valley since Little Ice Age maximum, 1850 – 2015

2.8 Moraines of Gepatschferner glacier

Since Little Ice Age maximum, a significant amount of terrain in Upper Kaunertal Valley became free of ice (c.f. Figure 9). Rapid glacial retreat since around 1850 AD was accompanied by gradual exposure of moraine deposits, as can be seen in the time series of Figure 11. Lateral moraines left-behind in the proglacial area of Gepatschferner glacier remain and display the particular study objects of the present research. Investigated sites include prominent LIA moraines up to ~ 200 m height as well as smaller deposits of recent years, on both sides of the valley. Moraines present in the study area differ not only in terms of size but also according to their time of de-icing, exposition, prevailing grain sizes, etc. Details on the setting of examined sites within the proglacial area of Gepatschferner glacier are given in the following passages.

Moraines are stony debris ridges deposited by glaciers. They may develop as product of long-lasting stable ice positions in front as well as at the lateral margins of a glacier (Sharp, 1988). *"Moraines consist of unconsolidated sediments, directly deposited by glaciers or deformed and accumulated by glaciers"* (Schomacker, 2011, p. 747). Sediments associated with moraines are typically non-bedded, unsorted, subangular and frequently showing scratch marks due to glacial transport (Embleton-Hamann, 2007). After glacial meltdown, deposits of frontal and lateral moraines are left behind. Nonetheless, due to their occurrence on unstable valley slopes, lateral moraines are generally less preserved (Schomacker, 2011). Figure 10 exemplifies the typical appearance of moraines in the forefield of an alpine glacier. In Upper Kaunertal Valley, prominent lateral moraine ridges deposited during LIA maximum (1855) are found on the right valley side. On the left valley side, comparable deposits have not been developed (e.g. due to cross-glacier asymmetry (Bennett and Glasser, 2009)) or have not been preserved. Moraine sections that have been investigated in particular are shown in Figure 14 and are shortly described in the following sections. Till material, forming the moraines of the study area, is derived from paragneiss and orthogneiss (c.f. section 2.4). Sand and coarser fractions dominate, but all grain sizes from silt to boulders can be found poorly sorted (Temme et al., 2016).

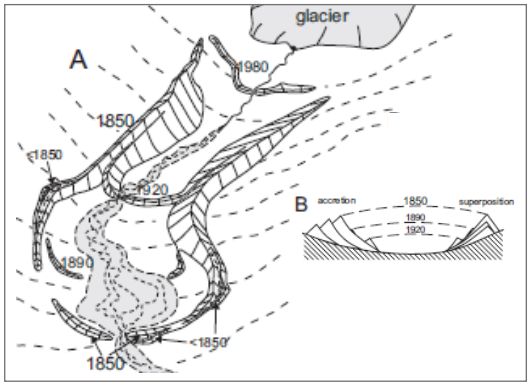

Figure 10: A, Pattern of typical moraine formation in the proglacial of an alpine glacier. Dates correlate to glacial advances. B, Profile of the depositional structure of a lateral moraine, comparison of two modes of moraine building: accretion and superposition (Zasadni, 2007)

The sharp LIA lateral moraine ridge on the right valley side is found roughly 1.6 km upstream from the maximum position of the glacier terminus in 1855 (Nicolussi and Patzelt, 2001) and continues to the present glacier snout and beyond (c.f. Figure 14, site A). The lateral moraine complex is up to 200 m high and very steep, especially at the upper parts of the slope with inclinations up to around 45°. The moraine´s exposure is west-southwest. In some locations, underlying bedrock has already been exposed due to erosive forces, visually dividing the moraine body (c.f. Figure 12). The moraine ridge itself is about thirty metres wide and free of ice

Figure 11: Retreating Gepatschferner glacier and progressively exposed LIA lateral moraine on the right valley side in A, 1904 in Keutterling and Thomas (2006), source: Gesellschaft für Ökologische Forschung, Munich, Germany; B, 1941 in Nicolussi and Patzelt (2001), photo: E. Schneider; C, 2015, photo: Czarnowsky V.

for roughly 100 years (e.g. picture a, in Figure 11). It is by now covered with vegetation and therefore less prone to erosive forces. Underneath a zone comprised of unconsolidated moraine material and widely free of vegetation continues. The whole moraine body was completely free of ice no later than 1971. Frequent fluvial and slope processes (e.g. debris flows, gullying, slope wash) (Dusik et al., 2014; Temme et al., 2016) are reworking those highly erosive sediments, as shown by Dusik et al., (2014, 2015b) and Hilger et al. (2014). For instance, an amount of 4400 m³ of sediments was mobilised between 2006 and 2012 (Hilger et al., 2014). In the upper fifty metres of the lateral moraine, where slope angles are greatest, erosive processes led to the formation of several deeply incised gullies (Neugirg et al., 2014). The LIA lateral moraine, as well as other unconsolidated moraines, therewith represent an important sediment source within the proglacial area. The middle slope of the moraine is mainly subject to sediment transport and intermediate storage within the sediment cascade. Eventually, mobilised material is transported to the footslope of the lateral moraine, where (re-)deposition as talus accumulation is happening. The base of the moraine is found at an altitude between 2070 and 2100 m a.s.l., adjacent to the braid planes of Fagge River. As ongoing fluvial processes of Fagge River cut into the accumulated material at the bottom of the moraine, a link between the morphologically highly active lateral moraine and other elements of the proglacial system is established.

A counterpart to the nicely developed LIA lateral moraine is missing on the left side of the valley. However, a second tongue of Gepatschferner glacier is flowing off the plateau to the NNE via the so-called *Münchner Abfahrt* and did confluence with the main tongue during LIA glacial maximum. This secondary tongue generated a symmetrically shaped moraine on the

Figure 12: Little Ice Age lateral moraine of Gepatschferner glacier on the right side of Upper Kaunertal Valley. Gullies and channels developed in unconsolidated sediments of the moraine. Fagge River cutting into talus accumulations at the foot of the slope (Kamleitner S. 2015)

left side of the tributary valley, which is reaching down to the main valley. Eventually, this moraine was cut off by erosive forces of the main glacier tongue and remains as a steep cut till today (c.f. Figure 13). Facing northeast, this moraine section is found on the left side of the valley roughly 2.6 km upstream of the LIA maximum position of the glacier (site B in Figure 14). It was free of ice prior to the 1970s. Today, parts of the moraine are vegetated while most surfaces are uncovered, highly unconsolidated and steep. Susceptible to fluvial and gravitational processes, a system of distinct gullies has formed.

Proceeding further to the current glacier front, at a north facing footslope on the left side of the valley, a moraine complex of roughly 300 m length and a maximum width of ~ 100 m has been equally investigated (c.f. Figure 14, C). Fully covered by the glacial extent of 1922, the moraine was largely disconnected from the glacier by 1971. Despite its exposure several decades ago, remaining dead ice is visible at certain spots within the blocky moraine matrix (c.f. Figure 13). This setting of the moraine conditions high geomorphological activity, especially rockfall, as could be observed in the field.

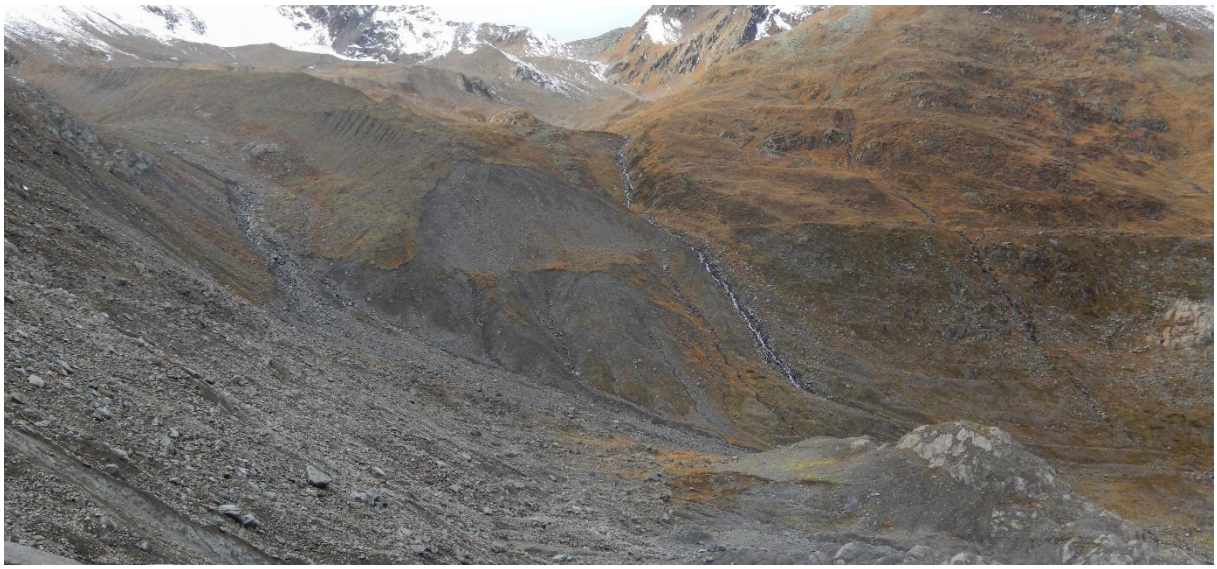

Figure 13: Frontal view of the lateral moraine coming from the *Münchner Abfahrt* into the main valley, where it has been cut off by Gepatschferner glacier. Moraine site C with outcropping ice is visible in the left front (Kamleitner S. 2015)

The lateral moraine of the next investigation site (D in Figure 14) is in comparison rather small (approximately 100 m length and 50 m width) but of very recent exposure. Given their current position, adjacent to the glacier mouth of Gepatschferner in 2015, these sediments were completely covered by ice in 2006 while lowest parts were still influenced by the glacier in 2012. Situated on the right side of the valley, the moraine is orientated to the south. Compared to other moraine sites, the constitutive sediments of this moraine show smaller grain sizes and boulder deposits are less frequent. Analogous to moraine site A and B, gullies and channels have been eroded into the fine grained material, however unevenly smaller. While upvalley, a heavily ice-cored moraine continues (Figure 14, E), no ice is visible at the surface of this lateral moraine.

From all moraine sections described numerous springs of varying discharge are evolving, both perennially and episodically. Anyhow, the hydrological systems of the moraines are not yet fully understood. Relative age dating aims to expand the understanding of the waters origin. More details on the radionuclide ^{129}I which is used for age determination are amplified in the following section.

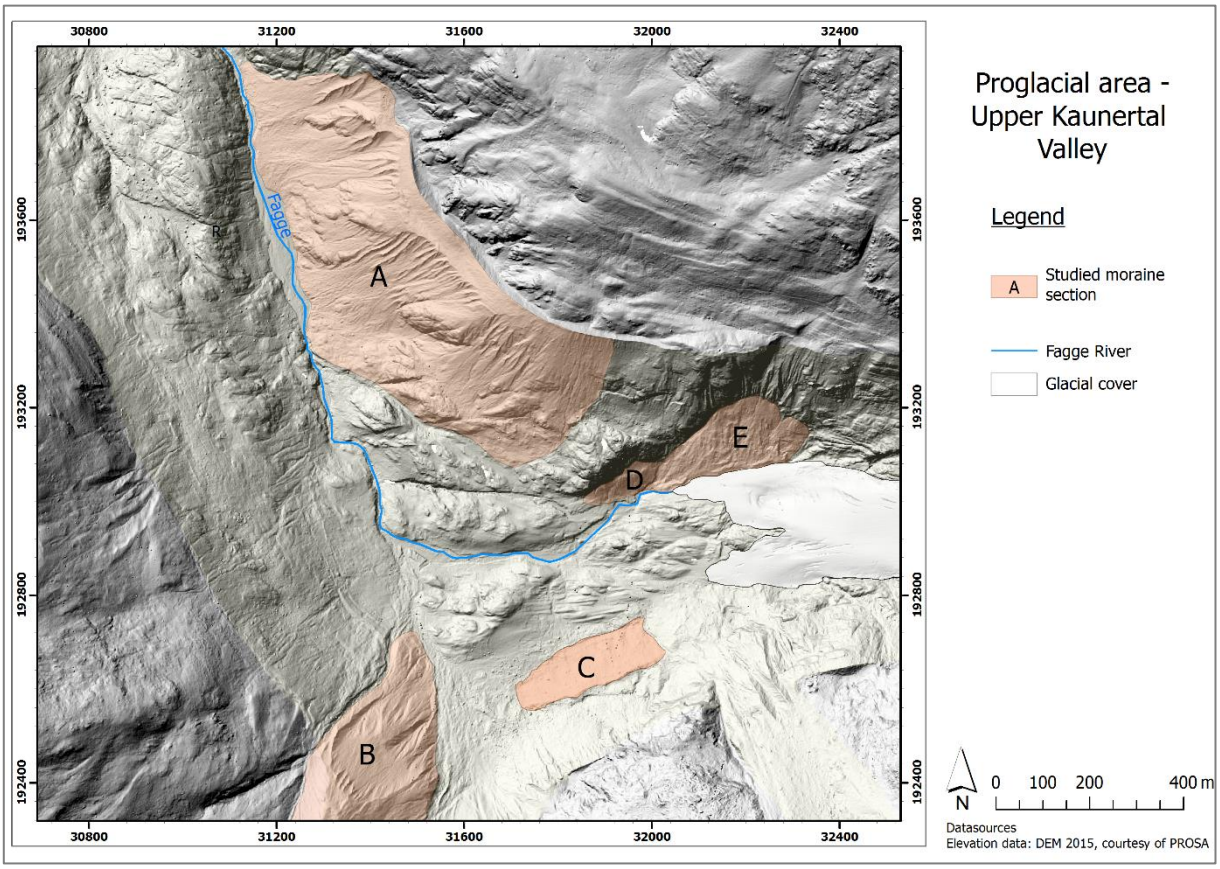

Figure 14: Spatial position of studied moraine sections (A-E) within the proglacial area of Gepatschferner glacier

3 Iodine 129

The present study aims to distinguish the source of ice-fed springs on lateral moraines of Gepatschferner glacier. Whether melt waters originate from seasonal segregation ice or old persisting dead ice shall be answered by testing the applicability of ^{129}I for relative age dating. As being only of recent interest to the scientific community (López-Gutiérrez et al., 2000b), which is even more true when working in a geomorphological context, the character, the natural and anthropogenic production as well as the global transport of ^{129}I are introduced in the following. Subsequently, the applicability of ^{129}I for (relative) age dating is addressed in general and in the distinct setting of the present study.

3.1 What is ^{129}I?

Iodine is member of the halogen group and a geochemically active element (Fehn, 2012). Given its high redox sensitivity and its biophilic nature it forms multiple compounds in natural environments, both organic and inorganic (Hou et al., 2009b). Iodine is characterised through high mobility (Fan et al., 2013) as it quickly transfers in different chemical species and time scales (Jabbar et al., 2013b). It easily moves between surface reservoirs and its natural isotopic composition at the earth surface is homogenous (Fehn et al., 2007a).

Iodine holds several isotopes, stable, long-lived and short-lived ones. ^{129}I is the only long-lived radioisotope of iodine with a half-time life of 15.7 Ma (Atarashi-Andoh et al., 2007). While several other short-lived isotopes of iodine exist (e.g. ^{125}I and ^{131}I) with half-lives just up to sixty days, there is only one stable iodine isotope available in nature, which is iodine 127 (^{127}I). Hence, the isotopic composition of iodine is usually given as the isotopic ratio of $^{129}I/^{127}I$ which is equivalent to $^{129}I/I$ (Fehn et al., 2007a). Contrary to stable ^{127}I, the formation of ^{129}I is defined by two natural paths. Atmospheric interactions of xenon with cosmic ray particles (Michel et al., 2012) and spontaneous fission of uranium in the earth crust and oceans (Jabbar et al., 2011) account for earth's natural ^{129}I reservoir. Anthropogenic nuclear activity represent the third source of ^{129}I and has been most effective in emitting this long-lived radionuclide since the 1950s (Fan et al., 2013). Anthropogenic ^{129}I entering the iodine cycle has substantially and permanently changed the natural isotopic ratio (Suzuki et al., 2006). Pre-anthropogenic isotopic ratios of 10^{-12} (Hou et al., 2010) have been thereby raised three to eight orders of magnitude up to 10^{-4} to date (Hou et al., 2009b).

Anthropogenic production and natural sources of ^{129}I are outlined in more detail in the following section, including their implication for the rise of the isotopic ratios and concentrations of ^{129}I. Subsequently the global circulation of released iodine and its spatial distribution in specific environmental reservoirs is discussed in chapter 3.3.

3.2 Natural production and anthropogenic release of ^{129}I

^{129}I is produced by natural processes as well as by anthropogenic releases since beginning of nuclear-age. The disequilibrium due to human drivers becomes apparent in Figure 15 which at the same time provides a summary of ^{129}I sources discussed in the following.

3.2.1 Natural production

All ^{129}I that was initially formed in the primordial nucleosynthesis has long been decayed to stable xenon 129. However, two major natural production processes addressed in the following, generate continuing steady-state ^{129}I concentrations (Hou et al., 2009b).

(1) Cosmic production

Cosmogenic ^{129}I is generated through the interaction of stable xenon isotopes with high-energy cosmic ray particles in the stratosphere which leads to their spallation. "*The production rate is a function of the flux of cosmic-ray nucleons, average nucleon energy, average cross-sections for ^{129}I production from xenon isotopes, and xenon isotopic abundances"* (Fabryka-Martin, 1984, p. 37). The average production rate of ^{129}I is given as $2.4 \cdot 10^{19}$ atoms per year (at a^{-1}) (Fabryka-Martin, 1984) but due to latitudinal dependence the fallout of ^{129}I by cosmic production varies. Production is about five times greater at a latitude of 45° compared to the equator or poles (Fabryka-Martin et al., 1987).

(2) Fissiogenic production

The second major source of ^{129}I is the production via spontaneous fission of uranium 238 in the lithosphere and oceans (Fabryka-Martin, 1984). Thermal neutron-induced fission of uranium 235 and neutron activation reaction of tellurium isotopes are of minor importance today (Fan et al., 2013; Jabbar et al., 2012b). Iodine produced either way can be mobilised to the "free" iodine inventory by volcanism or rock weathering. Modelling results indicate the exposure of $\sim 4.1 \cdot 10^{18}$ at a^{-1} to the surface from the latter. Fluxes of fissiogenic ^{129}I from volcanic activity were estimated to be as high as $2.5 \cdot 10^{19}$ at a^{-1} and therefore are comparable to cosmic-ray produced ^{129}I (Fabryka-Martin, 1984). Both fissiogenic and cosmic processes contribute to surface reservoirs in similar magnitude (Fehn et al., 2007a) of about 45 %, whereas rock weathering accounts for less than 10 % to the free inventory (Schmidt et al., 1998).

The earth's total natural ^{129}I inventory was estimated to be ~ 50,000 kg (Michel et al., 2012). While the majority is bound within the lithosphere (mainly oceanic sediments and continental sedimentary rocks (Lu et al., 2007)), only a small fraction of ~ 250 kg or less than 0.5 % is available on the surface area of the environment (Hou et al., 2009b). Present in hydrosphere, atmosphere and biosphere, this small portion is described as the free ^{129}I inventory (Fan et al., 2013). Exact numbers regarding the free inventory vary between authors.

Hou et al. (2009b) declares a steady state level of 180 kg for the entire hydrosphere, whereas Snyder et al. (2010) suggests an amount of 130 kg to be marine ^{129}I and another 11 kg to be situated in non-marine hydrosphere. Another 60 kg ^{129}I are believed to be free within the lithosphere (Hou et al., 2009b).

Natural isotopic ratios ($^{129}I/^{127}I$) of the marine environment have been proposed as $1.5 \cdot 10^{-12}$ (Hou et al., 2010) and pre-anthropogenic ^{129}I concentrations are given as $2.0 \cdot 10^{5}$ atoms per Litre (at L^{-1}) (Reithmeier et al., 2005). As on average lakes and rivers have a lower total iodine content, their presumed ^{129}I levels are only roughly $3.7 \cdot 10^{4}$ at L^{-1} (Snyder et al., 2010). The pre-nuclear isotopic ratios in the terrestrial system might differ from those of the marine compartment (Hou et al., 2010), but reliable initial values for the terrestrial environment are missing (Fan et al., 2013). Reported ratios differ crucially from $5 \cdot 10^{-12}$ to $1 \cdot 10^{-9}$ (Hou et al., 2010). Thus, the existing data base for pre-anthropogenic ^{129}I concentrations in atmosphere and biosphere remains inconsistent and incomplete (Schmidt et al., 1998).

Natural ^{129}I production and consequent pre-nuclear isotopic ratios and concentrations have been dramatically altered since the early 1940s (Aldahan et al., 2009). By now, the anthropogenic inventory of ^{129}I exceeds the natural abundance by several thousands of kilograms (Hou et al., 2009b). The main drivers responsible for the enlargement are outlined below.

3.2.2 Anthropogenic releases

Anthropogenic ^{129}I production was started with human-caused nuclear fission processes such as nuclear weapon tests (A). High quantities of ^{129}I are produced in nuclear power plants (B). Nuclear incidents (e.g. Chernobyl accident) (C) further enhanced concentration levels. However, reprocessing of spent fuel (D) from nuclear plants is by far the major source of present ^{129}I. Anthropogenic multiplication of the natural iodine inventory is exemplified in Figure 15.

(A) Nuclear weapon tests

Analogous to other anthropogenic radionuclides, testing of nuclear weapons initially was the primary source of anthropogenic ^{129}I (Snyder and Fehn, 2004). Atmospheric and underground nuclear weapon tests, executed between 1945 and 1975, released significant amounts of ^{129}I into the environment. Explosions of nuclear devices produced detectable amounts of ^{129}I as a consequence of neutron-induced fission of uranium 235 and plutonium 239 (Hou et al., 2009b). Concrete numbers vary, as uncertainties on the total fission yield of the explosions exist. Estimations range between 50 to 150 kg ^{129}I that have been introduced into the stratosphere by aboveground testing (Atarashi-Andoh et al., 2007). Meanwhile, releases from underground testing remain below ground (Zhou et al., 2013). The injection of ^{129}I into the stratosphere becomes especially relevant, as it allows for a long residence time, good mixing and large scale fallout of ^{129}I (Hou et al., 2009b). An elevated ^{129}I signal due to nuclear weapon tests can therefore be found around the globe, even in

remote locations (Schmidt et al., 1998). This is particularly true for the Northern hemisphere. Isotopic ratios have been raised from natural levels to between 10^{-11} and 10^{-10} and 10^{-11} and 10^{-9} respectively for marine and terrestrial environments (Hou et al., 2009b). The termination of the US American and Soviet above ground tests in 1962 (Reithmeier et al., 2010) and the successive nuclear test ban treaty in the following year marked the end of the nuclear weapon test era. Concentration levels of most radioisotopes elevated during this time have returned roughly to pre-bomb concentrations by today (e.g. ^{36}Cl) (Snyder and Fehn, 2004). Due to its long half-life time and ongoing emission this does not apply for ^{129}I. Its concentration is still increasing and values raised by nuclear tests have to be considered as today's background level (Fan et al., 2013).

(B) Nuclear power reactor

Following the nuclear test ban, the civilian use of nuclear energy became the major (anthropogenic) source of ^{129}I (Atarashi-Andoh et al., 2007). By fission of plutonium 239 and uranium 235 routine operation of nuclear power plants generates large quantities of ^{129}I (Schmidt et al., 1998). An amount of 68,000 kg ^{129}I was estimated to have been produced up to 2005 (Hou et al., 2009b). The majority is kept in encased spent fuel to prohibit gaseous releases in the environment. Emissions of ^{129}I into the environment are hence negligible and no significant ^{129}I accumulation could be found in the vicinity of nuclear reactors (Hou et al., 2009b).

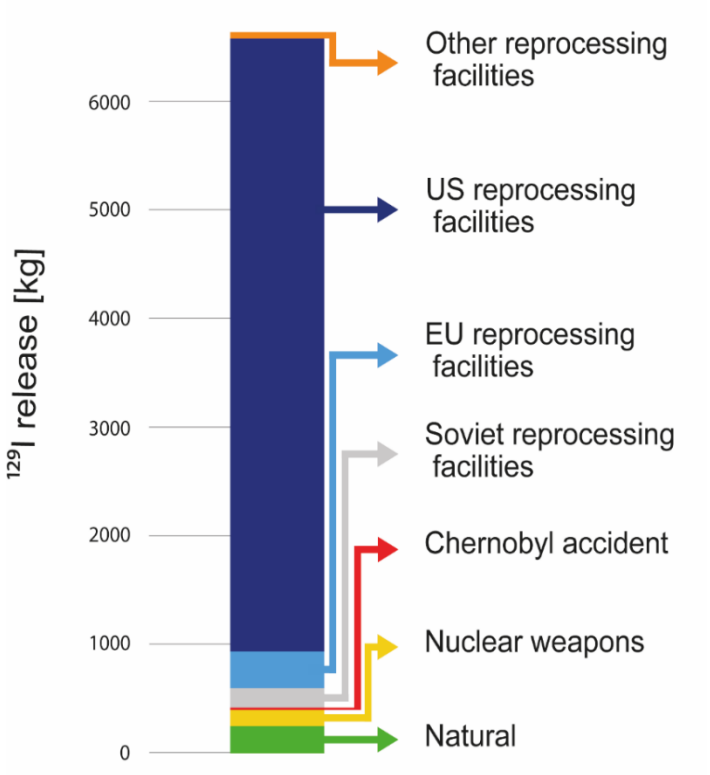

Figure 15: Natural ^{129}I content in comparison to anthropogenic release of ^{129}I after Jabbar (2012)

(C) Nuclear accidents

In addition to unintentional releases from nuclear power plants, nuclear accidents also emit small amounts of ^{129}I into the environment. Other than the incidents in Windscale (1957), and most recently Fukushima (2011), the reactor accident in Chernobyl in 1986 is most prominent. Estimated ^{129}I releases from Chernobyl range between 1.3 to 6 kg (Zhou et al., 2013), but affect a relatively small area (Schmidt et al., 1998). Nevertheless, they dominate the ^{129}I inventory in regions of Ukraine and Belarus (Reithmeier et al., 2005). On a broader scale, releases from nuclear accidents remain insignificant compared to total emission of reprocessing facilities of the Northern hemisphere (cf. Figure 15) (Snyder et al., 2010).

(D) Nuclear reprocessing

^{129}I is a by-product of routine operation of nuclear power plants and is kept in fuel elements. Reprocessing of this spent fuel mainly happens through PUREX (plutonium-uranium recovery by extraction) process which discharges formerly captured ^{129}I into the environment. During dissolution of the fuel with nitric acid, most iodine oxidises to I_2, which is volatile and consequently escapes the solution. Parts of released ^{129}I may then be trapped, stored or released into the environment, whereas others may be released aerially (Hou et al., 2009b). Consequently, ^{129}I is discharged directly into hydrosphere (ocean or rivers) and/or atmosphere, as nuclear reprocessing facilities (NRF) are operating (Persson et al., 2007). Both liquid and gaseous releases are pronounced and (civil) nuclear reprocessing represents the major source for anthropogenic ^{129}I today (Aldahan et al., 2009; Hou et al., 2009b; Michel et al., 2012; Reithmeier et al., 2005; Snyder et al., 2010; Zhou et al., 2013).

Even though several thousand kilograms of ^{129}I have been discharged since the early 1940s (cf. Figure 15) (Snyder et al., 2010), only a limited number of nuclear reprocessing facilities exists worldwide. Environmental ^{129}I releases are therefore perceived as point sources. As such they are mainly located in the Northern hemisphere, accounting for 99.8 % of all ^{129}I emitted by reprocessing. One does not find facilities with comparable releases, south of the equator. The facilities at Ezeiza, Argentina and Pelindaba, South Africa possibly ejected as much as 7 kg and 1 kg of ^{129}I (Snyder et al., 2010). Release numbers are therewith approximately in the range of the Chernobyl accident and are not considered by most authors. However, former and continuing releases from Soviet, US American and in particular European reprocessing are tremendously higher:

a) Soviet reprocessing facilities

Former reprocessing facilities of the Soviet military may represent major sources of ^{129}I for the Asian subcontinent and also Northern and Eastern Europe. Decommissioned in 1995, ^{129}I releases are still unknown as data remains unpublished till today (Reithmeier et al., 2010). The discharge during the operation time of the three soviet facilities can therefore only be roughly estimated. Reithmeier (2005) first approached aerial releases of Mayak (also known as Chelyabinsk-40 and -65), Seversk (Tomsk-7) and

Zheleznogorsk (Krasnoyarsk-26) based on quantities of produced plutonium. Estimations indicate that relevant amounts of 138 kg, 18 kg and 23 kg ^{129}I have been released to atmosphere by all three NRFs (Snyder et al., 2010). Approximations for liquid emissions e.g. into the Ob River (Reithmeier et al., 2010) have not been considered so far.

b) US American reprocessing facilities

The main US reprocessing sites are Savannah River (South Carolina) and Hanford (Washington). While the latter was finally decommissioned in 1988, the facility Savannah River is still operating. Past ^{129}I releases can only be estimated based on plutonium production rates as again little information is available (Reithmeier et al., 2010). It is estimated that 260 kg of ^{129}I has been discharged by the Hanford site during its primary operation (1944 to 1972) and another 14 kg during resumed operation (1983 to 1988) (Hou et al., 2009b). Peak emission occurred until the early 1950s when gaseous releases were not filtered (Schnabel et al., 2001). While the activity of the spent fuel is comparable, the airborne discharge of the Savannah River site is expected to be lower because of modern iodine filters utilised (Reithmeier et al., 2010). From 1951 up to the year 1990 Hu et al. (2010) state airborne releases of about 32 kg. Although releases of both sites happened mainly into the atmosphere (Hou et al., 2009b), raised ^{129}I signals have been observed in the drainage of the Savannah and Columbia rivers (Hoehn et al., 1999). In addition to Savannah River and Hanford, the former reprocessing sites of West Valley (New York) and Idaho Falls (Idaho) did release ~ 34 kg ^{129}I during their operation (Snyder et al., 2010).

c) European reprocessing facilities

Among all nuclear reprocessing facilities, the European ones are the most extensive sources of ^{129}I. More than 90 % of the total (anthropogenic) iodine inventory is contributed by them (Fan et al., 2013). The tremendous European releases arise mainly from two large nuclear fuel reprocessing plants: La Hague (France) and Sellafield (United Kingdom), both located at the coasts of Western Europe (Aldahan et al., 2009). In contrast to US American or Soviet facilities, more comprehensive release data is available for La Hague and Sellafield. The operation of the NRFs and with it the emission of ^{129}I started in 1951 (Sellafield) and 1966 (La Hague) and continues to date (Jabbar et al., 2012b). The majority of the releases are marine, ~ 85 % and ~ 97 % for Sellafield and La Hague respectively. Comparatively small amounts are emitted into the atmosphere (Michel et al., 2012). Up to the year 2007, the La Hague NRF was solely responsible for the release of 3,800 kg liquid ^{129}I into the English Channel and emitted 75 kg of gaseous ^{129}I into the atmosphere. Another 1,400 kg has been discharged into the marine environment of the Irish Sea by the Sellafield site. At the same time, 180 kg has been released into the air. ^{129}I concentrations in the English Channel, the Irish Sea and connected marine environments have significantly been raised as a consequence

(Hou et al., 2009b). Pre-nuclear concentrations of the ocean mixed-layer of $2 \cdot 10^5$ at L^{-1} increased to $\sim 7 \cdot 10^8$ at L^{-1} (Reithmeier et al., 2010) and $^{129}I/^{127}I$ isotopic ratios advanced from pre-nuclear values up to 10^{-8} to 10^{-5} (Hou et al., 2009a).

In addition, the former facility of Marcoule (France) released comparable gaseous amounts into the atmosphere, about 145 kg ^{129}I (Hou et al., 2009b) during its operation between 1957 and 1997 (Jabbar et al., 2012b). Liquid discharge into the Rhone River and consequently into the Mediterranean Sea (Michel et al., 2012) has been relatively smaller (45 kg) (Hou et al., 2009b). However, isotopic ratios measured close to the Rhone estuary reached up to $5 \cdot 10^{-7}$ (Jabbar et al., 2012b). In order to complete the study, the existence of minor European reprocessing plants such as the former NRF in Karlsruhe (Germany) with minimal releases of 1.1 kg ^{129}I (Hou et al., 2009b) are mentioned but are not considered relevant for global ^{129}I stock (Reithmeier et al., 2010).

d) Other reprocessing facilities

A few smaller NRFs exist outside of today's Russia, the US or Europe. Most of them are still operating. In addition to previously mentioned locations in Argentina and South Africa, reprocessing facilities in China (Guangyang), Japan (Tokai Mura), Pakistan (Kahuta), India (Bhaba, Trombay) and Israel (Dimona) raise the ^{129}I inventory. Though, estimated overall releases are less than 48 kg (Snyder et al., 2010).

As a consequence of ongoing emissions and its long half-life, ^{129}I is continuously accumulating in the environment (Atarashi-Andoh et al., 2007). The global dimension of ^{129}I deposition fluxes calculated by Reithmeier et al. (2010) is mapped in Figure 16. Displayed deposition maxima of the Northern hemisphere are obvious and linked to airborne releases of former Soviet, US-American and European reprocessing sites. Compared to global background deposition they are raised by up to two orders of magnitude. The Southern hemisphere is almost independent of Northern hemisphere emissions. The regular accumulation

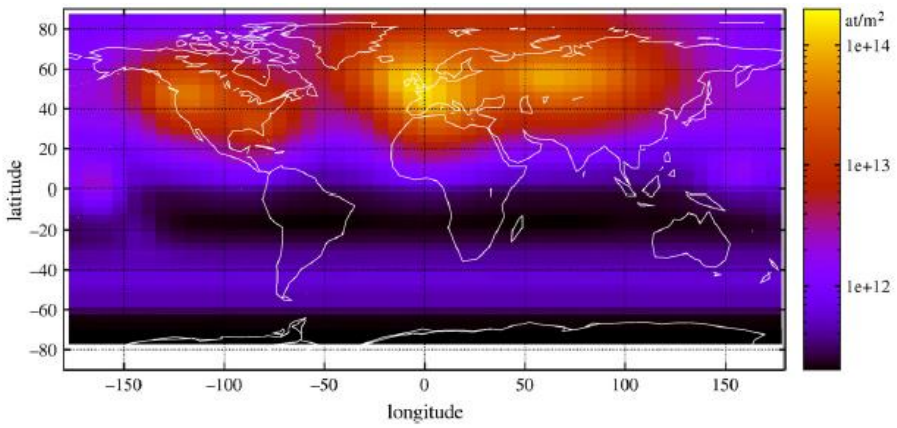

Figure 16: Calculated mean global deposition fluences of anthropogenic ^{129}I (at per m²) up to and including 2004 (Reithmeier et al., 2010)

pattern south of the equator clearly originates from the latitudinal dependence of stratospheric bomb fallout, which remains the dominate influence. The calculated ^{129}I fluences of the Southern hemisphere can be seen as today's global background deposition (Reithmeier et al., 2010).

Regardless of past emissions, anthropogenic increases of the ^{129}I inventory continue unabated. The main part of ^{129}I (an estimated amount of ~ 70,000 kg (Aldahan et al., 2009)) produced in nuclear reactors worldwide is stored in unprocessed nuclear fuel pending future reprocessing (Aldahan et al., 2009; Hou et al., 2009b). Variable sources and releases have, over time, led to a strongly inhomogeneous spatial distribution of ^{129}I. The huge emissions of La Hague and Sellafield in particular are the major drivers of the global ^{129}I variability. Accordingly, European ^{129}I concentration is 1000 times greater, compared to North America (c.f. Figure 17) (Aldahan et al., 2009). A disequilibrium for anthropogenic ^{129}I between atmosphere, hydrosphere and biosphere has been caused (Schmidt et al., 1998). Transport from anthropogenic and natural ^{129}I sources between the spheres to possible sinks and consequential concentrations of different surface reservoirs are discussed in the following.

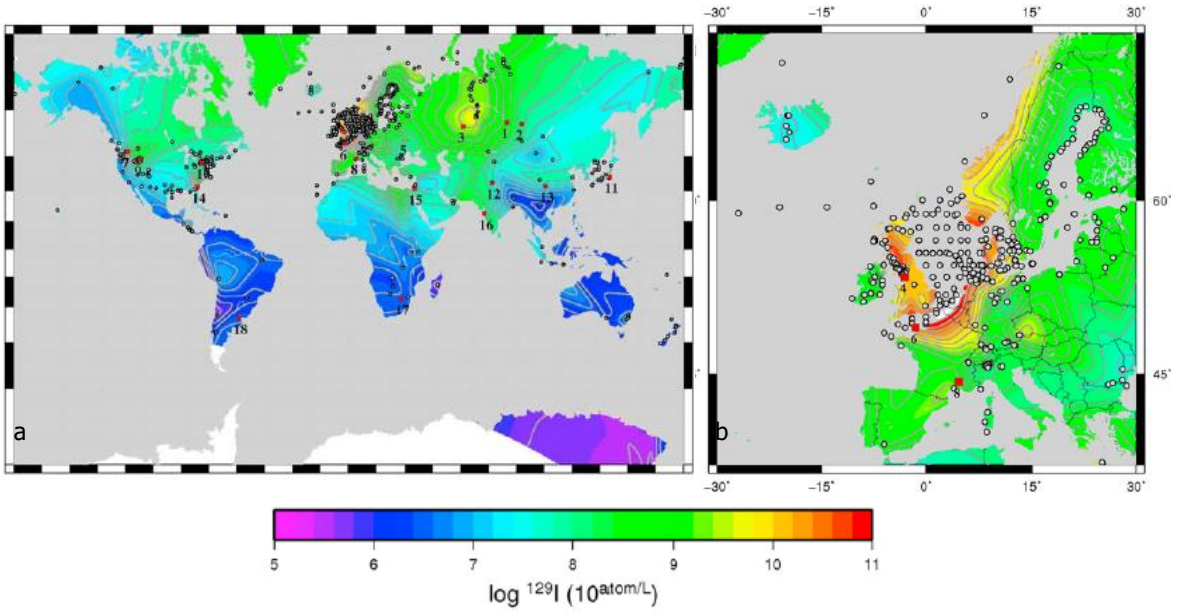

Figure 17: Distribution of ^{129}I globally (a) and on a regional scale for Europe (b). White circles represent sampling sites, red squares indicate nuclear reprocessing facilities (Snyder et al., 2010)

3.3 Transport of ^{129}I between sources and sinks within a global iodine cycle

The first global iodine cycle was describe by Kocher (1981) and extended by Fabryka-Martin, (1984) and Liu and v. Gunten (1988) (Wagner et al., 1996). The first iodine model was presented 35 years ago, yet little is known of ^{129}I pathways (Jabbar et al., 2012b) and several questions remain (Persson et al., 2007). Provided that total mixing, a steady state and no fractioning occur between ^{127}I and ^{129}I, general assumptions made for the stable iodine model

can also be assigned to ^{129}I in order to derive its environmental distribution (Fabryka-Martin, 1984). Especially as ^{129}I is believed to act similar to stable ^{127}I over long time periods (Muramatsu et al., 2004). The exchange of volatile iodine between all surface compartments is much faster than natural ^{129}I production. Initial iodine in atmosphere, biosphere and hydrosphere must have been well mixed, identical and in a natural equilibrium (Fehn et al., 2007a; Reithmeier et al., 2006). However, this natural balance has substantially been disturbed by human interferences as anthropogenic ^{129}I releases into the surface outstretched natural production (Fehn et al., 2007a). Anthropogenic ^{129}I caused a lack of equilibrium for surface reservoirs, at least north of the equator (Buraglio et al., 2001). It is easily detectable in waters anywhere in the Northern hemisphere (Hoehn et al., 1999) and has been marked even in remote background zones such as Antarctica (Snyder and Fehn, 2004). Oceanic discharge and gaseous releases into the atmosphere are the two main pathways of anthropogenic ^{129}I entering the environment (Buraglio et al., 2001). Based on these, transport between different surface reservoirs and the processes involved are examined in the following passages, using current knowledge and focusing on the European continent.

Oceans are the major reservoir for ^{129}I (Fehn et al., 2007a). The residence time of iodine in seawater of ~ 300,000 years in comparison with an oceanic turn-over time of only ~ 1,000 years should theoretically condition a homogenous marine ^{129}I content and a homogenous $^{129}I/^{127}I$ ratio, independent of crustal input and latitudinal differences in cosmic ray production (Snyder et al., 2010). Today liquid emissions, mainly from the NRFs of La Hague and Sellafield into the English Channel and Irish Sea, dominate the marine ^{129}I stock (Aldahan et al., 2009). Originating from these two point sources, emitted ^{129}I is transported by the Gulf Stream to the North Sea and further transferred along the Norwegian coast to the Barents Sea (Reithmeier et al., 2010) and the Greenland Sea to the North Atlantic (c.f. Figure 18) (Snyder et al., 2010). During the water mass transport processes, the initial ^{129}I signal is progressively being diluted as water masses of North Sea and North Atlantic act as buffer reservoirs, as can be seen in decreasing ^{129}I concentrations in Figure 18 (Christl et al., 2015). Nonetheless, elevated ^{129}I concentrations have been observed in the English Channel, the Irish Sea, the North Sea and the Norwegian Sea. Enhancements of these areas range in the order of four to five magnitudes compared to marine background zones that did not experience any direct exposure to oceanic emissions from nuclear reprocessing (Hou et al., 2009a). Highest ^{129}I concentrations have been traced downstream of La Hague, while lowest concentrations have been documented in the northern part of the central North Sea. This is due to the diluting effect of Atlantic water, which is flowing into this region and is relatively poor in anthropogenic radionuclides (Christl et al., 2015).

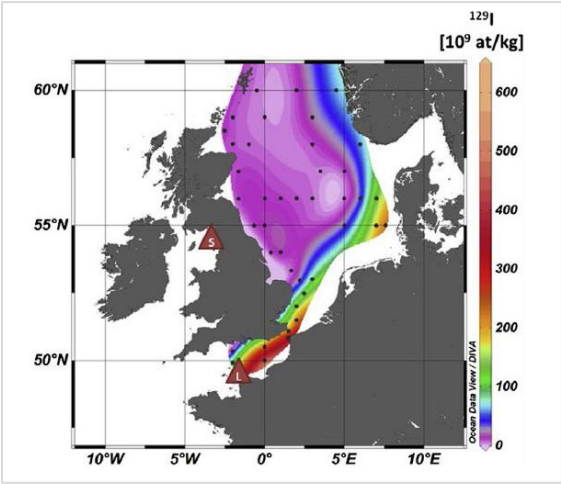

Figure 18: ^{129}I concentration (10^9 at kg^{-1}) of marine surface waters in the vicinity of NRF Sellafield (S) and La Hague (L) (Christl et al., 2015)

Neither the shallow nor the deep ocean is in equilibrium regarding ^{129}I. These disparities are fortified by continuing input from local point sources. Despite existing heterogeneities, the average global ^{129}I concentration for the shallow marine reservoir was estimated as $1 \cdot 10^9$ at L^{-1}, a value that would still exceed the pre-nuclear concentration by more than 3 orders of magnitude (Snyder et al., 2010). With respect to the shallow ocean reservoir, North Atlantic down welling is a major sink for ^{129}I as large amounts of iodine are transported from shallow to deep marine waters. They are carried by the thermohaline circulation for roughly 2,500 years before eventually emerging again in the Pacific Ocean. As the major European ^{129}I emitters, La Hague and Sellafield are incidentally located in the vicinity of the North Atlantic down welling. This represent a most efficient removal mechanism. A ^{129}I down welling flux of 60 kg a^{-1} has been reported which equals about 50 % of the combined annual discharge from Sellafield and La Hague. In contrast, ^{129}I released into shallow oceans far away from any down welling, as is the case with Asian sources, is expected to remain for some time. The only immediately effective sink in this case would be the atmosphere or marine particle scavenging (Snyder et al., 2010). The flux of the latter has been proposed as 2.3 kg a^{-1} (Snyder et al., 2010). Apart from scavenging and down welling in the North Atlantic, Snyder et al. (2010) proposed that another 56 kg ^{129}I per year must be transferred from shallow ocean to deep waters. With increasing depth, a general decrease of anthropogenic ^{129}I has been reported (Muramatsu et al., 2004). In combination with the much larger volume of the deep ocean, this should theoretically result in a lower current mean concentration of $1 \cdot 10^7$ at L^{-1} for the deep sea reservoir (even after the addition of 2,800 kg anthropogenic ^{129}I to the naturally present 126 kg). Recently discharged ^{129}I did not have time to spread evenly in the deep sea reservoir yet and bottom water circulation is not believed to have carried anthropogenic ^{129}I as yet. Upwelling in the Pacific Ocean therefore still preserves pre-nuclear concentrations of $4 \cdot 10^5$ at ^{129}I L^{-1} (Snyder et al., 2010).

In addition to intermediate-termed shallow-to-deep-water-sink, ^{129}I is primarily removed from active circulation within the hydrosphere by marine sedimentation. Assuming a mean sedimentation rate of ~ 0.25 cm per 1000 years, Fabryka-Martin (1984) suggested a net iodine removal of $7 \cdot 10^7$ kg a^{-1}. Snyder et al. (2010) calculated the marine net sedimentation for ^{129}I specifically to be 2.4 kg a^{-1}. However, iodine deposited on the sea floor cycles back into hydrosphere via several long pathways (Fabryka-Martin, 1984). As soon as iodine bearing organic matter reaches the sea floor, a large part of it undergoes diagenesis in the layer of bioturbation. Microbiological activity within this zone breaks up organic molecules and iodine is released to pore fluids. Iodine then quickly cycles back into the water column and remains in the pool. Still, up to 10 % of organic material does not undergo bioturbation. A minor but significant portion of iodine is consequently buried (Fehn et al., 2007a). Moving on into deeper sediment sequences, gravitational compaction might force out iodine-rich pore fluids. Estimations suggest that diagenesis could return roughly 85 % of iodine stored in marine formations back to hydrospheric circulation (Fabryka-Martin, 1984). The estimated time scale for transfer, deposition and diagenesis of organic matter ranges between several ten thousands to millions of years (Snyder et al., 2010). Once incorporated within the lithosphere, recycling of iodine back to the hydrosphere might occur via several pathways. These include leaching of sediments by ground water, weathering of uplifted

and exposed sediments, removal by sea-floor spreading, recycling in subduction zones and volcanic ejection along convergent zones. These processes gain relevance within a time scale of several millions of years (Fabryka-Martin, 1984).

From the perspective of marine iodine circulation, the atmosphere represents a clearly more immediate sink for iodine, in comparison to down welling and marine sedimentation. The ocean is the dominant source for iodine in the atmosphere and consequently also the terrestrial environment (Jabbar et al., 2011). Likewise most global iodine models describe aerial iodine as primarily originating from marine iodine (Szidat et al., 2000). Transfer of iodine into the troposphere is expected to happen through marine volatilization at the sea surface (Snyder et al., 2010) - a pathway where a dilution of ^{129}I with stable iodine is assumed to occur (Szidat et al., 2000). The total iodine flux from ocean to atmosphere is given as 240,000 t a^{-1} (Jabbar et al., 2013b) but depends on several parameters such as solar radiation, water temperature, water chemistry, water depth, spatial location, currents, waves, tides, biological activity, etc. (Aldahan et al., 2009). Iodine is thought to enter the troposphere mainly as methyl iodine (CH_3I) or other alkyl iodides (Hou et al., 2009a). Transfer through photochemical oxidation or through reaction with free ozone have also been suggested (Jabbar et al., 2013b) as well as molecular iodine (I_2) emissions from macro algae, especially during aerial exposure (Hou et al., 2009a). Only small amounts (0.3 %) of the ocean's surface ^{129}I inventory are affected by annual re-emission (Reithmeier et al., 2006). Nonetheless, a ^{129}I ocean-to-atmosphere-flux of 6.9 kg a^{-1} (Snyder et al., 2010) is comparable to annual gaseous emission of La Hague and Sellafield (Reithmeier et al., 2010). This means that liquid anthropogenic releases indirectly increase atmospheric ^{129}I concentrations via re-emission from oceanic surfaces (Reithmeier et al., 2006). However, transfer mechanisms are not entirely understood (Aldahan et al., 2009).

Other than marine re-emission, atmospheric ^{129}I can have several other sources. In any case, direct gaseous releases from nuclear reprocessing are one of them (Jabbar et al., 2013b). Indeed roughly 99 % of Europe's ^{129}I is released in liquid form, gaseous emissions are miniscule, yet they are believed to be the major source for European precipitation (Reithmeier et al., 2006). ^{129}I releases from La Hague and Sellafield are assumed to happen in the form of methyl iodine, which is fairly inert and stable and may therefore be transported on a global scale (Jabbar et al., 2011). Additionally, the effects of gaseous emissions are much more immediate because air's iodine content is more than three orders of magnitude smaller compared to the oceans (Szidat et al., 2000). ^{129}I emissions from the terrestrial environment including vegetation and soil may add to the atmospheres inventory. Some authors consider the input of the terrestrial pool to be of low importance (Reithmeier et al., 2010), while others suggest it to be of significance (Jabbar et al., 2013b). Snyder et al. (2010) estimates a comparatively little terrestrial flux through microbial volatilization and leaching of only 0.4 kg a^{-1} to the atmosphere. At this point, the input of cosmic-ray produced ^{129}I must also be mentioned. Facing average cosmic production rates of $2.4 \cdot 10^{19}$ at a^{-1} (Fabryka-Martin, 1984), an annual flux from this source should add up to roughly 0.5 kg a^{-1}. Regardless of its source of origin, once in the atmosphere, ^{129}I may be widely transported (Snyder and Fehn, 2004).

Air represents one of the key media within iodine cycling, especially regarding iodine species conversion and iodine transfer from the ocean to the terrestrial environment (Buraglio et al., 2001). Iodine transport in the atmosphere is a dynamic process (Hou et al., 2009a) depending on iodine's chemical speciation (Krupp and Aumann, 1999). During complex cycling within the troposphere, the reactive character of iodine might lead to the formation of iodine oxides through photolysis or the reaction with volatile active radicals (e.g. ozone) (Jabbar et al., 2011). Iodine in air consequently exists in multiple forms (Aldahan et al., 2009). Its atmospheric residence time therefore varies between eight days to just a few weeks (Snyder et al., 2010). Retention times of 10, 14 or 18 days are estimated for transfer of iodine's major atmospheric forms: inorganic gaseous iodine, iodine associated with aerosols or organic gaseous iodine (Hou et al., 2009a). This is rather short when compared to other nuclides, for example ^{14}C which has an atmospheric residence time of 10 years (Jabbar et al., 2013b). Short retention times suggest the majority of iodine released is returned to marine or terrestrial environments shortly thereafter (Snyder et al., 2010). However, when present in gaseous form (e.g. CH_3I), substantial mixing and transport of atmospheric iodine may still happen on a global scale (Hou et al., 2009a; Jabbar et al., 2011, 2013b). Despite iodine's ability to be transported long distances, global dispersion of ^{129}I and equilibration with its stable counterpart ^{127}I has not happened yet because point sourced emitted anthropogenic ^{129}I enters the global iodine cycle fairly slowly and its re-deposition occurs predominantly on a local scale (Jabbar et al., 2013b). Correspondingly, ^{129}I levels in the atmosphere were found to decrease exponentially with increasing distance from NRFs. Studies of Savannah River site further show that about 42 % of gaseous ^{129}I releases quickly attach to aerosol and consequently accumulate in the surroundings of the reprocessing plant. The residual amount of ^{129}I may experience long-distance transport (Jabbar et al., 2013b). Due to its long half-life, ^{129}I does not dissipate during atmospheric cycling and enters the terrestrial environment via precipitation (Jabbar et al., 2011).

Precipitation is the main source of iodine for the terrestrial reservoirs (Persson et al., 2007). It directly originates from the atmosphere and determines continental iodine concentrations and availability (Gilfedder et al., 2007), even in remote background areas (Reithmeier et al., 2010). Through the transfer of air masses from the oceans to the continents (e.g. via westerly winds), iodine may be transported in wet (clouds, moisture) or dry form (aerosols, gaseous) (Aldahan et al., 2009). Either way, 70 % of the iodine flux from ocean to atmosphere is re-deposited into the sea. The remaining 30 % may be distributed on land (Jabbar et al., 2013b). Deposition of iodine to the terrestrial surface may occur in dry (aerosol sedimentation and gas absorption) and wet precipitation (Aldahan et al., 2009; Jabbar et al., 2012b; Leeuwen, 1995). However, data on which form dominates vary, but is thought to depend on chemistry, particle size distribution, aerosol type and meteorological conditions (Jabbar et al., 2012b). Condensation of gaseous iodine in the atmosphere leads to the formation of new aerosols or to the growth of existing ones (Gilfedder et al., 2007). Further, water-soluble iodine species, e.g. elemental iodine, iodate, iodide, may absorb into aerosol or are contained in rain droplets or snow directly (Jabbar et al., 2013b). Likewise, aerosols may be easily captured in rain. The iodine of the particulate matter is leached to the water droplet and transforming into soluble iodine forms

(Hou et al., 2009a). Within this processes, inorganic iodine is more likely to be deposited, compared to organic compounds because of their higher water-solubility (Jabbar et al., 2013b). Concerning wet deposition, two types of scavenging are differentiated. Firstly, the processes of in-cloud scavenging (rain-out) where aerosols or gases are scavenged by cloud droplets directly in the cloud and are removed during the next rainfall. Secondly, the process of below-cloud scavenging (wash-out) where aerosols or gases are absorbed beneath the clouds by falling raindrops (Leeuwen, 1995). Nevertheless, it is still not fully understood how iodine is incorporated into rain droplets (Hou et al., 2009a) and even less known for snow (Gilfedder et al., 2007). Also, it remains uncertain what process of wet deposition applies for iodine (Aldahan et al., 2009). Nonetheless, an annual ^{129}I fallout of roughly 2.5 kg a^{-1} was calculated to result from precipitation over Europe. This is equivalent to one third of Europe's gaseous emissions but less than 1 % of its total releases (Persson et al., 2007). ^{129}I concentrations in precipitation from Europe range between 10^8 and 10^{10} at kg^{-1}, but usually lie above 10^9 at kg^{-1} (López-Gutiérrez et al., 2000a). Whether gaseous releases or marine re-emission of liquid discharge reflect the major source of precipitation in Europe is controversial. The dominating source may be a question of spatial location and temporal variations (Persson et al., 2007). Some studies have proven that aerosols in Vienna and precipitation of Central Europe are in good agreement with gaseous ^{129}I emissions from Sellafield and La Hague. Others claim liquid re-emissions as the dominant ^{129}I source in precipitation in Denmark (Hou et al., 2009a). Although spatial differences in ^{129}I contents of precipitation exist, a clear dependence on latitude is missing (Persson et al., 2007). Furthermore, due to conflicting results, a simple relation between decreasing ^{129}I levels with increasing distance from the sea is more and more doubted (Gilfedder et al., 2007). One explanation for varying concentrations observed in precipitation over Europe may be related to different sources of precipitation or moisture, e.g. West Atlantic, North Sea, North Atlantic (Buraglio et al., 2001). Also the alteration of iodine contents due to vertical transfer (Jabbar et al., 2012b) or orographic lifting (Gilfedder et al., 2007) were discussed.

^{127}I and ^{129}I which is dispersed on the terrestrial surface by dry or wet precipitation is transported into surface waters, intruding ground waters, cumulating in soils and incorporated into the biosphere. Anthropogenic ^{129}I values have been reported multiple times for stream waters in Europe, the US and the Southern hemisphere (Jabbar et al., 2013b). Likewise an inventory of 150 kg anthropogenic ^{129}I was calculated for European shallow soils at maximum depths of 50 cm, given an assumed ^{129}I concentration of $3 \cdot 10^5$ at kg^{-1}. Studies have further shown that "*soils , especially if of high organic matter content, are critically important for the storage of ^{129}I*" (Herod et al., 2016, p. 1220) and storage capacity seems to relate to soil organic matter content (Herod et al., 2016). In total, a value of 385 kg has been estimated for global anthropogenic ^{129}I yield in soils (Snyder et al., 2010). The flux of sedimentation on land was further estimated to be 7.7 kg a^{-1}, which is low when compared to the combined emission rate of Sellafield and La Hague of roughly 100 kg a^{-1} (Snyder et al., 2010). While the accumulation of iodine bound to organic matter in soils and terrestrial sediments represents a more effective sink, the freshwater system might only provide a temporary storage for iodine on its way to the marine system, hence closing the cycle of iodine.

In spite of the presented findings, knowledge on transport mechanisms and pathways of ^{129}I is vague and fairly incomplete (Jabbar et al., 2012; Persson et al., 2007). The combination of complex iodine chemistry and behaviour together with insufficient data (Aldahan et al., 2009, 2007) and an absence of systematic analysis (Jabbar et al., 2013b) leaves several questions of iodine circulation unanswered (e.g. sea-land transfer, metrological conditions, importance of liquid and gaseous emissions, etc.). Based on this, drawing conclusions is challenging. There is a crucial need to answer these question and to extend the knowledge about ^{129}I and its global pathways (Aldahan et al., 2009).

3.4 Application of ^{129}I for relative age dating

The long-lived and highly mobile nature of ^{129}I (Fan et al., 2013), detailed in the previous sections, together with its propensity to remain in liquid phase (Lu et al., 2007) and its sorb negligibility on most rocks or minerals (Fabryka-Martin, 1984) allows for a wide range of application within environmental and geological science (Fan et al., 2013). Interest in ^{129}I has increased recently (Jabbar et al., 2011) and related research is experiencing enhanced popularity (Fan et al., 2013).

Implementation of ^{129}I spans various fields being used in environmental & atmospheric research, geology (Fan et al., 2013, p. 201), hydrogeology (Atarashi-Andoh et al., 2007), hydrology (Fabryka-Martin et al., 1987), oceanography and nuclear waste management (Hou et al., 2009b). Within these fields, the isotopic system of iodine has been used for tracing as well as absolute age determination (Fehn et al., 2007b). Proposed for dating as early as 1962 (Fan et al., 2013), iodine dating has received increasing attention lately. It is based on the radioactive decay of cosmogenic ^{129}I and the consequent decline of the initial $^{129}I/I$ ratio within a closed system (Jabbar et al., 2013a). Given the long half-life of ^{129}I (15.7 Ma) $^{129}I/I$ dating is able to cover a major geological period (Fehn et al., 2007a) within a range of 3 to 80 Ma (Fan et al., 2013). This dating limit clearly exceeds those of radiocarbon dating (Jabbar et al., 2013a). Application of $^{129}I/I$ dating has been successful in numerous geological settings to date and meaningful dating results have been gained for e.g. brines, geothermal fluids, sediments (Fehn et al., 2007a), or salt domes. However, most reports focus on marine systems due to lower iodine contents and the uncertainty of the initial $^{129}I/I$ ratio in terrestrial materials (Jabbar et al., 2013a). For the sake of completeness, also I/Xe chronometer must be briefly mentioned. With this method, the radioactive decay of ^{129}I to its daughter nuclei ^{129}Xe and its consequent ratio to stable iodine are used for age determination (Hohenberg and Pravdivtseva, 2008). It is applied in e.g. meteorite dating (Fan et al., 2013). Both, $^{129}I/I$ and I/Xe dating prove the iodine system valid for age determination. Moreover, within this study the exploration of a different iodine dating variation is sought.

Vast anthropogenic releases of ^{129}I since the beginning of nuclear age and the consequent increase of the global ^{129}I inventory by several magnitudes (c.f. section 3.2) resulted in a very distinct (and continually expanding) environmental gap between pre-nuclear and nuclear ^{129}I

concentration values. Whilst environmental concentrations prior to any human action have been reported to be as low as $2 \cdot 10^5$ at L^{-1} (marine system) and $3.7 \cdot 10^4$ at L^{-1} (terrestrial hydrosphere) (Snyder et al., 2010), concentrations have been raised significantly but spatially unequal since 1940. Nuclear emissions have increased ^{129}I concentrations up to roughly $2 \cdot 10^{11}$ at L^{-1} in marine surface waters in the vicinity of NRFs (Christl et al., 2015). Analogous, anthropogenic altered precipitation over Europe has been measured to be as high as $1 \cdot 10^{10}$ at L^{-1} (López-Gutiérrez et al., 2000a). Based on this definite enhancement of ^{129}I concentration, the classification of sample materials as of pre-nuclear origin or of nuclear origin can be pursued. Relative age dating with ^{129}I therefore seems reasonable.

Following this implementation, relative age dating with ^{129}I is applied to answer the first hypothesis of the present study (c.f. 1.3). Ice-influenced spring waters are sought to be differentiated in terms of being of modern (young) or pre-nuclear (old) origin, based on their level of ^{129}I concentration. Accordingly, old pre-nuclear waters originating from dead ice would contain minor amounts of ^{129}I. This would apply to any remaining dead ice within the proglacial area, given the assumption that the ice was created prior to the 1950s and associated melt waters have not been in exchange with the atmosphere since. In contrast, modern waters influenced by nuclear emission would show clearly enlarged concentration values. Although, only information relative to the onset of major ^{129}I emissions starting in the 1950s (Snyder et al., 2010) can be gained by this method, descriptions such as "older than 1950" or "younger than 1950" seem sufficient within this context, given the Last Glacial Maximum in 1850 and the following rapid glacial retreat.

Relative ages of spring waters and thus their ^{129}I concentrations depend on their hydrological origin. Considerations on possible waterways and respective ages within the study site of the lateral moraines are described in more detail in the next section. The sampling procedure of the equivalent springs together with the further sample treatment and measurement follows in section 4.1.

3.5 Application of ^{129}I in the context of Upper Kaunertal Valley

For the purpose of using ^{129}I for relative age dating in the particular setting of Kaunertal Valley, the question of the moraines hydrological connectivity had to be addressed. Hence, a conceptual model shown in Figure 19 has been constructed. The oversimplified scheme summarises possible hydrological connectives of the lateral moraines. It suggests possible origins and pathways of spring waters, their linked ^{129}I concentrations and relative ages.

The existence of old ice within the lateral moraines can be assumed for the study site of Kaunertal Valley. As the remaining ice from the 1850 maximum certainly must have been formed prior to any anthropogenic isotope enrichments, its ^{129}I content has to be minimal. In the conceptual scheme of Figure 19, light blue ice lenses within the moraine sediments that contain very little ^{129}I, illustrate the assumption. While the old ice lenses inside the matrix were preserved over decades, nuclear age started and ^{129}I concentration outside of these preservations has been significantly raised. Emitted anthropogenic ^{129}I is transported to the Austrian

Alps by westerly winds. ^{129}I sources relevant for the Alps may be gaseous and/or liquid emissions of Sellafield and La Hague (and former Marcoule) located northwest of the study area. In fact, a recent investigation of aerosols from Vienna revealed a good correlation with gaseous emission of Sellafield (Jabbar et al., 2011). However, measurements at the high mountain metrological stations of Zugspitze (Bavarian Alps, Germany) and Sonnblick (Hohe Tauern, Austria) could not be traced back to one particular source (Jabbar et al., 2012a). Regardless of its source, ^{129}I transported to Kaunertal Valley may be deposited primarily by wet (in-cloud or below-cloud) precipitation, temperature-dependent as rain or snow. In addition, iodine concentrations in precipitation are likely to decrease with increasing altitude as has been proven by several studies. Orographic lifting of air masses and consequent rapid cooling favours enhanced precipitation and the removal of iodine by washout (Gilfedder et al., 2007). The development of strong altitudinal gradients has been reported for both, radiogenic as well as stable iodine. Gilfedder et al. (2007) could demonstrate halved total iodine concentrations over an altitudinal change of 800 m within a distance of 5 km in the Black Forest, Germany. Reithmeier et al. (2006) proved that ^{129}I concentrations of a glacial ice core from Fiescherhornglacier (~ 3.900 m a.s.l.) were a factor of 6 lower than precipitation collected near Zurich (~ 400 m a.s.l.). Jabbar et al. (2012a) further found the ^{129}I concentration in aerosols of two Alpine stations (with an altitude of 2962 m and 3106 m a.s.l.) to be one order of magnitude lower compared to those measured in Vienna (202 m a.s.l.). Based on these examples, it was suggested that the influence of orographically induced precipitation on iodine concentrations may be greater than latitudinal effects (Gilfedder et al., 2007). Given the environmental setting of Kaunertal Valley and highly differing altitudes, a decreasing $^{129}I/^{127}I$ isotopic ratios and ^{129}I concentration in precipitation from the valley mouth up to the head can be expected.

Once an event has been triggered, ^{129}I enriched precipitation is deposited on site. Three general water pathways, sketched in Figure 19, are feasible. Modern ^{129}I rich water infiltrates into the sediment matrix of the lateral moraine. Firstly, if this occurs while ground temperature is below freezing point, new ^{129}I rich ice will form. Alternatively, the development of segregated ice is possible (French, 2007) and may base upon new (^{129}I rich) or old (^{129}I poor) ice. Secondly, excessive rain will drain as overland flow, rich in ^{129}I. Thirdly, accumulation and temporal storage in surface waters (e.g. little pools on top of the moraine ridge) or snow will occur. When precipitation is occurring in a solid state, ^{129}I concentration might be lower - as suggested by findings of a study focussing on iodine in snow (Buraglio et al., 2001).

Given the described setting, springs on the lateral moraines may have multiple sources of origin and corresponding iodine concentrations. Overland flow, for example, may immediately trigger some springs during a precipitation event, while others will respond within a particular lag time as precipitation might be infiltrating first. If precipitation fed snow fields or little pools are formed at the top of the moraine ridge, their runoff/snowmelt might drain as overland flow as well, feeding springs on the moraine. Likewise infiltration and subsequent interflow within the sediments is possible, that may or may not re-emerge on the moraines surface. Either way, ^{129}I concentrations of springs fed by any of these sources will be high and traced back to

the water's modern origin. Even if evaporative water loss is occurring at any of this sources, $^{129}I/^{127}I$ ratios should not be biased as long as iodine is being available in the same chemical species (Snyder and Fehn, 2004). If ground temperatures rise above the melting point and potential ice lenses within the lateral moraine start melting, sufficient amounts of melt water may also feed little springs. If melt water arises from recently built ice lenses, it should, in regard of its ^{129}I concentration, significantly differ from those derived from old ice lenses. The former melt waters being rich, the latter being poor in ^{129}I. If different sources of different age (e.g. meltwater (old/modern), interflow, overland flow, etc.) contribute to the runoff of a spring, a mixed signal, showing medium concentrations is to be expected. In any case, this is founded on the basic assumption that no significant amounts of ^{129}I are retained by the till itself.

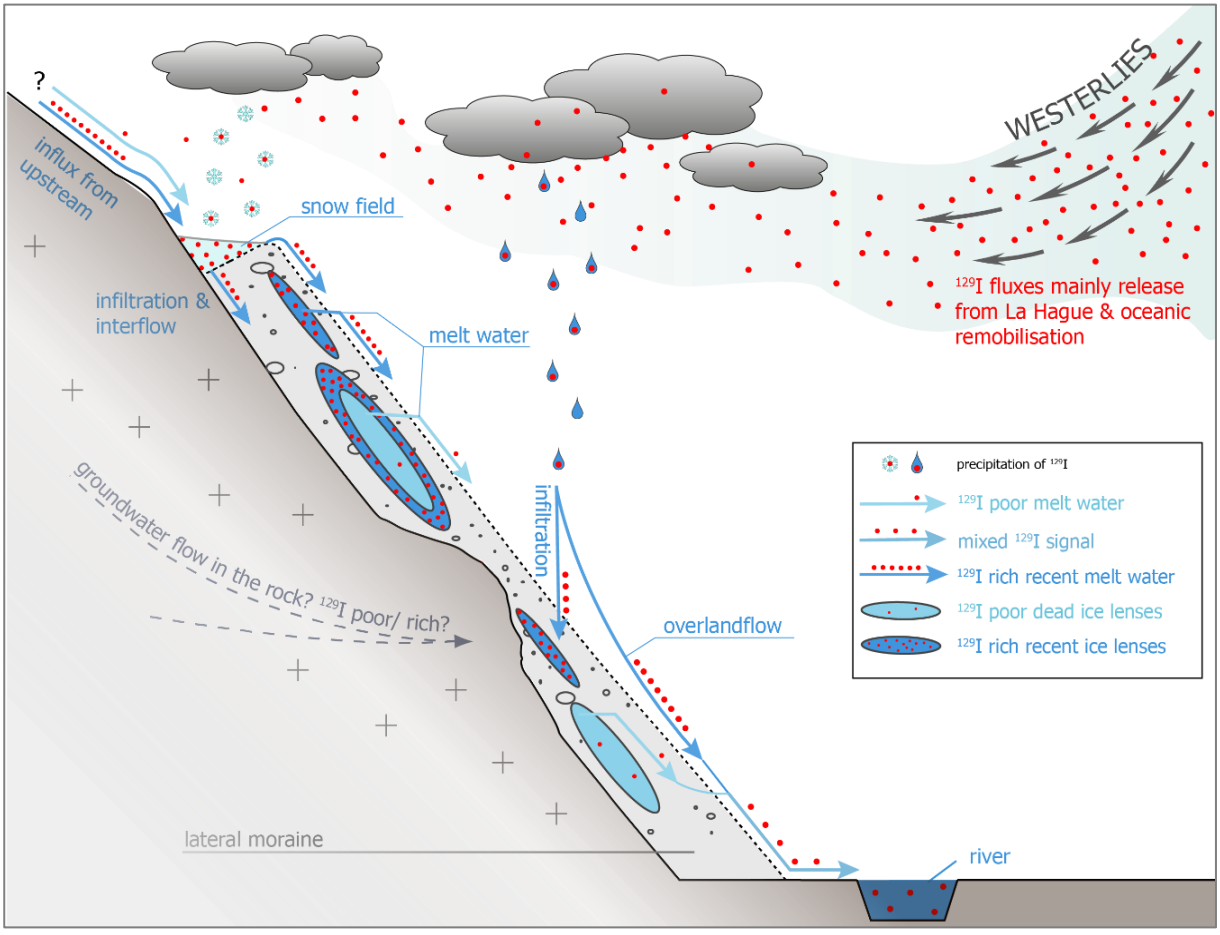

Figure 19: Conceptual model of ^{129}I input into the hydrological system of the lateral moraines including possible waterways and their equivalent ^{129}I concentration

Additionally, distorting fluxes beyond the moraine complex have to be addressed. The possibility of influxes from upstream areas or groundwater flows in the bedrock has to be recognised. For both, modern or pre-nuclear origin is feasible. Notably, through rock fissures, even the intrusion of waters from neighbouring catchments may be possible. Clarification of the latter is beyond the ability of the present study. While kept in mind, it is taken as general assumption that sub-surface and surface catchment areas are similar.

4 Methods

After comprehensively covering the basics of ^{129}I and its usage for relative age determination, this chapter focuses on the implementation of ^{129}I dating as well as on other methods applied to validate and answer previously raised hypothesis and research questions. Section 4.1 describes all steps involved in relative age dating in detail. This includes demonstration of water sampling, sample treatment, ^{129}I concentration measurements as well as raw data assessment. Methods used for statistical analysis of ^{129}I results are delineated, before the measurements of ground temperature are assessed in section 4.3.

4.1 Relative age dating

4.1.1 Sampling

Between July and October 2015, approximately 40 waters were sampled on a monthly basis. These waters stemmed from perennial and episodic springs, evolving from the lateral moraines, glacial runoff, (glacier) ice, the Fagge River, and a precipitation fed pond. Sampling happened on springs with concentrated flow, for reasons of representativeness (Kendall and McDonnell, 2006). In case of direct ice, dropwise sampling was performed. Potential contamination by overlandflow was excluded as far as possible. Sampling locations cover the whole study area and are equally distributed on both valley sides in terms of exposition and distance to the current glacier position. However, the locations vary slightly between months due to impact of precipitation events, different levels of discharge, morphological changes or glacial retreat.

Figure 20: Sampling of glacial runoff from Gepatschferner glacier, Kaunertal Valley (Czarnowsky V. 2015)

Sample volumes of ~ 500 mL were decided on (Szidat, 2000) as previous test runs with smaller sample volumes did not lead to sufficient outcome. Waters were collected with commercially available PET bottles, which had been cleaned with hydrochloric acid (HCl) and Millipore water prior to usage. Before taking samples, sample bottles were carefully rinsed three times on-site (Geboy and Engle, 2011). Sampling itself can be seen in Figure 20. Closure of the sample bottle happened whilst avoiding air pockets. In the course of sampling, total analytical duplicates were prepared. *"Total analytical duplicates are two samples collected in tandem from the same source at the same time and treated individually during preparation and analysis"* (Geboy and Engle, 2011, p. 12). They shall fulfil the purpose of quality control and ensure reproducibility of analytical results (Geboy and Engle, 2011).

As well as spring- and glacier waters, monthly precipitation samples were collected with an installed rain gauge (Palmex RS1B) at the altitude of the study area (~ 2152 m a.s.l., ETRS89-UTM-Zone-32-North-Coordinates: 632653.1447; 5193416.8907 m). Fitted one metre above ground, this rain gauge stored samples of up to 3 L within a HDPE container. Minimum evaporative losses compared to conventional rain gauges are to be expected (Gröning et al., 2012). A second rain gauge at a monitoring station maintained by the Austrian Central Institute for Hydrography (HZB Nr. 101873) approximately 18 km further down valley at Vergötschen (altitude of ~1263 m a.s.l., ETRS89-UTM-Zone-32-North-Coordinates: 633171.8149; 5211351.2477 m) provided additional precipitation samples. Both rain gauges were emptied after sampling of all other waters was concluded. Precipitation was collected as composite sample.

Samples were transported and stored refrigerated and protected from light for up to seven months. Long-time-stability of ^{129}I water samples is, according to Szidat (2000), given as greater than two years.

All sampling locations, except for the second rain gauge due to its position several kilometres down valley, can be seen in Figure 21. Details on sample codes are additionally found in the appendix.

Additional parameters

In the course of sampling, temperature and electrical conductivity has been reported for each sample using the hand-held conductivity meter GMH 3430 with integrated temperature sensor. For precipitation samples only the latter has been determined. Electrical conductivity is a measure of the concentration of ionisable dissolved solids. Following DIN EN 27888 it is measured as reciprocal of electric resistivity (Barsch et al., 2000). Resolution of conductivity measurements is 0.1 µS cm^{-1} for a range of 0.0 to 200.0 µS cm^{-1} and 1 µS cm^{-1} for a range of 0 to 2000 µS cm^{-1}. Accuracy of temperature measurements is given as 0.1 °C for a range of -5.0 °C to +100.0 °C. In the case of minimal discharge and precipitation samples, temperature and conductivity measures had to be performed inside the sample bottles. Minor deviation are therefore possible. As well as temperature and conductivity measures, spring discharge has been estimated and weather conditions have been noted.

Due to inaccessibility of most springs and frequent shifts in sample locations conditioned by high geomorphological activity in the proglacial area, using a differential GPS (global positioning system) for positioning was dispensed with. Instead, the location of all sampling sites was determined by hand held GPS (Garmin Dakota 20 and Garmin Oregon 300) with an accuracy of 5 m. Elevation was alternatively extracted from the digital elevation model (of 2015) as for the high error in z- value of the hand held. Further parameters of exposition and slope position have been noted for each sample taken and have been double-checked in a GIS environment using ArcGIS 10.4 and the DEM of 2015 with one metre resolution, which was gratefully provided by the PROSA Project. Notation of all parameters raised in the field can be taken from the appendix.

In addition to information collected in the field, the topographic parameters of slope has been derived in a GIS environment using ArcGIS Tools *Slope.* Details on the glacial extent of Geptaschferner glacier by Hartl and Fischer (2014) are available as open-source GIS data set of distinct time slices between 1850 and 2006. These datasets allowed, in combination with the existing DEM from 2012 and 2015 and field observation of the glacial extent in 2015, the identification of the year a certain sampling location was deglaciated.

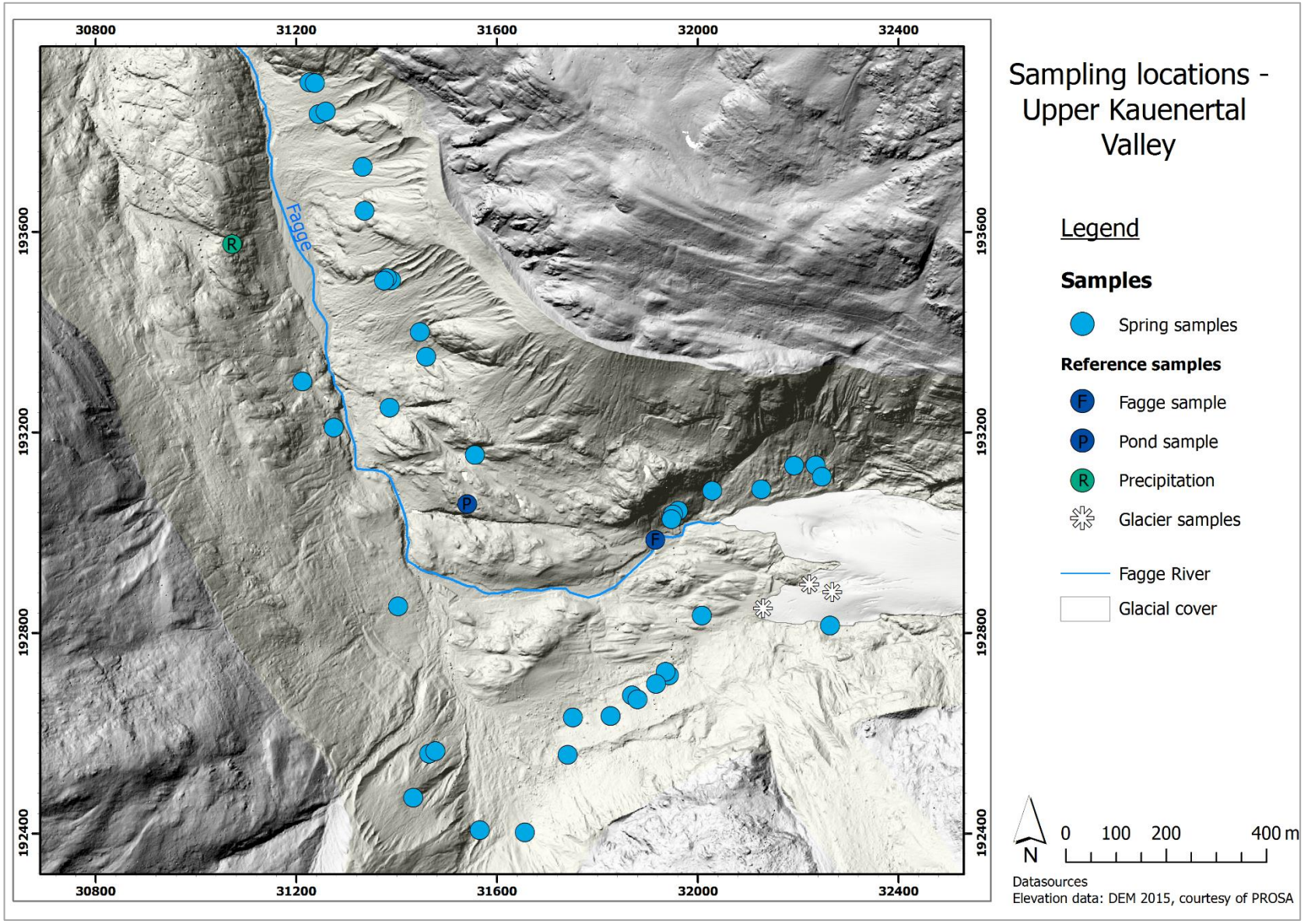

Figure 21: Location of spring sampling within the proglacial area of Gepatschferner glacier in Upper Kaunertal Valley. Single spring sampling sites can minorly differ between months due to morphological changes, variying discharge level or glacial retreat

4.1.2 Sample preparation: analytical method for separation of iodine

Sample treatment could only be applied to a reduced number of samples, due to financial restrictions and time limits within this study. Subject to these limitations, 39 samples from July 2015 (including 1 duplicate) were selected for preparation and consequent measurement. Air temperatures during sampling were the highest of all campaigns and melting of potential ice inside the moraines was therefore believed to be most likely. Also the influence of precipitation events, as a source of irritation, was the lowest during this campaign. Based on results of the first measurements, certain springs (45, 48, 49, 65, 67, 68 & 77/2) were selected to be measured for other months too (optionally August or September, again due to temperature and influence of precipitation during sampling). As ^{129}I concentration values of precipitation in literature are scarce (for the Alpine region in general and especially higher altitudes), all precipitation samples gained (10 samples, including 2 copies) were added for further analysis. A total of 53 samples and 3 duplicates has been processed.

The extraction of analytics from the sample is the general objective of any chemically or physically sample preparation step (Szidat, 2000). The amount of ^{129}I in environmental samples is usually very low. It does not exceed 10^{-7} mg g^{-1} for solid samples, or < 10^{-9} mg L^{-1} for water samples (Fan et al., 2013, p. 33). Hence, an iodine separation and pre-concentration from the liquid sample matrix is necessary. A wide variety of segregation routines exists for environmental samples (Schmidt et al., 1998) and finding a "*separation method with high iodine recovery and sufficient decontamination from interferences is the key point to obtain reliable analytical results"* (Fan et al., 2013, p. 35).

The chemical treatment of liquid ^{129}I samples has not been realised at the laboratories of the Institute for Isotope Research and Nuclear Physics, prior to this study. Several trial runs to identify the ideal analytical methodology for the separation of iodine were necessary.

The first iodine extraction scheme applied following Jabbar et al. (2011) led to insufficient conditioning of the anion exchange columns resulting in problems regarding the breakthrough of the columns and eventually in unsatisfyingly little deposition of iodine. Therefore, parts of the analytical procedure suggested by Povinec et al. (2013) renouncing the use of anion exchange columns were tested but did not lead to successful treatment of the samples either. Eventually, the analytical procedure compiled by Szidat et al. (2000), which is described in more detail in Szidat (2000), did show satisfying results. The suggested treatment procedure was consequently chosen for this study, yet slightly modified and combined with entries from Jabbar et al. (2011). The analytical steps of the sample treatment are explained in detail in the following. Single process steps are illustrated with several images in Figure 22. Summing up, the complete sample treatment can be seen in Figure 23. All glassware, containers, instruments and other tools, which have been in direct contact with samples during any step of the processing, were carefully washed with hydrochloric acid (HCl, 10 %) and rinsed with Millipore water before usage.

Only a few natural materials, e.g. thyroids, seaweed, brines, contain an iodine content high enough to allow for carrier-free ^{129}I measurements (Szidat, 2000). Other environmental or geological samples normally have relatively low iodine concentrations. The processing of these therefore demands the addition of a carrier medium in order to obtain iodine in a measurably sufficient amount using AMS (accelerator mass spectrometry) (Fan et al., 2013; Liu et al., 2015). This also applies to the waters sampled in Kaunertal Valley, and especially those believed to originate from the pre-nuclear era. Hence, an excessive amount of iodine carrier had to be added in the beginning of the chemical preparation. The intrinsic isotopic ratio ($^{129}I/^{127}I$) has thereby been changed, and more precisely been diluted (Szidat, 2000). The addition of the carrier, nonetheless poor in ^{129}I, might not only enhance the ^{127}I content but also slightly increase the ^{129}I concentration of the samples. This is probably negligible in case of modern environmental samples, where anthropogenic ^{129}I dominates anyway. ^{129}I introduced to pre-nuclear samples by the carrier generally needs to be seen more critically. After all, it is possibly comparable or even higher than the original amount of ^{129}I in the sample (Fan et al., 2013). Given the present study aim, this fact is not highly relevant, besides, possible ^{129}I contamination is monitored by chemical blank determination. An amount of 2 mg of iodide 127, which correlates with 222 mg of the used carrier solution with a concentration of ~ 10 mg per mL I^-, were thus mixed into the natural water samples.

The existence of iodine in an iodide (I^-) state is essential for the following solid-phase extraction. When treating natural waters this cannot be presumed (Klipsch, 2005). In addition to iodide, iodine in natural waters mainly exists as iodate (IO_3^-) and in small quantities also in organic form (Daraoui, 2010). Yet, dominant iodine species vary for ^{127}I and ^{129}I. Hou et al. (2009a) report, based on precipitation samples, that iodide is the major species for ^{129}I, whereas it is iodate in case of ^{127}I. All ^{129}I or ^{127}I has to be present in the speciation of iodide, since iodate for example, would, due to the salt load of the sample itself, already be washed out of the anion exchange column during the extraction. This must not happen. The original sample and also the iodine content of the carrier need to be held in the column in their entirety. Thus, the transformation of all species of iodine into iodide is essential (Szidat, 2000). Firstly, all iodine types present are converted into iodate through oxidation with 5 mL 2 M $Ca(ClO)_2$, and a reaction time of 5 minutes being sufficient. Secondly, the addition of 10 mL 1 M $NaHSO_3$ and 20 mL 1 M $NH_2OH \cdot HCl$ at pH 5 to 6 causes the reduction of all iodate to iodide (Szidat, 2000; Szidat et al., 2000). A reaction time of minimum 45 minutes (Szidat et al., 2000) is guaranteed. The steps of oxidation and reduction developed by Gabay et al. (1974) and validated by Szidat (2000) ensure that all iodine species present at this point of the processing have been transformed into iodide (Klipsch, 2005). According to Abdel-Moati (1999), the process of oxidation also destroys organic iodine compounds. The sample's inorganic as well as organic iodine can therefore be measured (Szidat et al., 2000). If a sample contained a greater amount of sediment it was necessary to centrifuge the sample at this point of treatment before continuing with the preparation.

The next processing steps involved solid-phase extraction of iodide through ion chromatography (IC) implemented with anion exchange columns. The anion exchange resin consists of polymer substrate and has been functionalised with a quaternary ammonium compound. This allows the bonding of anions based on their binding strength, where iodide binds more strongly than other anions (Klipsch, 2005). Equation 1 overviews the relative selectivity of iodide on a strongly alkaline anion exchanger in comparison with major anions (Daraoui, 2010):

$$I^- > NO^{3-} > Br^- > CH_3COO^- > OH^- > F^- \qquad \text{Eq. (1)}$$

For the preparation of the anion exchange columns (5 mL), synthetic resin (Dowex 1x8, 100-200 mesh Cl^- form) acting as anion exchange material, was elutriated with Millipore water and filled into glass columns (Figure 22b). As the anion exchanger comes in chloride (Cl^-) form, the anion chloride had to be replaced with nitrate (NO_3^-) beforehand. This increases the selectivity of the exchanger for iodide, as only iodide is able to replace nitrate (see equation 1) (Klipsch, 2005). The conversion to nitrate form was accomplished by adding 60 mL 2 M nitric acid (HNO_3). After completing the conditioning of the columns, the samples could be loaded on the column. By passing the resin dropwise, the sample's iodide was bound into the exchange matrix by replacing NO_3^- based on equation 2 (Daraoui, 2010):

$$Resin - N\,R_3, NO_3^- + I^- \Leftrightarrow Resin - N\,R_3, I^- + NO_3^- \qquad \text{Eq. (2)}$$

Anions other than iodide and miscellaneous matrix components were meanwhile flushed through the column (Klipsch, 2005). The extraction of iodide from the exchanger was subsequently initiated with a first rinse of 50 mL 0.5 M potassium nitrate (KNO_3) and continued with a second 10 mL 2 M KNO_3 rinse, before iodide was finally eluted with another 50 mL 2 M KNO_3. Following the preparation process of Szidat (2000), more than 90 % of elutable iodide should have been retained, but a certain remnant of analytes could not be avoided given a reasonable amount of eluant (Szidat, 2000). As a precaution the second rinse was reduced to 10 mL 2 M KNO_3 (instead of 15 mL) and the eluting solution was enhanced from 30 mL to 50 mL. Additionally, the possibility of a premature or delayed elution, e.g. during the second rinse or after the actual elution, was tested and could be excluded. Following the elution, 4 mL of 0.01 M silver nitrate ($AgNO_3$) solution was added. The samples were given minimum 24 hours to precipitate as silver iodide (AgI) and also silver chloride (AgCl). Observations during the trial run confirmed that a period of 24 hours is sufficient to precipitate all analytes. The addition of 15 mL ammonia (NH_3, 25 %) caused the separation of AgI and AgCl by dissolving the latter (Ohta et al., 2013), as well as other halides (Jabbar et al., 2011) and was conducted based on Jabbar et al. (2011). Figure 22c shows the amount of precipitated silver iodide. After washing the remaining AgI precipitate with Millipore water for a second time, the samples were dried at 60 °C. The dry samples (cf. Figure 22d) have been weighed, grained and mixed with silver powder (120 mesh) in a mass ratio of 1:1. Mixing of the samples with a conductive powder is needed in order to prevent the target from charging-up and in order to eliminate heat that is generated in the sample while caesium$^+$ ion sputtering (Liu et al., 2015). Samples

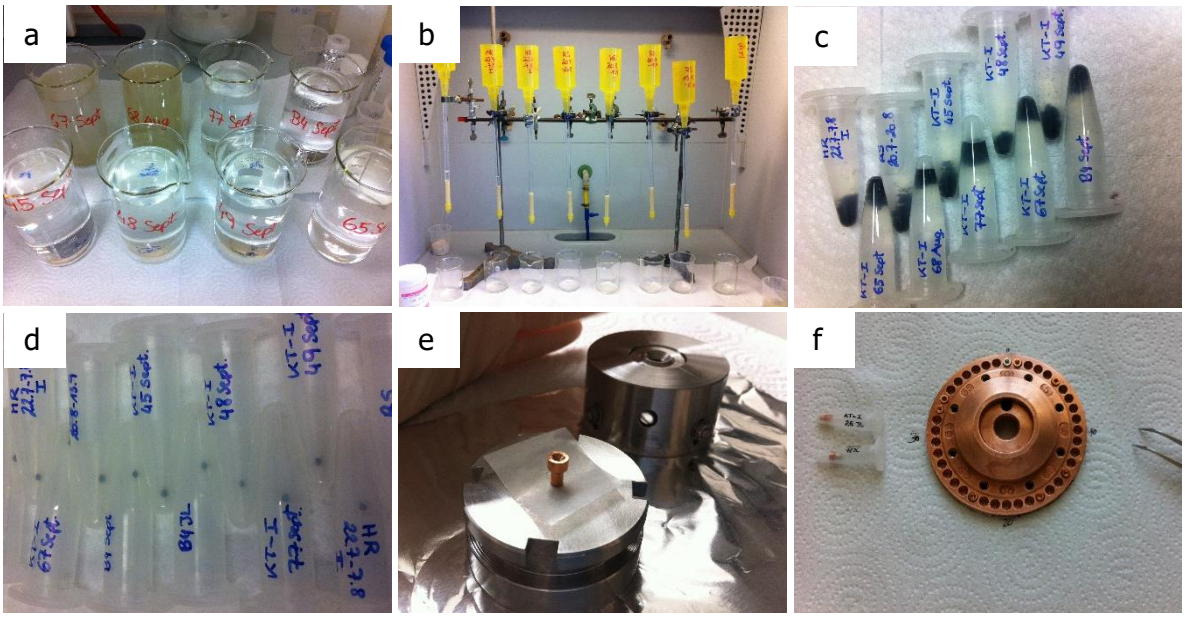

Figure 22: Selected steps of sample preparation scheme: a, addition of carrier, oxidation to iodate and reduction to iodide; b, solid-phase extraction of iodide through anion exchange columns; c, precipitation of AgI; d, dried AgI precipitate; e, pressing of sample targets; f, insertion of targets into the measuring wheel (Kamleitner S. 2016)

were pressed in a copper target holder with 15 kN (Figure 22e) and been placed in a copper wheel (Figure 22f). Copper rather than aluminium is the suitable material for targets and the measuring wheel during ^{129}I measurements as the holder material influences the stability of the samples (Liu et al., 2015). Chemical reactions between AgI and aluminium in air could cause the failure of AMS measurement or an unsteady current (Liu et al., 2015). Samples were complemented with several copies of the VIS 11 (Vienna Internal Standard) material with a known $^{129}I/^{127}I$ ratio of $1.0 \cdot 10^{-11}$. Machine blanks, so called Vienna AgI 111 targets, with a calibrated ratio of $1.8 \pm 0.2 \cdot 10^{-13}$ (Jabbar et al., 2013a) and an old carbon target were incorporated for the purpose of machine tuning and the issue of monitoring instrument background and memory effects (Liu et al., 2015) and therefore the sensitivity of the measurement (Reithmeier et al., 2005).

"Contamination is an important problem for low-level ^{129}I analysis, (…) it *can exceed the ^{129}I amounts in the samples itself by more than a factor of 10"* (Schmidt et al., 1998, p. 149). Natural and artificial samples contain a wide range of isotopic ratios and can lead to cross contaminations. As reported by some authors, chemical ingredients or sampling procedure may additionally alter the analysis (Schmidt et al., 1998). Loss of analytes or any contamination introduced during sampling, sample storage, sample preparation, target pressing or target measurement were therefore monitored by blank samples. Blanks were prepared with deionized water (Millipore pure water system), identical to real samples, immediately after the sampling campaign in the field. They underwent similar storage periods as the associated real samples. During iodine separation every sample sequence was accompanied by one blank sample which was treated equally. Within one process sequence, seven samples plus one blank sample were prepared.

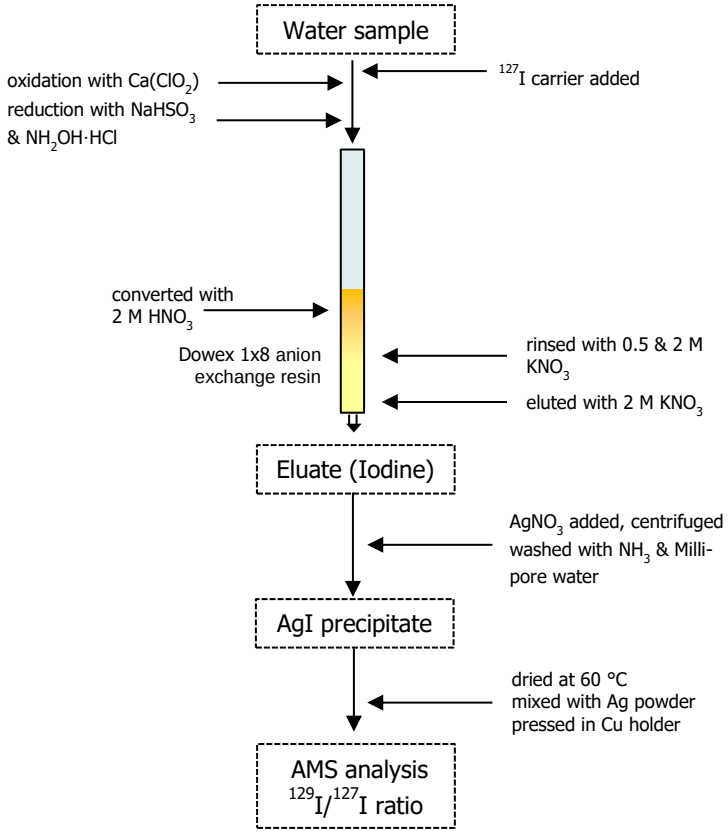

Figure 23: Scheme of ^{129}I sample preparation

4.1.3 Measurement of ^{129}I

According to Jabbar et al. (2013a, p. 49) *"iodine-129 is one of the hard-to-measure radionuclides, because of the long half-life and the low energy of beta- and gamma-rays emitted from it"*. The first successful determination of ^{129}I in environmental matrixes was at the beginning of the 1960s through radiochemical neutron activation analysis (RNAA). A technique which would keep its pre-eminence for nearly two decades, before being replaced by accelerator mass spectrometry (Szidat, 2000). Along with RNAA and AMS, inductively coupled plasma mass spectrometry (ICP-MS) has been efficient in measuring ^{129}I concentrations, too (Jabbar et al., 2013a). Using the emitting energy during the decay of ^{129}I, gamma- and x-ray spectrometry and liquid scintillation counters (LSC) can also provide information on ^{129}I concentration levels (Hou et al., 2009a).

All of these methods may be used for the determination of ^{129}I, but their sensitivity and detection limits vary considerably, thus defining their different areas of operation (Fan et al., 2013). Table 1 gives an overview on detection limits of the different measurement methods mentioned. While X-γ spectrometry has been successfully applied in determining iodine concentrations in high-level-samples such as thyroids or nuclear waste it is not sufficient for isotopic ratios above 10^{-6} (Hou et al., 2009a). Also LSC and ICP-MS may only be used for anthropogenic samples. Simply put, RNAA and AMS can be applied for environmental levels (Fan et al., 2013)

and accelerator mass spectrometry alone is sensitive enough to detect ^{129}I concentrations in pre-nuclear samples (Hou et al., 2010). With detectable $^{129}I/I$ ratios up to 10^{-14} (Snyder et al., 2010) AMS covers the entire range of isotopic ratios and concentrations in nature (Vockenhuber et al., 2015).

Table 1: Determination of ^{129}I – comparison of existing measurement methods (Hou et al., 2009a)

Detection method	Detection limit $^{129}I/^{127}I$ ratio	Reference
X-γ spectrometry	10^{-4} to 10^{-6}	(Maro et al., 1999; Suárez et al., 1996)
LSC	10^{-5} to 10^{-6}	(Suárez et al., 1996)
ICP-MS	10^{-5} to 10^{-7}	(Brown et al., 2007; Izmer et al., 2004)
RNAA	10^{-10}	(Hou et al., 1999)
AMS	10^{-14}	(Fehn, 2012; Snyder et al., 2010)

The isotopic ratios expected within this study are accessible with AMS only. It is therefore the method of choice for ^{129}I determination. AMS measurements are going to be examined in more detail in the following passages. Details on RNAA, LSC, X-γ spectrometry, ICP-MS are given elsewhere (Fan et al., 2013; Hou et al., 2009a).

4.1.3.1 Accelerator mass spectrometry (AMS)

AMS had been used in the analyses of other long-lived isotopes before being applied to ^{129}I analysis in 1980 (Schmidt et al., 1998). Improvements in analytical techniques over the last two decades finally led to an increasing number of AMS facilities applicable for ^{129}I around the world. Due to growing interest of environmental, geological and biological fields, the long-lived radionuclide is becoming one of the most popular and frequently measured isotopes today. Increasing demand is to be expected (Fan et al., 2013).

"Almost all AMS facilities can be understood as two mass spectrometers (called "injector" and "analyser") linked with a tandem accelerator" (Hou et al., 2009b, p. 187). Following Fan et al. (2013) an AMS system can typically be described in three sections: negative ion production, mass and energy selection (1), ion acceleration and molecular isobar destruction (2) and positive ion selection and ion detection (3). The schematic organisation of an AMS facility used for ^{129}I detection is shown in Figure 24, an illustration of the VERA (Vienna Environmental Research Accelerator) tandem accelerator. In the first section of the AMS facility, injection of the sample into the system happens using a caesium$^+$ primary ion source (Jabbar et al., 2013a; Liu et al., 2015). Iodine isotopes as well as other isotopes of the sample are sputtered out as negative ions (I^-) by Cs^+ ions. Negative iodine ions are easily produced in the sputter source while simultaneously main isobaric interferences (arising from isotopes of different elements with equal masses (Krieger, 2012) are instable and disintegrate quickly. Main interferences arising from xenon 129 ions should therefore not significantly restrict further measurement in any way (Hou et al., 2009b). The sputtered particles are then filtered and ions are separated firstly according to their energy and secondly by their magnetic rigidity

(Liu et al., 2015). The result of this selection are negative ion beams with the masses 127 and 129 that can now be sequentially injected into the tandem accelerator (Kieser et al., 2005). Entering the second section of the system, ions are accelerated in the first low-energy part of the accelerator. Thereby, several electrons of the iodine ions are stripped off and I^- is transformed into multiple positively charged ions (Liu et al., 2015) depending on the selected state of charge (Fan et al., 2013). Next, potentially interfering polyatomic molecules are disassociated (Liu et al., 2015), e.g. $^{127}IH^-$ and $^{128}TeH^-$ (Fan et al., 2013). Now positively charged ions are accelerated a second time and leave the accelerator (Liu et al., 2015). A Wien-filter follows the accelerator process and retains ions with velocities that vary from those of the selected ion (Reithmeier et al., 2010). Passing a magnetic-electrostatic mass spectrometer ions are selected based on their energy/charge and mass/charge ratio (Liu et al., 2015). Remaining background ions are thereby removed and the purified ^{129}I and ^{127}I is led to the detectors and measured (Hou et al., 2009b). Stable ^{127}I is detected as current with a gated Faraday cup (Jabbar et al., 2012b) which is in phase with the isotope injection time. The unstable ^{129}I is counted as single events by the gas ionization chamber (Liu et al., 2015) as is the case with VERA and/or time-of-flight (TOF) measurement (Hou et al., 2009b; López-Gutiérrez et al., 2000a).

"AMS is a relative analytical method" (Hou et al., 2009b, p. 187) and ^{127}I and ^{129}I signals are measured as relative values, as they depend on ion extraction and AMS status. Therefore, ^{127}I current and ^{129}I counts are reported as $^{129}I/^{127}I$ isotopic ratio (Fan et al., 2013). The theoretical detection limit of AMS facilities is reported as 10^{-15}. Still, blank materials with ratios below 10^{-14} are missing, which raises the practical detection limit up to 10^{-14} (Jabbar et al., 2013a).

Due to the specifications of AMS, it is possible that ^{127}I and ^{129}I are not detected in the same ratio as they are present in the sample. Additionally, instrument caused fluctuations are possible since the measurements last for days (Klipsch, 2005). It is therefore necessary to compute measurements in relation to standards with a known isotope ratio (Reithmeier et al., 2010) and correct the $^{129}I/^{127}I$ ratio as a function of the measured standards (Szidat, 2000). ^{129}I concentrations can be calculated based on the isotopic ratios (see section 4.1.4). However, information on the total ^{127}I content of the sample possibly need to be obtained via a separate method, e.g. ion chromatography, as synchronous determination of ^{127}I and ^{129}I is not possible with AMS (Schmidt et al., 1998).

4.1.3.2 Sample measurement at VERA

Determination of the $^{129}I/^{127}I$ isotopic ratio by AMS happened at VERA. First attempts of ^{129}I measurement at VERA were performed as early as 1998 (Wallner et al., 2007). ^{129}I measurements for the present study were performed in February and March of 2016 by Dr. Johannes Lachner and Dr. Peter Steier from the Isotope Research and Nuclear Physics group of the Faculty of Physics, University of Vienna. As the general functionality of an AMS facility has already been given in the previous section, specifics of the measurement at VERA are briefly mentioned in the following.

Samples were sputtered using a Cs negative ion source with an energy of 57 kV. For acceleration, a terminal voltage of 3 MeV was applied and argon gas was used for stripping. The charge state of 4^+ was selected, resulting in a total particle energy of 15.57 Mev. A transmission yield of 7 to 12 % for the selected state of charge was achieved. This AMS setup resulted in measured $^{129}I/^{127}I$ ratios being shifted by a factor of 0.8 and 0.6 in comparison to the isotope ratio of the reference material. A Bragg type gas ionization chamber was used for ^{129}I event detection. Measured ^{127}I currents were highly dependent on the specific sample measured but ranged between 100 nA to 3 µA (high energy side) and 65 nA to 3.5 µA (low energy side). Within the applied measurement design, single samples were continuously measured in three cycles á 40 seconds which add up to one run (t = 120 s). If one run is performed for all 40 samples a whole turn has been accomplished. However, depending on sample properties, between ten to twenty cycles were actually measured for each sample. The total measurement time therefore adds up to roughly 30 minutes per sample.

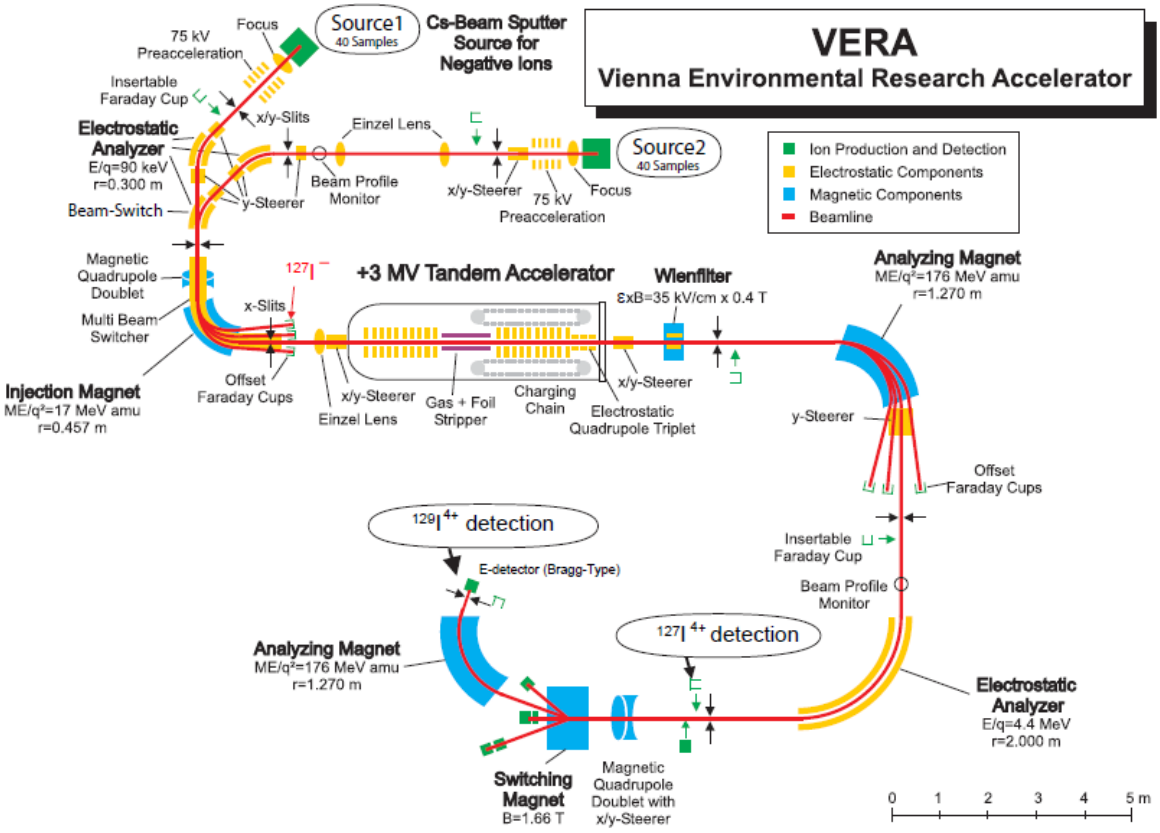

Figure 24: Schematic structure of an AMS facility used for ^{129}I detection by the example of VERA tandem accelerator (courtesy of the Isotope Research and Nuclear Physics group, modified after personal communication from Johannes Lachner)

4.1.4 Analysis of $^{129}I/ ^{127}I$ isotope ratio and ^{129}I concentrations

Computation of $^{129}I/ ^{127}I$ isotope ratios from AMS measurements represent the basic requirement for the calculation of ^{129}I concentrations. However, analysis of AMS data is a complex task. Based on the AMS generated isotope ratios, iodine concentrations can be calculated. The procedural method applied for data analyses is outlined in the following. Models used are described in more detail by Szidat (2000) and also Klipsch (2005).

In several cycles c over a certain test time t high energy ion current of mass 127 (I) was measured. Simultaneous single ^{129}I events (N) were counted. Taking into account the selected state of charge q (4^+) and the elementary charge e ($1.602 \cdot 10^{-19}$) the isotope ratio can be gained (Szidat, 2000):

$$\left(\frac{^{129}I}{^{127}I}\right)_c = q \cdot e \cdot \frac{N_c}{t_c \cdot I_c} \qquad \text{Eq. (3)}$$

All cycles of all runs are averaged and weighted by their test time and ion current following Szidat (2000). Measured standards weighted by test time and ion current determine the factor of correction. Depending on the chronological sequence of the standards, corrections can be carried out variably. If standards do have a constant arithmetic mean, as was the case within this measurement, the value is, likewise, subtracted from all samples. If standard values show steps or are drifting, more than one mean value may be applied for individual groups of samples (Klipsch, 2005). More details can be found in Szidat (2000). For every sample several standard corrected isotope ratios from numerous runs are available (Klipsch, 2005). A final averaging of these then leads to the measured value of the sample.

Based on the averaged and standard corrected $^{129}I/^{127}I$ ratio, the ^{129}I concentration of the sample can be calculated. The addition of iodide carrier is set as reference as this is the point where the intrinsic isotope ratio of the sample has been changed (Szidat, 2000).

The measured isotope ratio $\left(\frac{^{129}I}{^{127}I}\right)_{me}$ is given by the quotient of the amount of substance n of both isotopes, by their mass m and molar mass M (cf. Eq. 4) (Klipsch, 2005).

$$\left(\frac{^{129}I}{^{127}I}\right)_{me} = \frac{n_{129}}{n_{127}} = \frac{\frac{m_{129}}{M_{129}}}{\frac{m_{127,total}}{M_{127}}} \qquad \text{Eq. (4)}$$

Corresponding to equation 4 the determination of the ^{129}I concentration (m_{129}) is shown in equation 5. Next to the measured isotope ratio, the total mass of ^{127}I ($m_{127,total}$) and the quotient of the molar masses of both isotopes (M_{127},M_{129}) are needed. The last factor ($\frac{M_{129}}{M_{127}}$) is thereby converting the atomic ratio into a mass ratio (Szidat, 2000).

$$m_{129} = \left(\frac{^{129}I}{^{127}I}\right)_{me} \cdot m_{127,total} \cdot \frac{M_{129}}{M_{127}} \qquad \text{Eq. (5)}$$

The total ^{127}I mass is composed of the intrinsic iodine amount of the sample ($m_{127,intr}$) and the carrier addition ($m_{127,carrier}$) (Szidat, 2000):

$$m_{127,total} = m_{127,intr} + m_{127,carrier} \quad \text{Eq. (6)}$$

The intrinsic ^{127}I present before the addition of iodide carrier solution can be determined with an aliquot sample by IC or ICP-MS (Klipsch, 2005). As the intrinsic iodine mass is by far the smaller part of total ^{127}I, it is neglected by several authors (Fan et al., 2013), especially if the chance of ^{127}I determination is not given (Szidat, 2000). The information on intrinsic ^{127}I is therefore not needed (Schmidt et al., 1998). As this is also the case for the samples of Kaunertal Valley the study forewent on the determination of intrinsic ^{127}I mass. For the calculation of the ^{129}I concentration, this means that the intrinsic ^{127}I mass appearing in equation 6 can be withdrawn. The total ^{127}I mass then equals the ^{127}I mass of the carrier. The mass of the carrier is a result of the tracers weight taken ($m_{carrier}$) and the concentration of the carrier solution ($c_{127,carrier}$) (Szidat, 2000):

$$m_{127,carrier} = c_{127,carrier} \cdot m_{carrier} \quad \text{Eq. (7)}$$

The computed ^{127}I mass, the measured isotope ratio and the known molar masses can now be used to determine the ^{129}I mass by following equation 5. Admittedly, the calculated ^{129}I mass also contains ^{129}I that does not stem from the intrinsic sample, but has been introduced during sample processing and measurement. On account of this, a blank correction has to be performed (cf. Eq. 8). Blank concentrations are in most cases significantly lower than the samples intrinsic concentration and therefore have little to barely noticeable influence on the ^{129}I mass (Klipsch, 2005).

$$m_{129,sample} = m_{129} - m_{129,blank} \quad \text{Eq. (8)}$$

In the last step, the blank corrected ^{129}I mass has to be referred to the initial sample weight (Klipsch, 2005). The ^{129}I concentration by volume, represents the end results and can finally be obtained.

Regarding the measurement uncertainties of the isotope ratio, two factors have to be taken into account. Firstly, uncertainties that are resulting from the count of single ^{129}I events due to the partly small number of counts registered in a certain time period. Secondly, uncertainties arising from the standard deviation of repeated measurements. Detailed explanations can be found in Klipsch (2005) and Szidat (2000). Based on measurement uncertainties from the isotope ratio, the combined standard uncertainty was evaluated during ^{129}I mass determination with every calculation step following the law of error propagation (Klipsch, 2005):

$$y = f(x_1, x_2, \dots, x_n) \quad \text{Eq. (9)}$$

$$u^2(y) = \sum_{i=1}^{n} \left[\left(\frac{\partial f}{\partial x_i} \right) u^2(x_{i)} \right] \quad \text{Eq. (10)}$$

4.2 Statistical analysis

Based on the determination of ^{129}I concentration a statistical assessment of gained data is applied. First analyses aim to provide statistically grounded information on previously hypothesized differences of ^{129}I concentrations between several types of waters. Secondly, correlation between ^{129}I concentration and topographical and hydro-chemical characteristics of sampled waters are assessed in order to validate controls on dead ice preservation and indications of dead ice presence based on spring characteristics (c.f. section 1.3). Performed statistical calculations are accomplished with R Studio (Version 0.98.1062) by using the *sfsmisc* package (Maechler, 2016) and the *lsf* package (Navarro, 2015).

4.3 Ground surface temperature

"Ground surface temperature (GST) is defined as the surface or near-surface temperature of the ground (bedrock or surficial deposit), measured in the uppermost centimeters of the ground" (PermaNET, 2011, p. 1). Ground surface temperatures within the moraine till are of interest for the formation of seasonal segregation ice and have been accomplished within the study area. However, financial limitations only allowed for GST measurements at one distinct location. Measurements happened at the lower part of the west exposed LIA lateral moraine on the right side of the valley at an elevation of 2126 m. Inclination of the slope is 33°. GST measures were applied close to spring 45 (c.f. appendix) in a setting most comparable to other parts of moraine site A.

Ground temperature measurements were conducted by the use of iButtons (DS1922L). The coin-sized temperature loggers have a data log memory of 8 KB and measure a temperature range between -40 °C and 85 °C with a resolution of 0.5°C between -10 °C and 65 °C (Gubler et al., 2011). IButtons are described as water resistant but not waterproof (Maxim Integrated Products, 2015). Consequently, reports of iButton failures ascribed to water damage exist (Lewkowicz, 2008). In order to prevent water from entering the device, iButtons were packed within a conventional balloon before installation. A plastic string was fixed to the balloon to facilitate retrieval of the temperature loggers. Trying to reduce impacts on ambient sediment structure, holes of different depths were drilled into the moraine rather than dug. Multiple attempts were required due to the presence of large boulders within the till matrix. Three temperature loggers were placed at the bottom of the holes at roughly 20, 40 and 60 cm depth. The lateral distance between the iButtons did not exceed one metre. The location of the temperature sensors were determined using a hand held GPS (Garmin Dakota 20 and Garmin Oregon 300) with an accuracy of 5 m. Holes were filled up with sediments afterwards.

Ground surface temperatures were measured every four hours, starting at 2 AM. Daily mean temperatures have been calculated based upon the data collected. Further the ground freezing index (GFI), which is *"defined as the annual sum of negative daily mean temperatures, expresses as cumulated negative degree-days (°C.day)"* (PermaNET, 2011, p. 4), was determined. Temperature measures were conducted for a period of one year (26.07.2015 to 26.07.2016). For data backup, temperature loggers were read on September 12th 2015 and were put back in place afterwards.

The air temperature and the precipitation record of Gepatschalm is used for comparison of measured ground surface temperatures on the moraine site. The climate station of Gepatschalm and GST measurement site are within a linear distance of less than two kilometres and characterized by a difference in elevation of roughly 100 m. The data sets have been kindly made available by the PROSA project and are present in a resolution of 15 minutes.

5 Results

In the following section result of the present study are outlined. Firstly, ^{129}I concentration measures for relative age dating are addressed. Results of statistical analysis and ground temperature measurements are shown thereafter.

5.1 Relative age dating

^{129}I concentrations of 56 samples (including 3 duplicates) from Upper Kaunertal Valley, sampled between July and October 2015, have been determined through AMS measurements at VERA. An overview on topographic and hydro-chemical characteristics of sampled springs is given first before results are presented in section 5.1.2 and 5.1.3. Measurement uncertainties and -quality are subsequently addressed (section 5.1.4 and 5.1.5). This is followed by a discussion on the necessities of altitude correction and outlier treatment.

5.1.1 Topographic and hydro-chemical characteristics

Between July and October 2015, glacier-, spring-, and precipitation waters were sampled in Upper Kaunertal Valley. Fifty-three of these samples (and another three analytical duplicates) were selected for ^{129}I concentration measurement at the AMS facility VERA. Selected samples are characterised by varying topographic and hydro-chemical parameters, which have been raised directly in the course of sampling or in a GIS environment during post-processing. Frequency distribution of the samples regarding different topographic and hydro-chemical parameters are presented within this section.

Altitude

Processed water samples have been gathered between altitudes of 1260 and 2330 m. The accurate frequency distribution of all samples regarding altitude can be seen in the left barplot of Figure 25. Classification was done, similar to all other barplots shown, based on Sturges (1926). However, in some cases changes to the number and size of classes have been made for matter of better legibility.

The four samples obtained from an elevation of only 1260 m are precipitation samples from the locality of Vergötschen. Seven samples originating from an altitude between 2100 and 2149 m represent spring waters of lowest elevation. Fourteen samples have been taken between 2150 and 2199 m. Those include four precipitation samples from a rain gauge at 2152 m and a pond sample from 2183 m. In addition to the sample from Fagge River at 2207 m, another eleven springs have been sampled at an elevation range of 2200 to 2249 m. Twelve waters stem from an altitude between 2250 and 2299 m including two out of three samples from Gepatschferner glacier itself. Furthermore, four springs located within the highest elevation level of 2300 to 2320 m were also analysed. Three are on moraine site B on the left valley

side, while one originates from Gepatschferner glacier. Indeed, the altitude of all glacier samples is subject to some deviation due to large volume losses experienced at the Gepatschferner glacier snout and differences in timing of sampling and ALS (airborne laser scanning) survey.

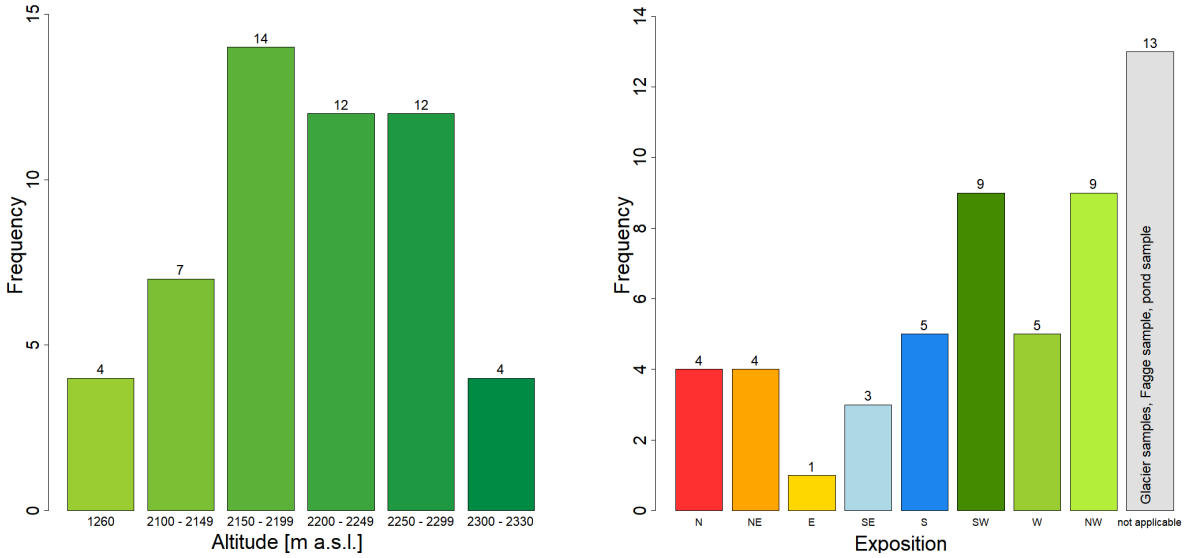

Figure 25: Frequencies of all samples taken for ^{129}I analysis regarding altitude (left) and exposition (right)

Exposition

As well as varying levels of elevation, samples taken from Upper Kaunertal Valley also have different expositions. The resulting frequency distribution of the selected 53 samples regarding exposition is shown in Figure 25 (right). Four samples have been taken from north and northeast exposed locations. Only one sample has been collected from east facing slopes. Three more samples stem from southeast facing slopes. Five samples are characterized by south and west orientation. Nine samples are characterised by southwest and northwest exposition. However, exposition is not an applicable parameter for all samples. Consequently, information on exposition is not to be found for precipitation and glacier samples as well as the pond sample and the sample from Fagge River.

Slope

Slope gradients associated with selected sampling locations are presented as frequency distribution in Figure 26. Inclination of the sampled slopes varies between 12° and 49°, with only one sample derived from

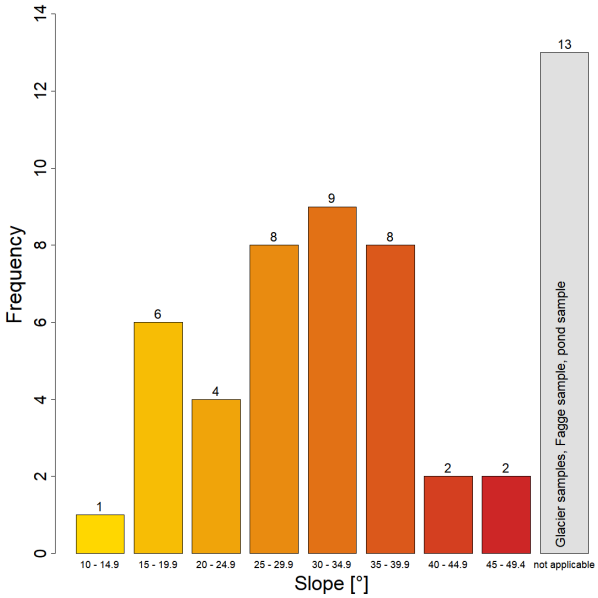

Figure 26: Frequencies of all samples taken for ^{129}I analysis regarding slope

a slope less than 14.9°. Six samples originate from slopes between 15° to 19.9°. Another four samples stem from parts of the study area that are characterized by a slope of between 20° and 24.9°. With eight, nine and eight samples, the majority of waters have been sampled from slopes between 25° to 29.9°, 30° to 34.9° and 35° to 39.9°. Two more samples fall into the class of 40° and 44.9°. Another two samples originate from slopes greater than 45°. As already the case for exposition, slope is not a reasonable parameter for all samples. Hence, a total of thirteen samples (precipitation samples, the pond sample, Fagge samples, glacier samples) are marked as non-applicable.

Year of deglaciation/ time since last glacial cover

The year that a certain sampling location has been deglaciated can been identified (c.f. Figure 27). However, large and dissimilar time steps within available data only allow to narrow the actual year of deglaciation and the time passed since glacial cover down to their minimum.

Only two spring samples originate from a location, which has been deglaciated at least since 1922 and is therefore free of glacial cover for a minimum 93 years. With 27 cases, the majority of samples has been taken from an area that is at least deglaciated since 1971 and is accordingly free of glacial coverage for minimum 44 years. In an area that more recently became part of the proglacial, four samples have been taken from zones that have been deglaciated at least since 2006. Another four sampling locations were deglaciated in 2012 at the latest. Five samples are found within the most recent proglacial area, which only became free of ice in 2015. Naturally, the three samples of glacial runoff and glacier ice stem from an area that is still glaciated. As this parameter does not apply for collected precipitation, these samples are marked as not applicable.

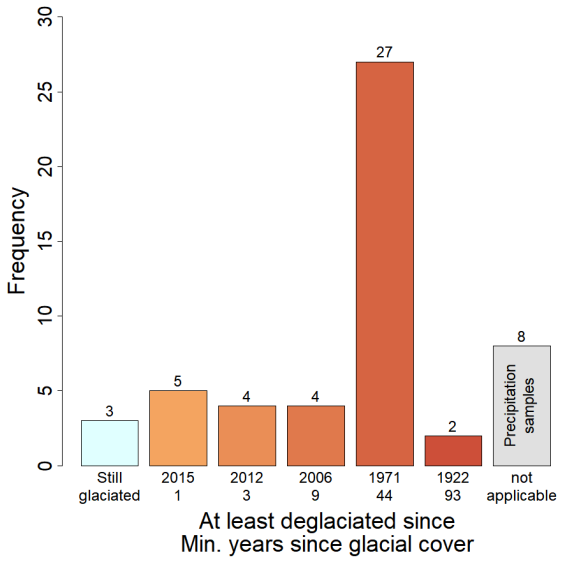

Figure 27: Frequencies of all samples taken for ^{129}I analysis regarding year of deglaciation/time since glacial cover

Water temperature

Results of routine temperature measures of spring and glacier waters and their frequency distribution is illustrated in Figure 28. The temperature of as many as eighteen springs sampled is below four degrees Celsius and therefore just above freezing. Within this class, only three waters have been sampled directly from the glacier. Another eight springs have shown temperatures between 4 °C and 7.9 °C. Seven samples were characterized by a temperature range of 8 °C to 11.9 °C. Six springs lie within a range of 12 °C to 15.9 °C and four springs have shown temperatures greater or equal to 16 °C but below 20 °C. With the pond, only one

sample is associated with a comparatively high temperatures of 23.6 °C. Temperature measurements of precipitation samples have not been conducted and temperature records of KT-I 74 JL are missing.

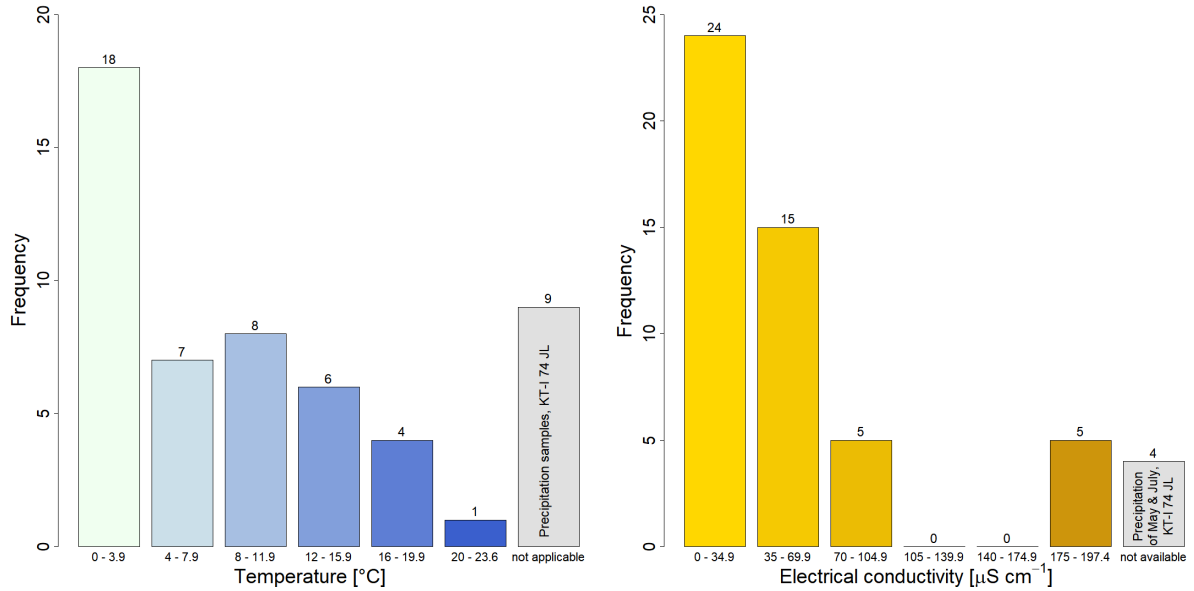

Figure 28: Frequencies of all samples taken for ^{129}I analysis regarding water temperature (left) and electrical conductivity (right)

Electrical conductivity

As with temperature measures, electrical conductivity has also been determined for sampled waters. Dimensions and frequencies of electrical conductivity in selected springs of Upper Kaunertal Valley are shown in Figure 28 (barplot on the right). 24 out of 53 samples are characterised by very low electrical conductivity (below 35 µS cm^{-1}). Another 15 springs follow with values between 35 µS cm^{-1} and 69.9 µS cm^{-1}, while only five samples range between 70 µS cm^{-1} and 104.9 µS cm^{-1}. None of the springs measured are found within the wide range of 105 µS cm^{-1} to 174.9 µS cm^{-1}, whilst five samples are characterised by comparatively high electrical conductivity values above 175 µS cm^{-1}, with the highest value measured as 197.4 µS cm^{-1}. Samples with noticeable high electrical conductivity values originate from moraine site B on the left valley side which has been deglaciated since the 1970s, as well as the only recently deglaciated site D on the right valley side. In contrast to temperature measurements, measures of electrical conductivity have also been conducted for precipitation samples. Yet, conductivity records for precipitation collected at the monitoring station of the Austrian Central Institute for Hydrography at Vergötschen are missing for May and June, as well as the sample KT-I 74 JL.

5.1.2 Descriptive statistics - ^{129}I concentration of glacial waters, spring waters and precipitation

^{129}I concentrations of 53 samples from Upper Kaunertal Valley sampled between July and October 2015 have been determined through AMS measurements at VERA. A summary on measures of central tendency and statistical dispersion of ^{129}I concentration of different waters, is further given in Table 2. Results of ^{129}I concentration of collected precipitation are given in Table 3. Concentrations of glacial ice, glacial runoff, Fagge River, a pond sample and several spring waters are given separately in Table 4. ^{129}I concentrations and absolute errors are expressed as atoms per litre. Relative errors are given in percentage. Time of sampling and sample specifications are listed additionally. For information on sample location please refer to the appendix. Visual information on ^{129}I concentration levels of different sample categories can additionally be gained from Figure 30.

^{129}I concentrations of all waters sampled from Upper Kaunertal Valley range from $1.10 \pm 0.23 \cdot 10^6$ to $1.14 \pm 0.04 \cdot 10^9$ at L^{-1}. This includes precipitation, glacial- and spring waters as well as the samples from the Fagge River and a small pond but not any duplicate samples. The median ^{129}I concentration of all samples is $1.86 \cdot 10^7$ at L^{-1}, the mean value is given as $9.07 \cdot 10^7$ at ^{129}I L^{-1}. Mean values as well as minimum and maximum values are highly influenced by extreme values present within the data set, while the median is recognised as less sensitive and more robust measure (Kronthaler, 2016) and probably more appropriate given the present data. The standard deviation, as measure for statistical dispersion, is $1.85 \cdot 10^8$ at ^{129}I L^{-1}.

Table 2: Descriptive statistics of ^{129}I concentration of different sample categories including blanks

Descriptive Statistics

	n	Minimum	1st Quantile	Median	Mean	3rd Quantile	Maximum	Std. deviation
All samples	53	1.10E+06	7.62E+06	1.86E+07	9.07E+07	8.87E+07	1.14E+09	1.85E+08
Precipitation samples	8	8.87E+07	1.17E+08	1.41E+08	1.77E+08	2.26E+08	3.24E+08	8.26E+07
Spring samples	42	1.10E+06	7.50E+06	1.50E+07	7.99E+07	2.71E+07	1.14E+09	2.04E+08
Glacier samples	3	1.68E+06	2.59E+06	3.50E+06	3.82E+06	3.82E+06	6.29E+06	1.90E+06
Blank samples	8	7.15E+05	9.69E+05	1.07E+06	1.08E+06	1.14E+06	1.60E+06	2.44E+05

Combined ^{129}I concentrations of precipitation from Vergötschen and the study area itself provide the highest median and mean values measured. Those measurements of central tendency are $1.41 \cdot 10^8$ and $1.77 \cdot 10^8$ at ^{129}I L^{-1}. The precipitation samples also hold the highest minimum value of $8.87 \pm 0.16 \cdot 10^7$ at ^{129}I L^{-1} within all categories. The precipitation sample with the highest ^{129}I concentration yielded $3.24 \pm 0.11 \cdot 10^8$ at L^{-1}. Standard deviation is $8.26 \cdot 10^7$ at L^{-1}.

Precipitation at the monitoring station of the Austrian Central Institute for Hydrography at Vergötschen (altitude of 1263 m a.s.l.) shows concentrations roughly between 1 to $3 \cdot 10^8$ at ^{129}I L^{-1}. Results from the second rain gauge within the study area at an altitude

of 2152 m a.s.l. present ^{129}I concentrations in precipitation between $8.87 \pm 0.16 \cdot 10^7$ and $2.94 \pm 0.06 \cdot 10^8$ at L^{-1}. This concentration range is similar to those observed from precipitation nearly 900 m below. Sample KT-I 50 JL originating from a small pond solely feed by rainwater evidences a ^{129}I concentrations very much in line with precipitation concentrations.

Table 3: ^{129}I concentrations and errors of precipitation samples from Upper Kaunertal Valley. Period of sampling and sample descriptions are further given

Sample				^{129}I Concentration			
Code		Time of Sampling	Description	^{129}I Concentration [at L^{-1}]		Absolute Error [at L^{-1}]	Relative Error [%]
KT-I	HR	20.05 – 12.06	Precipitation (1263 m)	1.07E+08	±	2.06E+06	1.93
KT-I	HR	12.06 – 22.07	Precipitation (1263 m)	3.24E+08	±	1.10E+07	3.40
KT-I	HR	22.07 – 07.08	Precipitation (1263 m)	1.48E+08	±	2.20E+06	1.49
KT-I	HR	20.08 – 13.09	Precipitation (1263 m)	1.34E+08	±	2.63E+06	1.96
KT-I	RS	09.06 – 20.07	Precipitation (2152 m)	2.94E+08	±	6.24E+06	2.12
KT-I	RS	20.07 – 20.08	Precipitation (2152 m)	1.20E+08	±	2.95E+06	2.47
KT-I	RS	20.08 – 13.09	Precipitation (2152 m)	2.03E+08	±	5.46E+06	2.69
KT-I	RS	13.09 – 08.10	Precipitation (2152 m)	8.87E+07	±	1.55E+06	1.75

The category of spring samples includes all 40 springs of unknown origin that have been sampled in Kaunertal Valley and corresponds to all samples listed as a spring in Table 4. All samples derived from known origin, such as precipitation, the glacier, the pond or Fagge River are hence excluded. The results of spring waters indicate a wide variety in ^{129}I concentrations, spanning three orders of magnitude from $1.10 \pm 0.23 \cdot 10^6$ to $1.14 \pm 0.04 \cdot 10^9$ at L^{-1}, with the highest standard deviation of $2.04 \cdot 10^8$ at ^{129}I L^{-1}. As such some waters show even lower ^{129}I concentrations as samples taken from glacier ice or glacial runoff. Specifically KT-I 45 and KT-I 77 taken in July as well as KT-I 45 and KT-I 77 from September show values below the minimum ^{129}I concentration derived from glacier samples. Concentrations of named samples are as small as measured blank values (c.f. section 5.1.5.2). Further there are three more samples (KT-I 29, 78, 74) having concentrations within the range of glacier ice and glacial runoff. Most spring waters show medium ^{129}I concentrations ranging between values of glacial ice and precipitation. Median and mean values are given as $1.50 \cdot 10^7$ and $7.99 \cdot 10^7$ at ^{129}I L^{-1}. At the upper end of the measured scale, some spring waters coincide with the concentration range set up by gained precipitation values, while others (KT-I 20 JL, 27 JL, 68 JL) even exceed those. However, the ^{129}I concentration of KT-I 68 July is the only sample out of all waters measured that has been determined to be above 10^9 at L^{-1}.

Samples from glacier ice and glacial runoff evidence lowest ^{129}I concentrations with measured values of $1.68 \pm 0.20 \cdot 10^6$ at L^{-1} (KT-I 95), $3.50 \pm 0.29 \cdot 10^6$ at L^{-1} (KT-I 80) and $6.29 \pm 0.27 \cdot 10^6$ (KT-I 93). Median and mean values of $3.50 \cdot 10^6$ and $3.82 \cdot 10^6$ at ^{129}I L^{-1} are considerably lower than those of precipitation or spring samples. Standard deviation of the three glacier samples sums up to $1.90 \cdot 10^6$ at ^{129}I L^{-1}.

Table 4: ^{129}I concentrations and errors of spring and glacier samples from Upper Kaunertal Valley. Time of sampling and sample descriptions are further given

Sample				^{129}I Concentration			
Code		Time of Sampling	Description	^{129}I Concentration [at L^{-1}]		Absolute Error [at L^{-1}]	Relative Error [%]
KT-I	04	July	Fagge River	3.78E+07	±	6.59E+05	1.74
KT-I	05	July	Spring	1.31E+07	±	4.94E+05	3.77
KT-I	06	July	Spring	8.98E+06	±	3.76E+05	4.18
KT-I	08	July	Spring	1.20E+07	±	3.45E+05	2.87
KT-I	20	July	Spring	3.90E+08	±	8.13E+06	2.09
KT-I	26	July	Spring	2.73E+07	±	6.57E+05	2.40
KT-I	27	July	Spring	5.52E+08	±	1.10E+07	1.99
KT-I	29	July	Spring	2.02E+06	±	2.03E+05	10.04
KT-I	32	July	Spring	2.87E+08	±	7.01E+06	2.44
KT-I	40	July	Spring	7.62E+06	±	4.06E+05	5.33
KT-I	41	July	Spring	1.71E+07	±	6.04E+05	3.54
KT-I	42	July	Spring	9.54E+06	±	3.69E+05	3.87
KT-I	43	July	Spring	1.51E+07	±	5.67E+05	3.77
KT-I	45	July	Spring	1.46E+06	±	2.22E+05	15.22
KT-I	46	July	Spring	2.19E+07	±	6.40E+05	2.93
KT-I	47	July	Spring	7.14E+06	±	2.76E+05	3.87
KT-I	48	July	Spring	6.57E+06	±	4.11E+05	6.25
KT-I	49	July	Spring	1.89E+07	±	8.87E+05	4.69
KT-I	50	July	Pool	1.42E+08	±	5.23E+06	3.69
KT-I	51	July	Spring	1.56E+07	±	5.26E+05	3.38
KT-I	52	July	Spring	2.54E+07	±	8.69E+05	3.43
KT-I	61	July	Spring	1.22E+07	±	3.78E+05	3.09
KT-I	65	July	Spring	9.35E+06	±	3.56E+05	3.81
KT-I	66	July	Spring	4.02E+07	±	1.67E+06	4.16
KT-I	67	July	Spring	2.37E+07	±	1.07E+06	4.51
KT-I	68	July	Spring	1.14E+09	±	4.04E+07	3.56
KT-I	74	July	Spring	5.36E+06	±	3.78E+05	7.05
KT-I	76	July	Spring	7.84E+06	±	3.62E+05	4.62
KT-I	77	July	Spring	1.35E+06	±	2.66E+05	19.71
KT-I	78	July	Spring	2.72E+06	±	3.26E+05	11.95
KT-I	79	July	Spring	2.70E+07	±	6.34E+05	2.35
KT-I	80	July	Glacier Ice	3.50E+06	±	2.87E+05	8.20
KT-I	90	July	Spring	1.86E+07	±	7.93E+05	4.27
KT-I	91	July	Spring (Dead Ice)	2.31E+08	±	3.94E+06	1.71
KT-I	92	July	Spring	4.19E+07	±	2.15E+06	5.13
KT-I	93	July	Glacial Runoff	6.29E+06	±	2.68E+05	4.26
KT-I	94	July	Spring	5.38E+07	±	1.13E+06	2.09
KT-I	95	July	Glacier Ice	1.68E+06	±	1.98E+05	11.81
KT-I	68	August	Spring	8.28E+07	±	1.33E+06	1.60
KT-I	45	September	Spring	1.10E+06	±	2.32E+05	21.07
KT-I	48	September	Spring	6.54E+06	±	3.32E+05	5.07
KT-I	49	September	Spring	1.49E+07	±	4.84E+05	3.25
KT-I	65	September	Spring	8.29E+06	±	3.33E+05	4.02
KT-I	67	September	Spring	2.60E+07	±	5.96E+05	2.29
KT-I	77	September	Spring	1.40E+06	±	2.69E+05	19.13

5.1.3 Monthly variability of measured ^{129}I concentrations

^{129}I concentration in precipitation has been determined for several months in order to ascertain monthly variability. ^{129}I concentration in precipitation generally does not vary greatly across different months. At the locality of Vergötschen May/June, July/August and August/September precipitation is fairly similar. July precipitation is two to three times greater than values reported from preceding and following months. Variations of monthly precipitation collected at the study area are somewhat larger. Similarly to Vergötschern, July precipitation is highest here too. The concentrations determined in precipitation for the following months are lower, although August/September precipitation reaches a concentration above $2 \cdot 10^8$ at $^{129}I\ L^{-1}$. Then again, the September/October value is clearly lower. In fact it is the only precipitation mixed sample with a ^{129}I concentration in the order of 10^7.

As with precipitation, the ^{129}I yield of selected springs were not only measured for July but also for one following month as indicated by different months listed as *time of sampling* in Table 4. Selection of individual springs happened based on first measurement results and in order to support or challenge first results. Months to be tested where then individually chosen based on weather conditions during sampling of the selected springs. Months with highest temperatures and lowest disturbance by rainfall on sampling date where favoured. In the case of sample KT-I 45, 48, 65, 67 and 77 favoured weather conditions occurred during September sampling, while spring KT-I 68 was (besides July) only present in August. A summary on ^{129}I concentration differences of all six springs tested for two dates is given in Table 5.

The ^{129}I concentration of the July and September samples of spring KT-I 45 are similar and lie within each other's range of measurement uncertainty. Nearly identical ^{129}I concentrations and barely existing variability between the selected months have been reported for spring KT-I 48. A concentration of $6.57 \pm 0.41 \cdot 10^6$ at $^{129}I\ L^{-1}$ measured in July is accompanied by $6.54 \pm 0.33 \cdot 10^6$ at $^{129}I\ L^{-1}$ measured in September. Similar findings have been made for spring 77 ($1.35 \pm 0.27 \cdot 10^6$ at $^{129}I\ L^{-1}$ in July and $1.40 \pm 0.27 \cdot 10^6$ at $^{129}I\ L^{-1}$ in September), where concentrations between months appear to be identical. Waters of spring KT-I 65 and 67 show absolute variation between the months that are outside of measured error ranges. Yet, variations of ^{129}I concentration did stay within the same order of magnitude. This does not apply for sampling site 68. Here variability between July and August is very high and spans two orders of magnitude. As mentioned before the July concentration represents the by far highest value measured in Kaunertal Valley. Therefore, the sample of KT-I 68 JL is treated specifically in section 5.1.7. Vast differences between the samples of this specific spring are therefore not to be overestimated at this point.

The analysis on monthly variabilities of spring waters within the study area certainly covers neither enough cases nor a sufficient time period. Presented results can clearly not be used to infer general assumptions. Nonetheless, they represent first estimations about monthly ^{129}I variations within the study area.

Table 5: Comparison of monthly variability of ^{129}I concentration (including errors) of selected springs in Upper Kaunertal Valley

Sample				^{129}I Concentration			
Code		Time of Sampling	Description	^{129}I Concentration [at L^{-1}]		Absolute Error [at L^{-1}]	Relative Error [%]
KT-I	45	July	Spring	1.46E+06	±	2.22E+05	15.22
KT-I	45	September		1.10E+06	±	2.32E+05	21.07
KT-I	48	July	Spring	6.57E+06	±	4.11E+05	6.25
KT-I	48	September		6.54E+06	±	3.32E+05	5.07
KT-I	65	July	Spring	9.35E+06	±	3.56E+05	3.81
KT-I	65	September		8.29E+06	±	3.33E+05	4.02
KT-I	67	July	Spring	2.37E+07	±	1.07E+06	4.51
KT-I	67	September		2.60E+07	±	5.96E+05	2.29
KT-I	68	July	Spring	1.14E+09	±	4.04E+07	3.56
KT-I	68	August		8.28E+07	±	1.33E+06	1.60
KT-I	77	July	Spring	1.35E+06	±	2.66E+05	19.71
KT-I	77	September		1.40E+06	±	2.69E+05	19.13

5.1.4 Measurement uncertainties

Taking into account results of ^{129}I concentration presented above, specified measurement uncertainties have to be considered for any sample. Calculated errors include AMS measurement errors of $^{129}I/^{127}I$ ratio as well as net weight uncertainties introduced during sample preparation. Mean measurement uncertainty for samples from Kaunertal Valley (including duplicates) is 5.52 %. Standard deviation, at 6.15 %, is high as a wide error range exists due to large differences in ^{129}I concentration magnitude of various samples. In general, the value of error seems to relate to the dimension of ^{129}I concentration, where samples with naturally low initial ^{129}I amounts are associated with largest errors. This is caused by the measurement procedure of ^{129}I by AMS, where ^{129}I atoms are counted as single events and repeated measurements are averaged (Klipsch, 2005; Szidat, 2000). For instance the sample with the lowest detected ^{129}I concentration (KT-I 45 (2)) coincides with the sample that has the highest error value of 36.31 %. Other low-level samples are likewise characterised by high error values, e.g. 15.22 % (KT-I 45 JL), 19.71 % (KT-I 77 JL), 19.13 % (KT-I 77 SEP) and 21.07 % (KT-I 45 SEP). On the contrary precipitation samples (including duplicates) which are among the samples with the highest ^{129}I concentrations show fewer errors with a mean relative error of 2.25 ± 0.61 %.

5.1.5 Quality control

5.1.5.1 Duplicate samples

Three pairs of total analytical duplicates have been individually treated and analysed for evaluation of sample treatment and measurement precision. Table 6 compares the ^{129}I concentration values determined for one spring- and two precipitation samples and their respective duplicates.

The first duplicate pair was taken from spring KT-I 45 in July (c.f. Figure 21). The samples have been determined to contain a ^{129}I concentration of $1.46 \pm 0.22 \cdot 10^6$ at L^{-1} and $7.48 \pm 2.71 \cdot 10^5$ at $^{129}I\ L^{-1}$, which is the lowest concentration measured in all samples from Upper Kaunertal Valley. The concentrations determined are of similar range, yet the two duplicates do not, given their associated uncertainties, overlap. Duplicates do not necessarily show identical measurement results as a result of natural variation or the heterogeneity of spring waters (Geboy and Engle, 2011). Hence, this duplicate measurement is still seen to confirm reproducibility of ^{129}I concentration results and as an indicator of good operational procedure.

Another duplicate was taken from the composite sample of precipitation in the period of 22.07.2015 to 12.08.2015 at the lower altitude rain gauge. Analysis has proven a ^{129}I yield of $1.48 \pm 0.02 \cdot 10^8$ at L^{-1} and $1.51 \pm 0.03 \cdot 10^8$ at L^{-1}. Recognizably, the concentration values correspond. This time the total uncertainties associated with both samples also overlap. Results of these duplicate samples prove the reproducibility and quality of the measurement procedure.

Table 6: ^{129}I concentrations and errors of selected samples of Upper Kaunertal Valley and their duplicate

Sample				^{129}I Concentration			
Code		Time of Sampling	Description	^{129}I Concentration [at L^{-1}]		Absolute Error [at L^{-1}]	Relative Error [%]
KT-I	45	July	Spring	1.46E+06	±	2.22E+05	15.22
KT-I	45 (2)	July	Duplicate	7.48E+05	±	2.71E+05	36.31
KT-I	HR	20.05 – 12.06	Precipitation (1263 m)	1.07E+08	±	2.06E+06	1.93
KT-I	HR (2)	20.05 – 12.06	Duplicate	1.34E+07	±	3.98E+05	2.98
KT-I	HR	22.07 – 07.08	Precipitation (1263 m)	1.48E+08	±	2.20E+06	1.49
KT-I	HR (2)	22.07 – 07.08	Duplicate	1.51E+08	±	2.64E+06	1.75

The correspondence of the first two duplicates, could not be achieved with the third duplicate tested. The duplicate of the composite precipitation sample taken from Vergötschen between 20.05 and 12.06.2015 did not deliver similar ^{129}I concentrations as its counterpart. The concentration of the original sample was measured to be $1.07 \pm 0.02 \cdot 10^8$ at $^{129}I\ L^{-1}$, while the duplicates concentration has been determined as $1.34 \pm 0.04 \cdot 10^7$ at $^{129}I\ L^{-1}$ (c.f. Table 6). As such, the deviating concentration measurements of both sample and duplicate exceed associated uncertainties and vary by more than one magnitude. The duplicate sample KT-I HR 20.05 – 12.06 (2) contains a ^{129}I concentration about eight times lower than its counterpart taken from the very same composite sample. Moreover, the concentration of the duplicate is the by far the lowest concentration measured for all precipitation samples. It is neither comparable with precipitation measures originating from an altitude of 1260 m or 2150 m a.s.l. (c.f. Table 3). Geboy and Engle (2011) state that measures for duplicate samples do not necessarily need to be identical, they may even vary widely due to heterogeneity or natural variation. However, the precipitation duplicate was taken from the same well-mixed, homogenous, composite precipitation sample. It is therefore not to be expected that deviating

results for ^{129}I measurements are justified by natural variations. Reasonable doubts concerning the validity of the duplicate are raised. Concerns are reinforced by literature. European precipitation is believed to be of ^{129}I concentration above 10^8 (López-Gutiérrez et al., 2000a) or $3 \cdot 10^7$ at L^{-1} (Aldahan et al., 2007), respectively. On balance, it is assumed that the duplicate sample cannot be trusted and the original sample is more likely to display the true concentration of the May/June precipitation, as it is also well in line with precipitation measures of other months (c.f. Table 3). In doing so, it is believed that there have been one or more errors during sampling, treatment or measurement that have caused differing results, but these errors can no longer be identified.

5.1.5.2 Blanks

In order to monitor potential ^{129}I contaminations during sampling, storage, treatment and measurement procedure to ensure quality control every eighth sample prepared was a blank sample. Results of ^{129}I concentration measurements, including errors, for the total of eight blanks are given in Table 7. Blank values range between $7.15 \cdot 10^5$ and $1.60 \cdot 10^6$ at $^{129}I\ L^{-1}$, with a mean ^{129}I concentration of $1.08 \pm 0.25 \cdot 10^6$ at L^{-1}. Average measurement error is $1.01 \pm 0.43 \cdot 10^5$ at L^{-1} or 9.11 ± 2.28 %.

Table 7: ^{129}I concentrations and errors of blank values from each run of sample treatment

Sample			^{129}I Concentration			
Code		Description	^{129}I Concentration [at L^{-1}]		Absolute Error [at L^{-1}]	Relative Error [%]
KT-I	B1 JL	Blank	1.05E+06	±	7.20E+04	6.86
KT-I	B2 JL	Blank	1.60E+06	±	1.88E+05	11.71
KT-I	B3 JL	Blank	7.15E+05	±	6.41E+04	8.98
KT-I	B4 JL	Blank	1.12E+06	±	1.15E+05	10.26
KT-I	B5 JL	Blank	8.45E+05	±	5.26E+04	6.23
KT-I	B6 JL	Blank	1.18E+06	±	1.13E+05	9.58
KT-I	B7 JL	Blank	1.01E+06	±	6.57E+04	6.53
KT-I	B4 S	Blank	1.08E+06	±	1.38E+05	12.74

The ^{129}I concentration of most samples differ from those of the blank samples by one order of magnitude or more. Though, samples with a very low initial amount of ^{129}I, e.g. glacier ice believed to be of old origin or springs believed to be fed by old waters, are naturally lacking large concentration and partly plot within the range of blank values. A comparison of ^{129}I blank concentration and ^{129}I concentration of different sample categories, using Wilcoxon-rank-sum-test, assured a statistically significant difference on a level of 0.001 for all samples, precipitation samples and spring samples. Even glacier samples differentiate significantly from blank values by a level of 0.05 (c.f. Table 9).

5.1.6 Altitude correction

Iodine concentration in precipitation is believed to decrease with increasing altitude (Fabryka-Martin, 1984). Yet, only a few studies, examining altitude effects on iodine isotopes and more specifically ^{129}I, exist. Gilfedder et al. (2007) has shown that total iodine concentrations in snow more than halves over an elevation change of 840 m, indicating the importance of iodine depletion due to orographically induced lifting. Aerosol studies confirm that stable iodine as well as ^{129}I decrease by a factor of 1.5 or by one order of magnitude over an altitude change between Vienna (202 m a.s.l.) and Zugspitze/Sonnblick (2962/3106 m a.s.l.) (Jabbar et al., 2012a). ^{129}I deposition fluxes at Fiescherhorn glacier (~ 3900 m) have further shown to be a factor of six lower than precipitation from Zurich (408 m) (Reithmeier et al., 2006). Consequently a strong altitudinal gradient is suggested for ^{129}I, "*typical for water-soluble atmospheric trace species which are removed from the atmosphere in the course of days by precipitation scavenging"* (Reithmeier et al., 2006, p. 5891). However, progressive isotopic depletion by rain might not be the only factor conditioning vertical ^{129}I gradients as gaseous injections of NRF, a main source of ^{129}I, do not reach high elevations (Jabbar et al., 2012a).

Mindful of observations made in previously published studies, the question of whether spring samples from Upper Kaunertal Valley are affected by a regional altitude effects is raised. Yet, when looking at a scatter diagram for an initial overview, no general tendency of decreasing ^{129}I concentrations with increasing altitude were apparent. A classification of ^{129}I concentrations by distinct classes of altitude following Sturges (1926), also fails to indicate distinct trends (Figure 29). Spring samples of highest elevation are associated with the lowest median, yet the range of the box is fairly wide, nearly covering those of all other altitude classes. Moreover, median values of the first four classes rise with increasing altitude rather than fall. Based on present data no altitude effect may be inferable.

That an altitude effect could not be identified based on the spring data set may be ascribed to the low number of samples (n=39). Moreover, altitude effects might be masked as the origin and composition of the spring waters used to identify present altitude effects are largely unknown, but are believed to be of different ^{129}I concentration. At the same time it is also possible that moisture within the study area is released evenly during rain events. After all the proglacial area is characterized by comparably small differences in both elevation and distance. Altitude effects due to orographic lifting may be reduced or not develop at all. Elevation effects could also be suppressed due to the regional setting of Upper Kaunertal Valley within the Alpine range, as it has been shown that typical altitude gradients of other isotopes are often not observed in interior mountains (Kendall et al., 2004).

Given mentioned uncertainties associated with a potential altitudinal effect, it is believed that the application of any corrections for spring samples ^{129}I concentration would introduce errors than rather reduce them. Altitudinal corrections are therefore not performed.

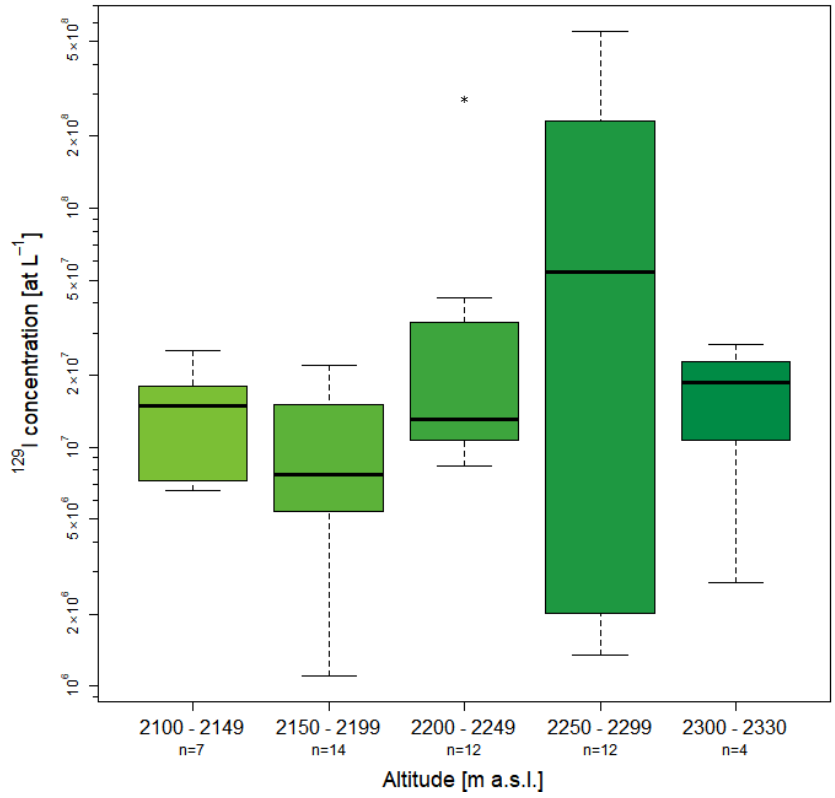

Figure 29: Distribution of ^{129}I concentration of spring samples by altitude

5.1.7 Outlier treatment

Statistical measures of central tendencies and dispersion have been delineated in the above section 5.1.2. Regarding minimum and maximum values, it has been mentioned that single samples are characterised by concentration values that are beyond the generally observed spectrum. Observations located conspicuously far off the central part of a measurement are outliers (Steland, 2016). Groß (2010) further argues that outliers need particular attention due to their wide controls on correlations between variables. On account of this, the following section is dedicated to outlier detection and treatment.

Boxplots can be valid instruments to visualise dispersion of ordinal and metric variables (Kronthaler, 2016). Additionally, they assist in outlier detection as extreme values are displayed (Steland, 2016). Figure 30 compares ^{129}I concentration values of different sample categories in a combined box-whisker-plot based on the measures of dispersion and central tendencies stated in Table 2. The upper and the lower edge of each box are defined as the first and the third quartile of the underlying data set. Fifty percent of all samples are placed within the box. The height of the box corresponds to the interquartile range (IQR). The bold line drawn within the box represents the median value of the data set. In order to identify extreme values the IQR is used to compute restrictions, so called *fences.* Inner and outer fences are calculated based on Eq. (11) and Eq. (12) respectively.

$$Q_1 - 1.5 \cdot IQR \quad \& \quad Q_3 + 1.5 \cdot IQR \qquad \text{Eq. (11)}$$

$$Q_1 - 3 \cdot IQR \quad \& \quad Q_3 + 3 \cdot IQR \qquad \text{Eq. (12)}$$

The so called *whiskers* range from the first (Q_1) or the third quantile (Q_3) to the outermost values within the inner fences. Single values that plot outside the inner but within the outer fences are so called *outs* and are visualised as unfilled circles. Most extreme data points, that lie outside the outer fences (*far outs*), are marked with an asterisk (c.f. Figure 30)(Benesch, 2013).

Figure 30 visualises varying ^{129}I concentration ranges of different sample categories, with ^{129}I concentration given on a logarithmic scale for issues of graphical representation. Concentrations of spring samples from Upper Kaunertal Valley have, clearly, the widest span. Glacier and precipitation samples cover a much more distinct concentration range. Indeed, a smaller number of observations exists for them. From a visual point, differences between concentration levels of glacier- and precipitation are evident as no intersections between both sample categories are apparent. The range of spring samples however covers those of both precipitation samples and glacier samples. Some springs even exceed minimum values of glacier samples down to the level of blank values, as well as maximum values measured for precipitation. As indicated, highest values of spring samples have been automatically classified as outliers. Five of them as far outs, one spring value as out. That the lowest spring values are also located within the whiskers seems confusing at first sight, but it is a result of the logarithmic scale used. Glacier and precipitation samples do not contain any samples that spread out across inner or outer fences.

Observations do not become outliers due to technical definition, but rather because of conscious classification. Insofar boxplots can provide indications on values that might be classified as outliers, at the most (Benesch, 2013). Extreme values, identified by the box-whisker plot must not be excluded from the present data set automatically. In fact, many of the extreme concentrations within the spring data set are plausible values. Four of them are still in line with concentrations measured in precipitation and may simply indicate a corresponding origin. Even those samples exceeding the values within the precipitation range might be valid measurements given the unknown origin of the water and its composition. However, the ^{129}I concentration of KT-I 68 JL has been determined as to be in the order of 10^9. A concentration twice as high as the concentration of the second highest spring sample and more than thrice as high as the highest measured concentration of precipitation collected in the study area. In light of these extreme values, ^{129}I concentrations of the same spring were also determined for the following sampling period. Contrary to July, August concentrations of KT-I 68 are moderate and determined to be only $8.28 \pm 0.13 \cdot 10^7$ at $^{129}I\ L^{-1}$. More than thirteen times less than specified for the July sample. The waters origin and composition is subject to change and waters of July and August may be completely different. Nonetheless, monthly variability of others spring nearby (KT-I 67 and 65) has been shown to be small (c.f. 5.1.3).

Given the extreme value measured and without published reports of similar high values in a comparable setting as well as non-compliant measures in the following month, the validity of KT-I 68 JL is doubted. The sample is therefore excluded from any further analysis or discussion. Figure 30 shows the concerned sample marked in red.

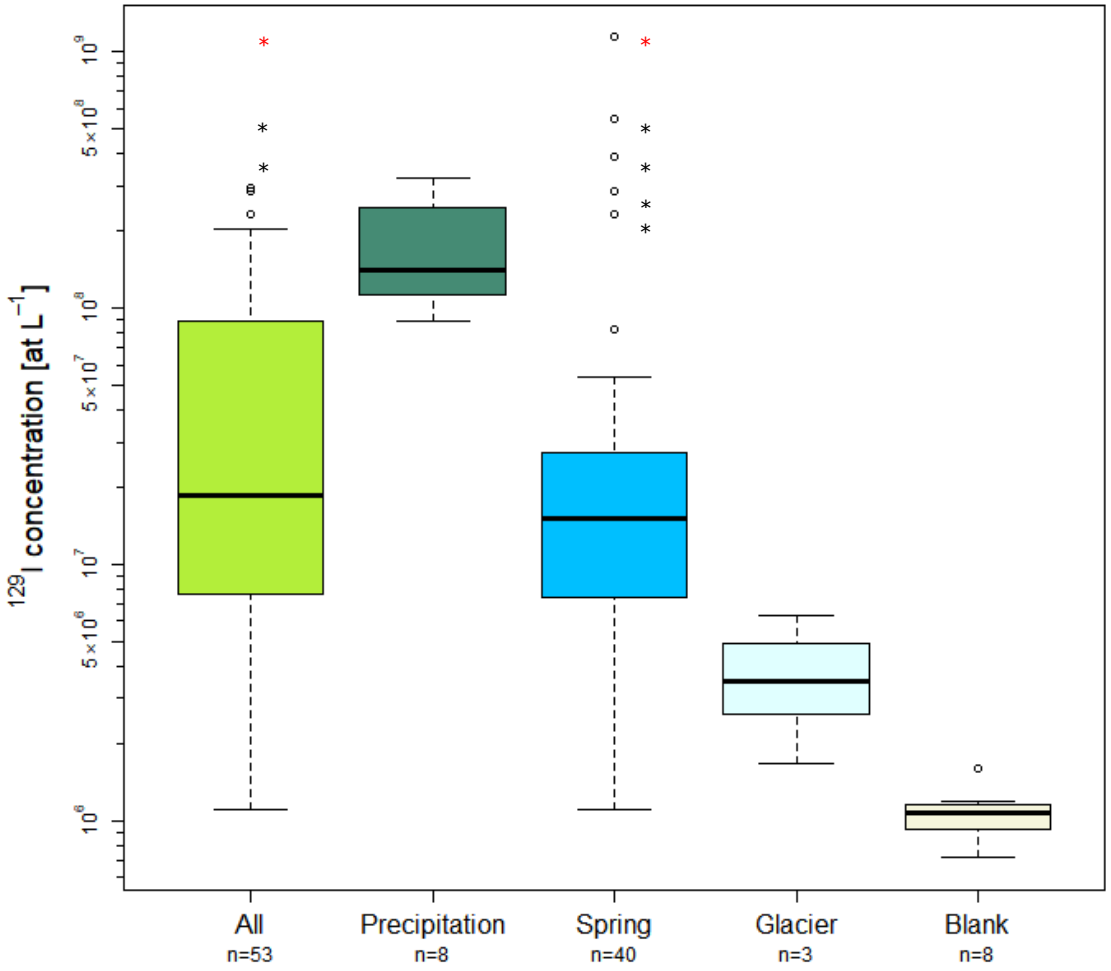

Figure 30: Summary of ^{129}I concentration ranges of different sample categories including blank samples. Red selections mark one extreme values, excluded from further data analysis

5.2 Statistical analysis

Statistical analysis of ^{129}I results carried out are presented in section 5.2. They focus on the assessment of differences between sample categories as well as on correlation of ^{129}I results with independent topographic and hydro-chemical parameters.

5.2.1 Statistical assessment of differences between samples

Evident differences of ^{129}I concentration between precipitation, glacial- and spring waters have been pointed out in the previous section. Yet, objective proof is needed. Assessments presented in this section aim to provide statistically grounded information on hypothesized differences of ^{129}I concentration between different types of waters.

In order to define whether a parametric or a non-parametric test is to be used, a Shapiro-Wilk test of normality was first applied for all sample categories. A histogram of the samples ^{129}I concentration is further shown in Figure 31, ^{129}I concentration is logarithmised due to visualisation issues. Results of the Shapiro-Wilk test declare that normal distribution is, regardless of approximations of normality shown in the histograms and with a probability of 99.9 %, not a given for all samples categories. Precipitation, glacier and blank samples are, following Shapiro-Wilk, normally distributed. However, only a very low number of samples is available for each of these categories. A summary of the Shapiro-Wilk test results is given in Table 8. As the normal distribution assumption is not a given for all sample categories, a non-parametric test has to be applied.

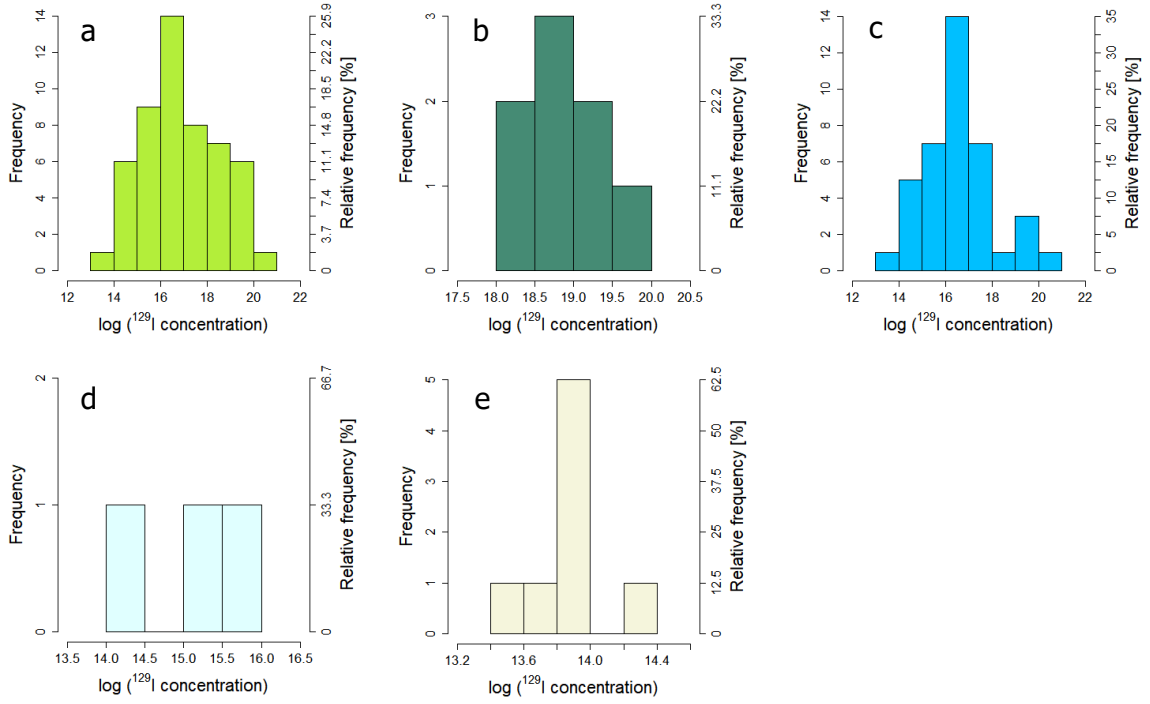

Figure 31: Histogram of logarithmised ^{129}I concentration of all samples (a), precipitation samples (b), spring samples (c) and glacier samples (d) and blank samples (e)

Table 8: Shapiro Wilk Test of normality for ^{129}I concentration of all sample categories including blanks

Test of Normality

	Shapiro Wilk		
	n	p- value	
All samples	52	4.41E-10	***
Precipitation samples	8	0.123	
Spring samples	39	9.49E-11	***
Glacier samples	3	0.7691	
Blank samples	8	0.4437	

* p <0.05, ** p <0.01, *** p <0.001

The non-parametric alternative to a two-sample t-Test for unpaired samples is the Wilcoxon rank sum test. The Wilcoxon rank sum test checks for differences in central tendency of two samples and is robust against outliers (Steland, 2016). It is equivalent to the Mann-Whitney-U-test (Benesch, 2013). Wilcoxon's test requires independent and random samples with equal or similar distributions (Hedderich and Sachs, 2016; Steland, 2016). Using QQ-plots (Groß, 2010), the latter seems not to be met for all variables. This could be conditioned by the small sample sizes (n=3, n=8, n=8, c.f. Table 8) present in different sample categories and might not have been an issue if more data would have been available. The alternative for unequally distributed samples is the median test, a test described to be of little power (Benesch, 2013). Further the median test is facing suggestion for its retirement from general use (Freidlin and Gastwirth, 2000). It has hence been decided to use the Wilcoxon rank sum test as it is assumed that with sufficient large sample sizes variables would follow the same or a similar distribution. The Wilcoxon rank sum test was executed as two samples Wilcoxon test. During the test both samples are combined, sorted according to size and ranked. Taken apart, ranks of one sample should either tend to be small or large, if the test is to be significant (Groß, 2010) and samples originate from different populations. Results of the rank sum test, given in Table 9, confirm what has been described earlier. Differences within precipitation, spring and glacial waters are significant with levels of 0.05, 0.01 or 0.001. All categories further show significant differences

Table 9: Results of Wilcoxon Rank-Sum Test for all sample categories including blanks

Wilcoxon Rank-Sum test

	p-values									
	All samples		Precipitation samples		Spring samples		Glacier samples		Blank Samples	
All samples			0.002	**	0.364		0.038	*	0.000	***
Precipitation samples	0.002	**			0.000	***	0.012	**	0.000	***
Spring samples	0.365		0.000	***			0.041	*	0.000	***
Glacier samples	0.038	*	0.012	**	0.041	*			0.012	*
Blank Samples	0.000	***	0.000	***	0.000	***	0.012	*		

* p <0.05, ** p <0.01, *** p <0.001

to blank samples. Even differences tested for the total of samples and single sample categories are significant. Individually the difference between all samples and spring samples is not statistically verifiable.

5.2.2 Correlation of ^{129}I concentration and topographic and hydro-chemical parameters

Topographical and hydro-chemical characteristics of samples of Kaunertal Valley have been presented in section 5.1.1. If a correlation between described parameters associated with certain waters and their ^{129}I concentration exists and weather this association correlates sufficiently strong to ^{129}I values is assessed in the following.

Scatter diagrams support analysis of correlations. Information on relations between two metric attributes is provided and potentially existing dependencies may be derived (Benesch, 2013). Figure 32 shows several scatter diagrams, where ^{129}I concentration of springs is given as dependent variable on the y-axis and varying explanatory variables are plotted on the x- axis. Regardless of whether plotting altitude, slope or temperature as independent variables, the result are rather diffuse. Springs at high altitude are characterized by both high ^{129}I content as well as low ^{129}I content. Lowest ^{129}I yields are found in waters of low elevation as well as higher parts of the study area. Low as well as high slopes correlate with springs of medium ^{129}I concentrations, while the highest concentration range is found around medium slopes. Waters with highest temperatures show moderate ^{129}I concentrations. Interestingly, springs

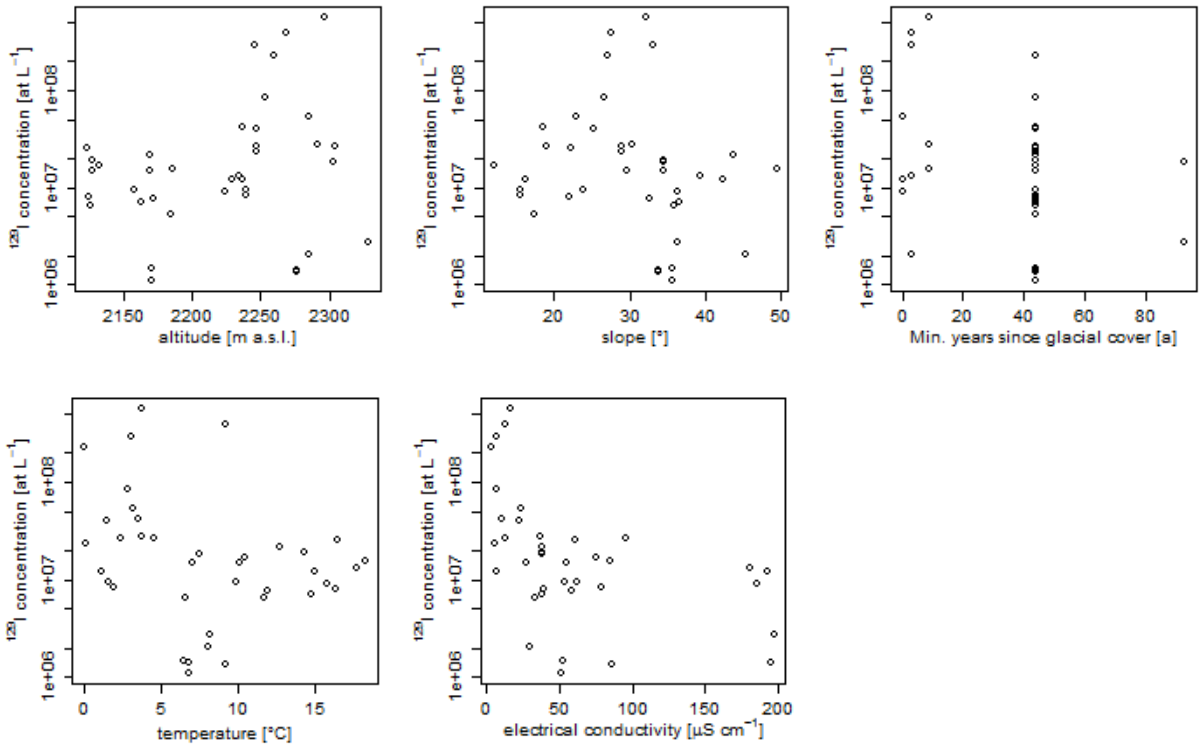

Figure 32: Scatter diagrams of ^{129}I concentration and metric explanatory variables: altitude (top left), slope (top centre), min. years since glacial cover (top right), temperature (bottom left) and electrical conductivity (bottom centre)

below 5 °C are characterized by medium and high ^{129}I values, while lowest ^{129}I concentrations plot at temperatures between 5 and 10 °C. Summarizing the visual information from the scatter diagrams, neither altitude nor slope, nor years since glacial cover or temperature seem to sufficiently correlate with measured ^{129}I concentrations. If electrical conductivity is plotted against ^{129}I concentrations, however, the existence of a negative correlation may be derived. Highest values of electrical conductivity are only associated with low or medium ^{129}I values. Furthermore, with lower electrical conductivity, a water's ^{129}I concentration seems to increase. The function of the correlation thereby seems to be exponential rather than linear, but as not all springs of lowest ^{129}I concentration show high electrical conductivity, the correlation may be less strong.

Scatter plots provide indications on the strength of a correlation between two variables (Groß, 2010), though no numerical value is derived from it (Benesch, 2013). The assessment of correlations with the use of statistical coefficients is therefore essential.

As Pearson's correlation coefficient is restricted to linear correlations between variables, Spearman's rank correlation coefficient is the favoured measure of association. Spearman's correlation coefficient is a measure for monotonic relationships, suitable for metric and ordinal data. Further it is almost robust against outliers (Benesch, 2013). Spearman's rank correlation coefficients are not only generated for the spring sample-set alone, but also for all samples and the combined data-set of spring and glacier. Not all variables meaningfully correlate to the named categories. Therefore, correlations for the variables, *years since glacial cover* and *temperature,* are conducted solely for glacier samples and spring samples. The variable of *slope* is further tested for correlations with spring data only. The independent variables of *altitude* and *electrical conductivity* are assessed for all sample categories.

Results of Spearman's rank correlation are given in Table 10. The number of asterisks indicates the level of significance of single correlations. Three out of five topographic and hydro-chemical variables tested show significant correlation with waters ^{129}I concentration, namely slope, temperature and electrical conductivity. All three are negative. No correlations of significance have been found to exist between the ^{129}I concentration and altitude, nor with time passed since deglaciation.

Table 10: Result of Spearman's Rank Correlation Test between ^{129}I concentration of different sample sets and independent variables

Spearman's rank correlation ρ

	Altitude	Slope	Min. years since glacial cover	Temperature	Electrical Conductivity
All samples	-0.178	-0.334 *	-	-	-0.400 **
Spring & glacier samples	0.130	-0.334 *	-0.039	-0.130	-0.334 *
Spring samples	0.290	-0.334 *	-0.245	-0.334 *	-0.566 ***

* p <0.05, ** p <0.01, *** p <0.001

The correlation between ^{129}I concentration and slope are significant for all categories tested. Spearman's correlation coefficient is the same for each category. This is unsurprising because precipitation and glacier samples as well as the Fagge and the pond samples were excluded as slope is not an applicable parameter for those samples. Hence, all three data sets only include the spring samples. Even though the relationship is of statistical significance, after Zöfel (2008), a correlation coefficient of -0.33 is a weak relationship. This also explains why no correlation has been stated in the scatterplots before. The same applies to the significant negative correlation between the ^{129}I concentration of springs and their temperature. The highest correlation coefficient of -0.57 is found for electrical conductivity when tested for spring samples only. It is of highest significance ($p<0.001$). Additionally, the relationship between electrical conductivity is also significant for the categories of all samples as well as spring and glacier samples, yet with lower coefficients and significance. A correlation coefficient above -0.5 indicates a correlation of medium strength (Zöfel, 2008).

As well as metric and ordinal topographic and hydro-chemical characteristics, the nominal variable of exposition has been checked for possible correlations with the ^{129}I concentration of sampled waters. As Spearman's correlation coefficient is not suitable for nominal data, a possible correlation between ^{129}I concentration and exposition has been tested using Cramer's V contingency coefficient (Benesch, 2013). Distribution of springs' ^{129}I concentration across different expositions is shown in Figure 33. Clearly, different orientations overlap each other and none of the categories covers an entire concentration range of its own. Certainly, springs exposed to the south are characterised by a very high median. However, the upper quantile is

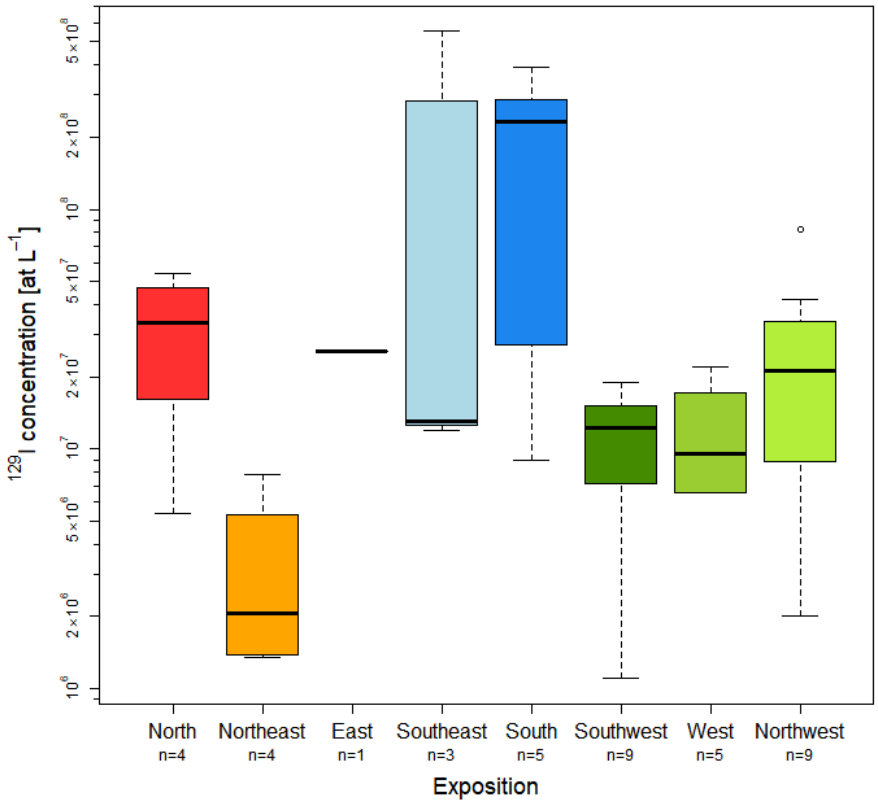

Figure 33: Distribution of ^{129}I concentration of spring samples by exposition

similar to those of southeast exposed springs and the upper end of the whisker is even smaller. Samples from the northeast facing slopes show the lowest median. Yet, its minimum does not differ much from those of the springs from southwest orientation. Springs of other expositions more or less coincide with each other within a small median ^{129}I concentration range of $9.54 \cdot 10^6$ to $3.36 \cdot 10^7$ at L^{-1}. The conducted Cramer's V of 0.0009 is very low. This acknowledges visual impression gained from the box-whisker-plot, that for springs tested, no correlation between ^{129}I concentration and the spring's exposition exists.
Particular influential parameters tested reveal weak to medium correlations with ^{129}I concentration. Nevertheless, independent variables might not only correlate with the waters ^{129}I concentration, but also with each other. In order to identify potential correlations between variables, scatter plots (c.f Figure 34) have been produced and Spearman's correlation coefficients (c.f. Table 11) have been calculated for numeric variables. For potential correlations of the nominal variable of exposition, Cramer's V has been checked (c.f. Table 12).

Table 11: Result of Spearman's Rank Correlation Test between numeric independent variables

Spearman's rank correlation rho

	Altitude	Slope	Min. years since glacial cover	Temperature	Electrical conductivity
Altitude		-0.066	-0.132	-0.510 ***	-0.095
Slope	-0.066		-0.148	0.510 **	0.241
Min. years since glacial cover	-0.132	-0.148		-0.074	0.123
Temperature	-0.510 ***	0.510 **	-0.074		0.582 ***
Electrical conductivity	-0.095	0.241	0.123	0.582 ***	

* p <0.05, ** p <0.01, *** p <0.001

Following Spearman's coefficients, significant correlation exist exclusively with the variables of spring temperature. Positive correlation between temperature and slope and temperature and electrical conductivity have been found as well as a negative correlation between temperature and altitude. Strength of the significant correlation varies between 0.510 and 0.582. That characterises a medium relationship (Zöfel, 2008) between named variables and is also apparent in the scatter plots of the correlation matrix. Results of Cramers' V further indicate low correlations (Zöfel, 2008) between exposition and time since last glacial cover, temperature as well as electrical conductivity.

Table 12: Results of Cramers' V between nominal variable of exposition and other independent variables

Cramers' V

	Altitude	Slope	Min. years since glacial cover	Temperature	Electrical conductivity
Exposition	0.02	0.16	0.423	0.35	0.311

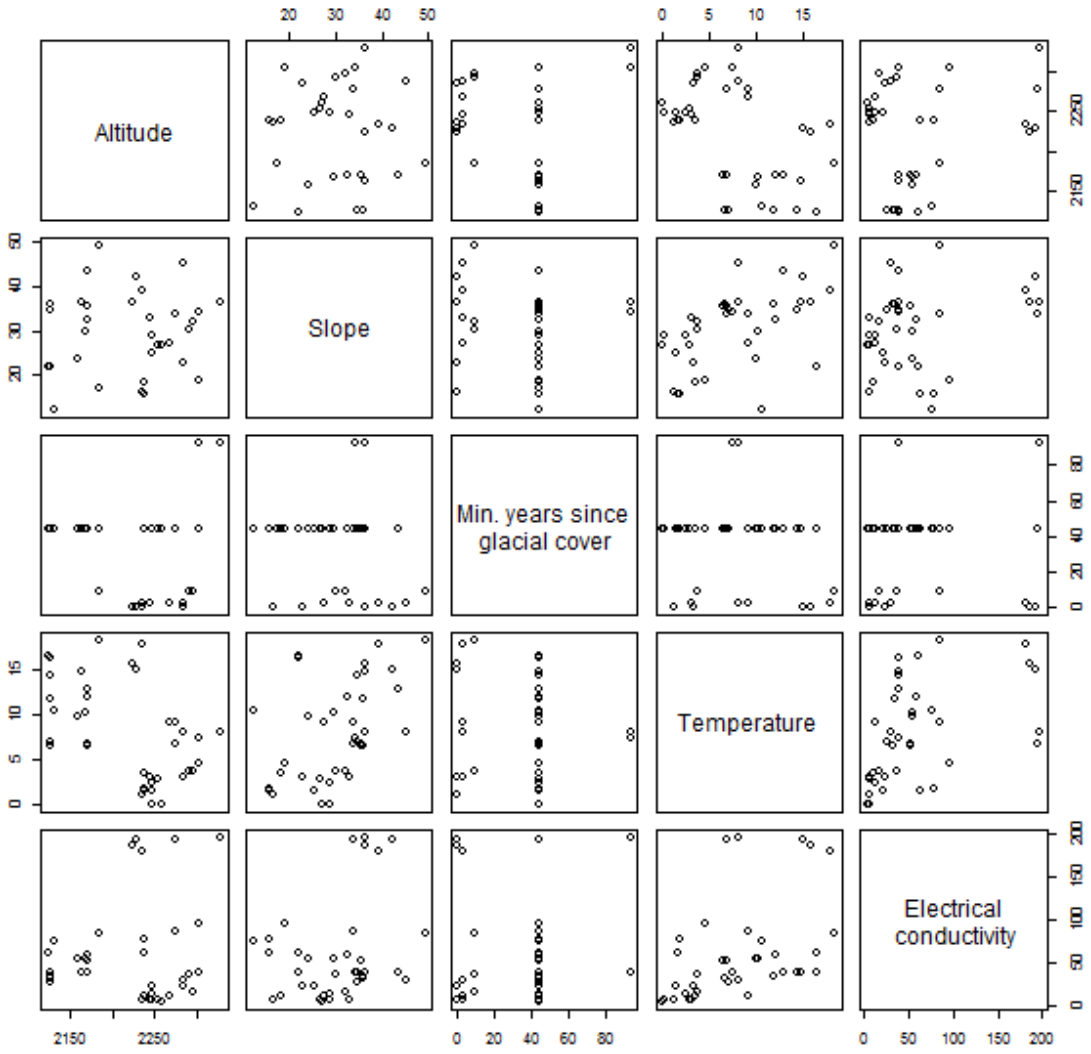

Figure 34: Correlation matrix of independent variables altitude [m], slope [°], min. time since glacial cover [a], temperature [°C] and electrical conductivity [µS cm^{-1}]

5.3 Ground surface temperature

Ground surface temperatures on the prominent LIA lateral moraine on the right valley side have been measured at ~ 20, 40 and 60 cm depths for the time period of July 2015 to July 2016. Daily mean ground surface temperatures are shown in Figure 35 and are compared to daily mean air temperatures and daily precipitation measured at Gepatschalm climate station.

In the first months recorded, ground surface temperature oscillates in tandem with air temperature. If air temperature increases so does the GST. Expectedly the temperature response in the upper centimetres is stronger and decreases with increasing ground depth (e.g. two temperature peeks in August in Figure 35). During cooling periods, however, GST of different depths converge and differences between depths minimise. Unfortunately the temperature record for 60 cm depth exists only up to September 11th 2015. The record for the time period after the conducted interim backup was lost due to a failure of the temperature logger. The iButton was, despite the covering balloon, most likely affected by water damage as indicated by rust marks on the device. As a consequence all data values recorded have been lost. Hence, GST record for 60 cm depth is available only up to mid-September.

Highest mean daily temperatures of 20.47 ± 1.74 °C (20 cm depth), 18.83 ± 0.88 °C (40 cm depth) and 17.64 ± 0.58 °C (60 cm depth) were reached on 12.08.2015 and 13.08.2015. A second peak with somewhat lower temperatures is evident at the end of August and the beginning of September. Following temperatures continue to oscillate but show a decreasing trend. Mean daily air temperatures first reach below zero in mid-October. From the end of November up to end of March air temperatures are mainly characterized by sub-zero temperatures of varying degree down to -18.9 °C. Yet, distinct days of positive mean temperature have been intermittently recorded.

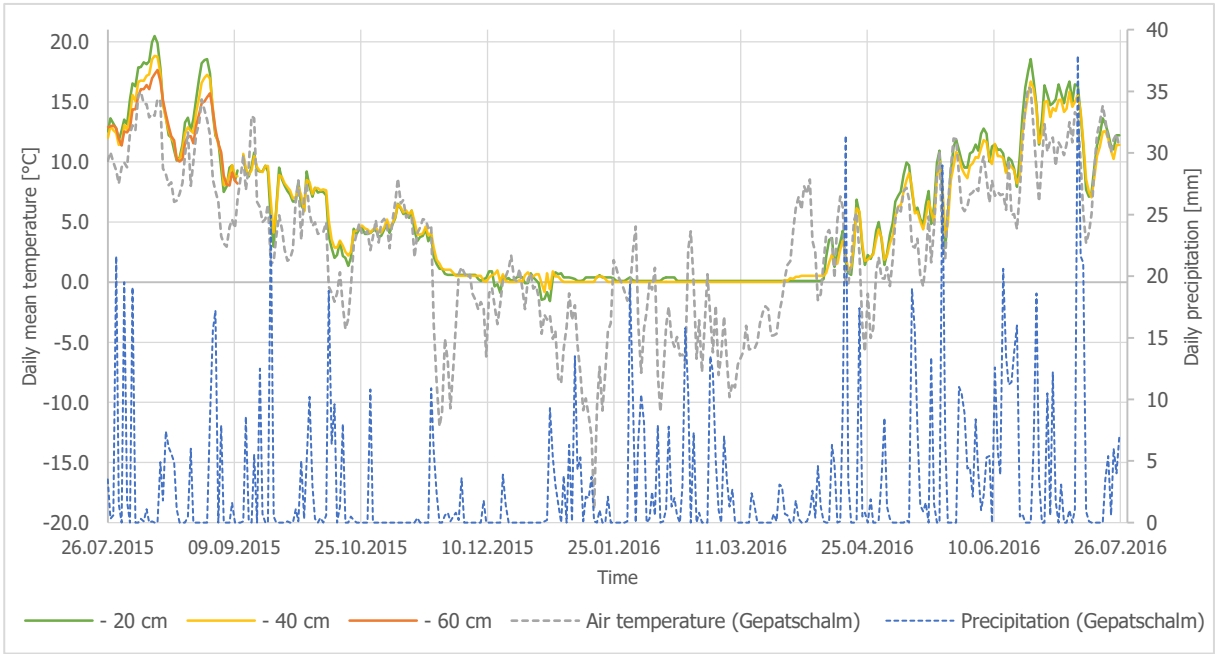

Figure 35: Daily mean ground surface temperatures in 20, 40 and 60 cm depth, measured between 26.07.2015 and 26.07.2016 at a distinct location of moraine site A, precipitation and air temperature data from Gepatschalm have kindly been provided by the PROSA project

GST oscillates following air temperatures up to the first major cooling period at the end of November, but seem to be decoupled from air temperature variations during the following months. A cold snap at the end of November reduces GST at both 20 and 40 cm depths, yet ground temperatures do not drop below zero and stabilise between 0 °C to 1 °C for roughly two weeks. A three week period of varying GST follows and ground temperatures intermittently fall below zero around the turn of the year. Precipitation during this time was minimal. Thereafter, precipitation events are recorded more frequently and GST levels off once more at just above freezing point. The period of early January to early April is characterized only by minor temperature variations that eventually come to a halt in February. Mean GST from 5.1.2016 to 10.4.2016 is 0.18 ± 0.50 °C and 0.11 ± 0.50 °C at 20 cm and 40 cm depth respectively. By the end of March air temperatures increase again. Ground surface temperatures follow but are subject to a lag time of several days. Temperatures at 40 cm depth rise first but only by several fractions of a degree, while at the same time temperatures at 20 cm depth remain constant during the first days of positive air temperatures. By April 10th GSTs oscillate again following air temperatures and do not drop down to 0 °C anymore until the end of the measurement period.

For the entire measuring period mean GSTs are stated as 5.74 ± 0.52 °C at 20 cm depth and 5.56 ± 0.51 °C at 40 cm depth (c.f. mean air temperature at Gepatschalm is 3.0 °C). Mean GST for the depth of 60 cm could only be obtained for the period of 26.7.2015 to 11.9.2015 as a result of the failure of the device. It is 12.96 ± 0.52 °C at 60 cm depth in comparison to 13.47 ± 0.53 °C at 40 cm depth, 14.03 ± 0.56 °C at 20 cm depth and 10.2 °C air temperature. The GFI is -6.9 °C.day for 20 cm depth and -1.5 °C.day for 40 cm depth.

6 Discussion

Results presented in the preceding passages are put into context and are discussed in the following. In the first step, ^{129}I yield of waters from Kaunertal valley is compared with previously published literature on the subject. Different critical values necessary for relative age differentiation are applied and validated. Potential dead ice sites are identified. Correlations between ^{129}I concentrations and topographic or hydro-chemical parameters are assessed and the possibility of seasonal ice growth within the study area is evaluated based on local ground surface temperatures. Thereafter, implication of dead ice for sediment dynamics and sediment budget studies are specified.

6.1 Relative age dating

6.1.1 Comparison of ^{129}I concentrations published in literature

Reports on ^{129}I concentration in different environmental spheres are, as mentioned earlier, scarce (c.f. section 3.3) (Aldahan et al., 2009, 2007). Most of the present data relates to the hydrosphere. European research clearly focuses on North Sea, Baltic Sea and associated coasts (cf. Figure 17). Continental Europe is under-represented and so are high altitudes. Studies on ^{129}I concentration in Austrian's hydrosphere have not been found as research of Jabbar et al. (2012a, 2012b, 2013a) and Wallner et al. (2007) focuses on ^{129}I in air, aerosols, petrified wood and lignite. Quantification of ^{129}I concentration of natural waters has been conducted for a few other locations outside of Austria but within the Alpine foreland and within an aerial distance of less than 300 km from the study site. Still, knowledge on ^{129}I concentration at high altitudes is limited. Only a few studies by Gilfedder et al. (2007), Jabbar et al. (2012a) and Reithmeier et al. (2006) include samples from high altitudes or engage with the impact of elevation on (stable) iodine concentration. Despite scattered data availability, this section aims to put generated ^{129}I data from Kaunertal Valley into the context of latest research.

Precipitation

Aldahan et al. (2007) specify modern global precipitation to range between $1 \cdot 10^6$ and $6 \cdot 10^{10}$ at $^{129}I\ L^{-1}$. European precipitation is, due to proximity to operating nuclear reprocessing sites, however characterized by higher ^{129}I concentrations. While Aldahan et al. (2007) quote concentrations of between $3 \cdot 10^7$ and $6 \cdot 10^{10}$ at $^{129}I\ L^{-1}$ for European precipitation, López-Gutiérrez et al. (2000a) consider precipitation to be of a higher range of 10^8 to 10^{10} at $^{129}I\ L^{-1}$ and typically above 10^9 at L^{-1}. Referring to the latter, precipitation measured in Kaunertal Valley ranks at the bottom end of the scale. A comparison with precipitation measured within the broader region further confirms the low ^{129}I yield of rain from Kaunertal Valley.

The following comparisons of ^{129}I concentrations of Kaunertal Valley and precipitation from distinct locations within the broader Alpine region, referenced in literature, have to be considered cautiously. Temporal and spatial variability of precipitation is generally high and representativeness for a larger region cannot be presumed in general (Reithmeier et al., 2007). References have been selected to be closest to Kaunertal Valley but the linear distance between both locations may be

as much as ~ 300 km. Measurements of ^{129}I in precipitation in relative proximity to Kaunertal Valley exist for selected periods, roughly on a monthly basis, for the following locations: Swiss Alps 1983 to 1987 (Schnabel et al., 2001), Schauinsland (Black Forest) 1995, Brotjacklriegl (Bavarian Forest) 1994 to 1995 (Krupp and Aumann, 1999), Dübenbach (near Zurich) 1994 to 1997 (Schnabel et al., 2001), Marnate (Northern Italy) 1998 (Buraglio et al., 2001) as well as Stierberg (Upper Bavaria) 2003 to 2004 (Reithmeier et al., 2005). Comparison with more recent data cannot be accomplished as references covering recent years have not been found for the respective regions. The vast majority of precipitation from Alpine regions shows higher ^{129}I concentrations than precipitation collected in Kaunertal valley with values up to ~ $4 \cdot 10^{10}$ at L^{-1}. Precipitation from the Swiss Alps obtained between 1983 and 1987 shows slightly higher concentrations of $3.3 \cdot 10^{8}$ to $4.66 \cdot 10^{8}$ at $^{129}I\ L^{-1}$ (Schnabel et al., 2001). The named data sets contain four samples that are within the concentration range measured for precipitation in Kaunertal Valley. However, in none of these references does concentration of precipitation fall below $1 \cdot 10^{8}$ at $^{129}I\ L^{-1}$.

^{129}I concentration of precipitation from Kaunertal Valley is comparatively low to those of other studies. Indeed, assumptions on ^{129}I decrease with increasing altitude have been mentioned (Gilfedder et al., 2007; Jabbar et al., 2012a; Reithmeier et al., 2006) and precipitation values used for comparison have been derived mainly from lower altitudes. Exceptional cases are the samples taken from Schauinsland and Brotjacklriegel, which have been collected at 1205 m and 1016 m a.s.l. (Heideman, 1993; Krupp and Aumann, 1999). These altitudes are comparable to those of Vergötschen. However, precipitation from Vergötschen has considerably lower ^{129}I levels.

Supporting the presence of an ^{129}I elevation effect, as mentioned by Gilfedder et al. (2007), Jabbar et al. (2012a) and Reithmeier et al. (2006), with data from Kaunertal Valley is problematic. Three precipitation samples collected from the study area itself are associated with a sample from Vergötschen. But, only one of these exists for an identical period (August/September). The other precipitation pairs (June/July and July/August) differ by several days (c.f. time periods noted in Table 3) and indicate a decrease of ^{129}I concentration between 1263 and 2152 m a.s.l. of $3 \cdot 10^{7}$ and $2.8 \cdot 10^{7}$ at L^{-1}. Existing temporal discrepancies make it difficult to assess the validity of the altitudinal gradient suggested by those sample pairs. Especially as it seems equally plausible that concentration differences between both altitudes originate from rain of different air masses and their unique ^{129}I concentration, which are not covered by either one of the sample pairs. The August/September samples, however, are present for exactly the same time period. While the lower altitude sample has a concentration of $1.34 \cdot 10^{8}$ at $^{129}I\ L^{-1}$, precipitation collected at the higher altitude station contains $2.03 \cdot 10^{8}$ at $^{129}I\ L^{-1}$. These results would have been expected to be reversed and do not support ^{129}I decrease with increasing elevation hypothesized by others (Reithmeier et al., 2006; Jabbar et al., 2012a; Gilfedder et al., 2007).

The number of precipitation samples from Kaunertal Valley is, especially given partly diverged sampling periods, unsatisfactory to identify any altitudinal effects on ^{129}I concentration in precipitation. The altitudinal difference between the two sampling station is ~ 890 m and might not be sufficient to identify a distinct elevation effect. Since findings of Reithmeier et al. (2006) and Jabbar et al. (2012a) are based on much greater elevation differences of ~ 3500 m, 2750 m and 2900 m.

Nonetheless, Gilfedder et al. (2007) was able to show an altitudinal gradient for stable iodine in snow over roughly the same difference in height. Perhaps the interior location of Kaunertal Valley within the Central Alps also plays a vital role in undermining the altitudinal gradient of ^{129}I concentrations observed elsewhere. Similarly, typical altitude gradients of other isotopes are often not observed in interior mountains (Kendall et al., 2004).

Glacier ice and glacial runoff

Samples from Gepatschferner glacier are not the only records on ^{129}I concentration in glacial ice. Nine samples have been taken from a Greenland ice core covering the years 1900 to 1985 (Aldahan et al., 2007), and therefore, partly pre-nuclear times. Further, two ice cores from Fiescherhornglacier (Bernese Alps, Switzerland), roughly 200 km southwest from Gepatschferner glacier, have been analysed for ^{129}I concentration. Combined, both ice cores cover the time period of 1950 to 2002 with annual resolution (Reithmeier et al., 2006; Wagner, 1995) and provide a unique source of information on anthropogenic ^{129}I release history, starting from the very beginning (Reithmeier et al., 2006). European NRF started operating in 1951 (Sellafield), 1957 (Mercoule) and 1966 (LaHague) and the vast majority of ^{129}I introduced by nuclear weapon tests has not been disposed until 1957 (Snyder et al., 2010). Hence, the first years of the ice cores from Fiescherhornglacier could approximate pre-anthropogenic concentrations of Alpine glacial ice. Their record may further provide an approximation of a first critical value applicable for a distinction between modern waters influenced by nuclear activities and pre-nuclear waters free of any anthropogenic ^{129}I signal. However, comparatively small inputs of anthropogenic ^{129}I originating from early nuclear weapon tests have possibly enhanced the natural concentrations of the ice layers by 1950. Also, *"a relocation of ^{129}I deposited in one year to the layer of previous year(s) due to meltwater percolation and refreezing cannot be excluded"* (Reithmeier et al., 2006, p. 5894).

Glacial ice of Fiescherhornglacier associated with the year 1950 is characterised by a ^{129}I concentration of $1.01 \cdot 10^7$ at L^{-1}. The concentrations of ice layers from the following years document an increasing ^{129}I trend with annual fluctuations. From 1951 to 1958 concentrations vary from $5.5 \cdot 10^6$ to $3.28 \cdot 10^7$ at $^{129}I\ L^{-1}$. In later years, ^{129}I concentrations frequently reach levels of 10^8 at L^{-1} (Wagner, 1995). The highest value of the record reaches up to roughly $1 \cdot 10^9$ at $^{129}I\ L^{-1}$ (Reithmeier et al., 2006). Ice sampled directly from the tongue of Gepatschferner glacier revealed clearly lower ^{129}I concentrations than any ice layer of the Fiescherhornglacier since 1950. ^{129}I concentrations derived from Greenland ice are stated to be between $1 \cdot 10^6$ and $1 \cdot 10^7$ at L^{-1} (Aldahan et al., 2007). Because no numeric dates are named for the Greenland ice samples, it is assumed that samples of lowest concentrations are also associated with pre-nuclear time. Values of Gepatschferner glacier are in line with those. Nonetheless, neither records from glacial ice of Gepatschferner glacier, Fiescherhornglacier nor Greenland ice cap come close to the ^{129}I concentration of $3.7 \cdot 10^4$ at L^{-1} presumed as the natural ^{129}I content for the non-marine hydrosphere by Snyder et al., (2010). Glacial runoff of Gepatschferner glacier is further characterized by a slightly higher value of $6.29 \cdot 10^6$ at $^{129}I\ L^{-1}$, possibly caused by contributions of externally derived, modern atmospheric waters through rainfall, snowmelt (Bennett and Glasser, 2009) or seasonal ice.

Relatively lower concentration determined for ice of Gepatschferner glacier in comparison to Fiescherhornglacier may be explained by the latter's shorter distance to the sea, shorter distance to NRFs or its location in the interior of the Central Alps. Oceans are a main source of iodine for continental environment (Hou et al., 2009a) and distance to the coast is, aside from longitude and latitude, expected to cause highly variable isotopic concentration of glaciers (Aldahan et al., 2007). While differences in longitude and latitude are minor for Fiescherhorn and Gepatschferner glaciers, differences to Greenland are obvious and the validity of a comparison with Greenland ice is questionable. Alternatively, it seems possible that ^{129}I concentrations of glacier samples are lower because ice derived from Gepatschferner glacier snout was formed before 1945. If so, the ice would not contain the ^{129}I signal of early nuclear weapon testing and would represent the natural ^{129}I concentration. This cannot be assumed with certainty for the early samples of Fiescherhornglacier. However, as no numerical age is available for Gepatschferner glacier samples and reference values from other Alpine glaciers are missing, the cause of concentration differences between the two glaciers cannot be resolved at this point. Apart from that, comparisons with ^{129}I data from literature support the assumption that ice sampled from Gepatschferner glacier is likely to be of pre-nuclear origin or is at least not influenced by anthropogenic ^{129}I from European NRF.

Spring waters

Spring samples from Upper Kaunertal Valley are derived from small perennial and episodic springs, typically characterized by little discharge. Associated ^{129}I concentrations recline between $1.1 \cdot 10^6$ and $5.52 \cdot 10^8$ at L^{-1}, ranging below and beyond values measured for glacier and precipitation. Comparisons of measured values with ^{129}I concentrations from literature are difficult as references for spring waters of similar size have not been found. In general, a reduced ^{129}I concentration in rivers compared to precipitation is suggested due to iodine's affinity to soil organic matter (Herod et al., 2016; Reithmeier et al., 2007). More detailed information on ^{129}I concentration in rivers is poor and comparisons are practically unfeasible. Reports on global ^{129}I concentrations of (large) rivers exist, but focus on areas mainly outside of Europe (Snyder and Fehn, 2004). Only one reference has been found within the Alpine region, referring to a Swiss river (Hoehn et al., 1999). Conditions of Glatt River are non-comparable to those of springs from Kaunertal Valley. The Glatt River sample contains a ^{129}I concentration of $2 \cdot 10^9$ at L^{-1}, many times higher than those determined for any sample from Kaunertal Valley.

Blank samples

Comparable blank values published in literature are scarce, due to a general limited number of ^{129}I studies. Different sample matrixes and volumes as well as varying preparation and detection techniques further complicate direct comparisons. Blank values specified in literature are commonly referred to as $^{129}I/^{127}I$ ratios only. Even though details given in Reithmeier et al. (2010) and Szidat (2000) specify ^{129}I concentrations of blank values from water samples, data only allows for a rough comparison as blank values are referred to samples without itemising sample sizes. Blank values from Reithmeier et al. (2010) of 0.2 to $1.1 \cdot 10^6$ atoms ^{129}I per sample and from Reithmeier et al.

(2007) of 10^5 to 10^6 atoms ^{129}I per sample cover a similar range of magnitude as blank values presented herein. Average blank concentrations of 8.88 $\cdot 10^6$ atoms ^{129}I per sample which were stated by Szidat (2000) following similar sample treatment but using larger sample volumes (2 to 10 L).

In summation, the comparison of ^{129}I concentration measured in water samples of the study area and published concentration values from comparable waters in relative proximity is illustrated in Figure 36. The ^{129}I concentration in atoms per litre is plotted on the y-axis. The x-axis displays the year a specific sample has been taken or the year a sample is associated with, in case of ice cores samples from Fiescherhornglacier. Data points from Kaunertal Valley intentionally cover a time range associated with more than one year. This aims to increase readability and comparability. Nevertheless, all samples from Upper Kaunertal Valley originate from 2015. The bars and the top of the graphic further indicate the operation period of the European NRFs Sellafield, Marcoule and La Hague.

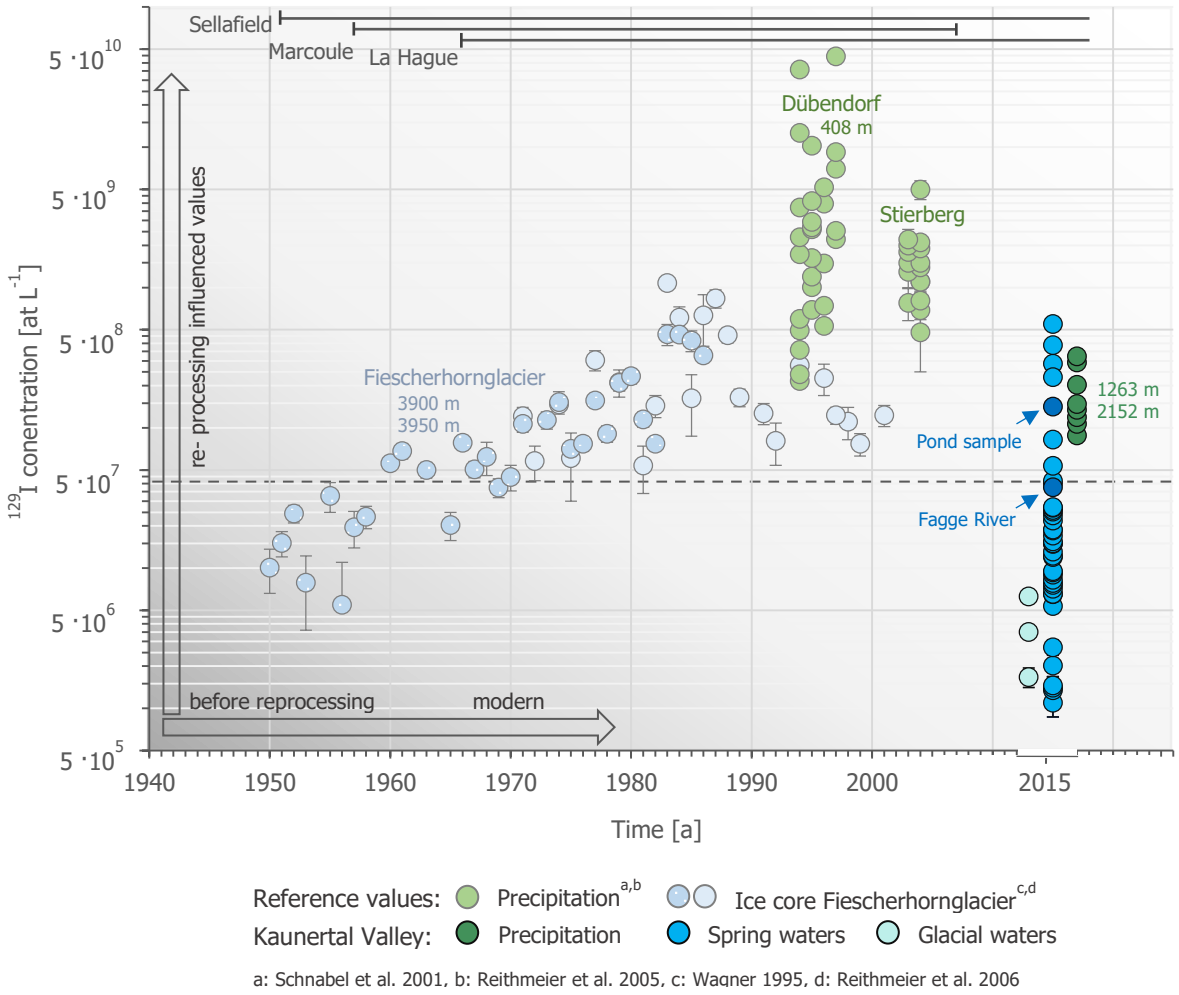

Figure 36: ^{129}I concentration of waters from Kaunertal Valley compared to values from literature; dashed line represents a first threshold to differentiate modern and pre-nuclear waters

6.1.2 Towards a critical value to address relative age determination

Results of ^{129}I measurements of springs from Kaunertal Valley provide concentration values covering several orders of magnitude. ^{129}I measures aimed at separating springs influenced by modern and pre-nuclear waters. In order to do so, a plausible threshold must be agreed upon. Since natural ^{129}I concentration levels within the non-marine hydrosphere and the cryosphere as well as their spatial and temporal variability are not known, defining a threshold value is not straightforward. Yet, finding another approach to assess ^{129}I concentration of springs tested is essential if relative age determination is to be applied. The following section reflects the process of decision making and addresses the applicability of considered thresholds.

Springs evolving from the lateral moraines are thought to be fed by melt water of buried dead ice, which remains from the LIA maximum. A spring solely fed by such melt waters should therefore have similar ^{129}I concentrations as glacier ice formed prior to nuclear age (c.f. conceptual model, section 3.5). The early ^{129}I concentration records of the Fiescherhornglacier ice core, not impacted by European NRF, might hold a threshold allowing its application to spring samples from Upper Kaunertal Valley. The ice core analysed by Wagner (1995) only contains one year which is not influenced by ^{129}I emissions of European NRF with certainty. Yet, establishing a threshold based on one value is critical and would completely exclude natural variability. Additionally, ice layers of 1953 and 1956 show lower concentrations than those of 1950 (c.f. Figure 36). When attempting to include natural ^{129}I fluctuations the ^{129}I concentration of a period greater than one year has to be considered. At the same time, it is crucial not to include ice layers with significant anthropogenic ^{129}I inputs. Given these needs, it is suggested to use the time range from 1950 to 1957 as 1957 coincides with the launching of the second European NRF Marcoule and further marks the beginning of the majority of ^{129}I releases by nuclear weapon testing (Snyder et al., 2010). The highest ^{129}I concentration recorded in the Fiescherhorn ice core between 1950 and 1957 is roughly $3.3 \cdot 10^7$ at L^{-1} (in 1955). Including measurement uncertainties, the value rises to $\sim 4 \cdot 10^7$ at $^{129}I\ L^{-1}$ (Wagner, 1995). This value hence represents a first literature-based approach towards a threshold for relative age classification.

Applying the threshold derived from Fiescherhornglacier to the waters of Upper Kaunertal Valley (c.f. Figure 36), 82 % of all spring samples plot below the threshold while only 18 % show higher ^{129}I concentrations. This translates to 32 springs classified as waters formed prior to the onset of nuclear age, while only seven springs would be classified as being of modern origin. Samples derived from the Gepatschferner glacier or precipitation would be classified accordingly. Yet the small number of springs derived from modern waters is striking. Especially as observations from the field demonstrate that springs categorised as of old origin, are only presents after intense rainfalls. That waters of Fagge River are of pre-nuclear origin is further questionable as Fagge is draining the total catchment area and is assumed to represent a mixture between sources of both origins (Bennett and Glasser, 2009). Also, the lowest ^{129}I concentration measured for precipitation from the study area is just twice as high as the threshold. On the whole, it is believed that the threshold derived from Fiescherhornglacier is too high especially when taking into account the

different geographical position of both locations (c.f. section 6.1.1.). The number of springs influenced by pre-nuclear waters are overestimated by the literature-based threshold. Literature seems not to provide sufficient information for classification. Hence, it is necessary to improve the threshold based on ^{129}I concentration derived directly from the study area.

If a threshold is to be adapted to the specifics of Kaunertal Valley it has to be grounded on the ^{129}I concentration measures of two ice samples and one run off sample from Gepatschferner glacier. These glacial samples have been proven to be significantly different to other sample categories (c.f. section 5.2). Yet, it is a low number of values to base a thresholds on and especially as the question regarding the true age of the ice samples remains unanswered, corresponding uncertainties arise. It is hence suggested that the deduced threshold is not seen as rigid but is rather understood as boundary for necessary delimitations. It is proposed that springs below the boundary value are recognised as high likelihood of being fed by old water. This likelihood increases with decreasing ^{129}I concentrations. At the same time, springs characterised by ^{129}I concentrations higher than the guideline are less likely to be of pre-nuclear origin with increasing concentration levels. Further delineating the waters origin, a second boundary based on ^{129}I concentration measured in precipitation is introduced. ^{129}I concentrations for precipitation have also been shown to be of significant difference to spring and glacier samples. The function of the second boundary is equally understood as those of the first boundary. Yet, this time samples that plot above the guiding value are very likely to originate from modern waters. The lower a spring's concentration falls the lesser its likelihood to be fed by modern water becomes (c.f. Figure 37).

Based on the higher value of two direct ice samples and its uncertainty, the first boundary might be set at $3.79 \cdot 10^6$ at $^{129}I\ L^{-1}$. Further, glacial runoff is, after modern meteoric water (Bennett and Glasser, 2009), expected to contain significant parts of melt water of pre-nuclear origin. Hence, the first guiding limit is raised up to $6.56 \cdot 10^6$ at $^{129}I\ L^{-1}$. The lowest ^{129}I concentration measured for precipitation, in consideration with associated measurement uncertainties, is set as second boundary at $8.71 \cdot 10^7$ at $^{129}I\ L^{-1}$.

Implementing these boundaries (c.f. Figure 37), a total of eight waters are most likely to be of old origin. If uncertainties associated with the measured ^{129}I concentrations of single springs are taken into account the number rises to nine. Four springs plot above the precipitation boundary and are most likely to be derived from modern waters. The twenty-six springs plotting between both boundaries have different likelihoods to be associated with old or modern waters. They may represent mixtures of varying proportions, such as Fagge River which ranks between both boundaries.

The spatial distribution of springs and their likely origin is further shown in Figure 38. Springs with high likelihood to originate from old waters can be found spread across the whole study area. All three waters sampled from the north-east exposed moraine complex C in July and September 2015 are associated with old waters. Their location is further characterized by high elevation (2276 and 2329 m) and steep slopes (34° and 36°). Additionally, another spring, situated on the lower elevated and less steep parts of the left valley side, is also most likely

fed by pre-nuclear waters. Old origin is further assigned to two, west and south-west oriented springs of the prominent moraine on the right valley side, measured in July as well as in September. The location of all named springs has been deglaciated between 1922 and 1971. Sampled just above the glaciers lateral margin, a ninth sample characterized by pre-nuclear origin is found on a very steep part of the right valley side. Springs clearly associated with modern waters are present on both sides of the valley, yet they are less scattered and found closer to today's glacier front. Waters that can neither be ascribed to modern nor old origin with certainty evolve all over the proglacial, close to the glacier snout as well as in areas that are furthest away from it.

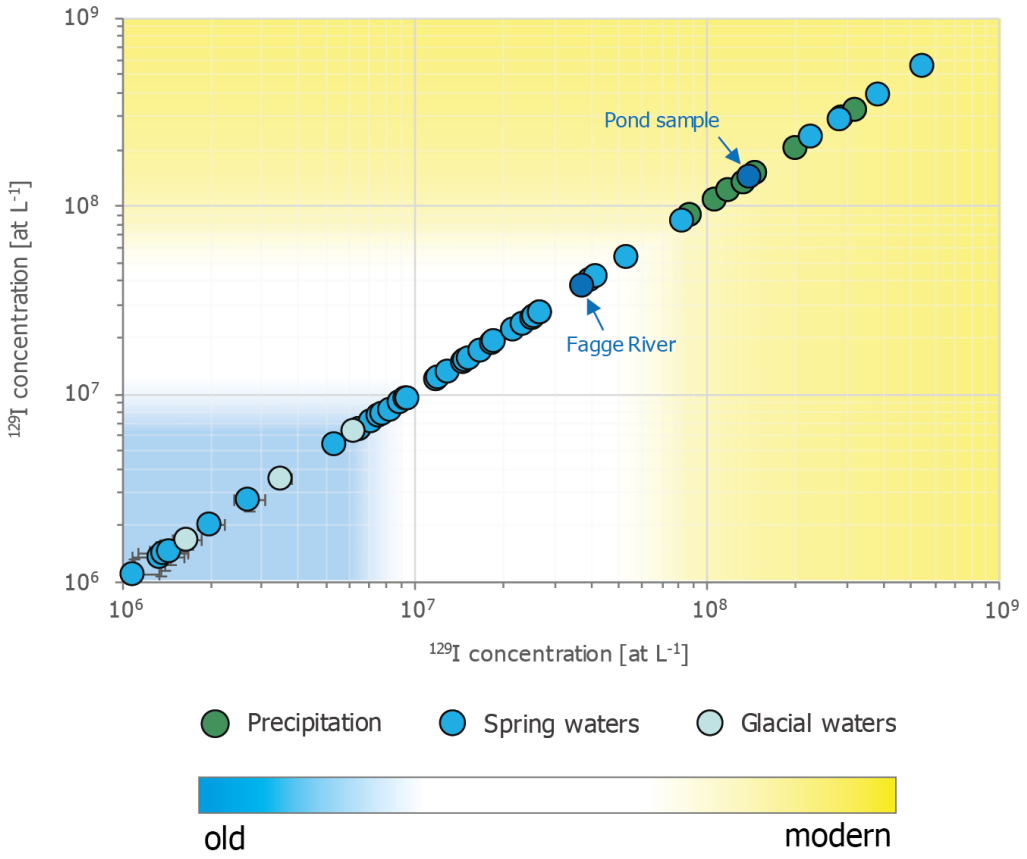

Figure 37: Relative age assessment of springs from Upper Kaunertal valley based on guidelines derived from glacial waters and precipitation

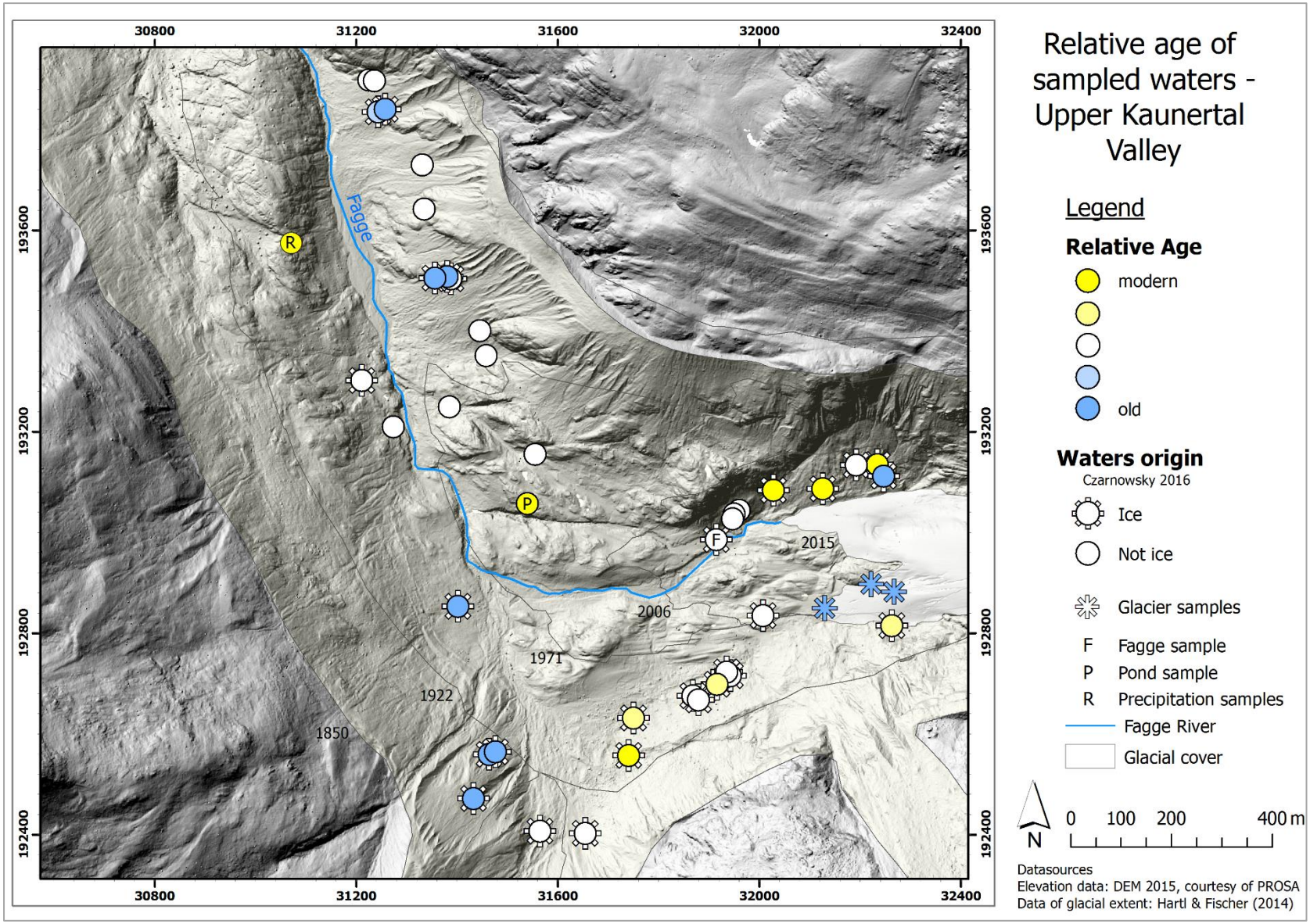

Figure 38: Relative age assessment of waters of Upper Kaunertal Valley

6.1.3 Evaluation of the relative age assessment

Nine springs are most likely fed by waters formed prior to nuclear age. Yet, the estimated relative age alone does not allow for a conclusion that they originate from dead ice. The spring may as well be ascribed to old groundwater which has so far not been in exchange with modern waters. Short residence times below five years have been shown for groundwater just downslope of the study area (Strauhal et al., 2016). Yet, the study of Strauhal et al. (2016) did not extend to the study area of the present analysis and therefore groundwater composition, storage and flow within the proglacial area remain unclear. Between June and October 2015 springs of the study area were part of a hydro-chemical monitoring programme conducted by Czarnowsky (2016). Stable isotopes ($\delta^{18}O$, $\delta^{2}H$), temperature and electrical conductivity of spring waters were used for spring characterization. Results identified two different types of spring waters. One type shows light isotopic signature, low temperature and electrical conductivity and suggests the existence of subsurface ice. The other type of spring water is characterized by heavier isotopic signature, higher temperatures, increased electrical conductivity and is subject to evaporation. Springs of the second type are thought to be fed predominantly by precipitation (Czarnowsky, 2016). The comparative findings from the hydro-chemical analyses and results of the relative age assessment (illustrated in Figure 38) attempts to address the issue of old groundwater as the spring's source. Along with field observations, it will allow to validate present results and define potential dead ice occurrences.

Twenty-seven out of thirty-nine springs analysed have been characterized as being influenced by ice. Irrespective of the fact that all of these springs originate from ice, they show highly varying ^{129}I concentrations thus evidencing ice of varying age.

All nine springs that have been evaluated as high likelihood of pre-nuclear origin have also been shown to originate from ice. It is these springs that are indicators of dead ice buried within the moraine's matrix. Accordingly, dead ice is potentially present in moraine complex B on the left valley side as well as moraine complex A and moraine complex E, both on the right side of the valley. The existence of dead ice within the latter moraine can be acknowledged by observations made in the field, with ice cropping out at several locations and sampling done directly from top of the ice body. Obvious signs of the existence of ice within the moraine sections A and B are not to be found. This may be related to the greater thickness of superimposed tills. At the same time it has to be kept in mind that the evidence of old icy waters does not necessarily indicate buried dead ice. Waters from upstream areas could possibly infiltrate the moraine body or feed evolving springs directly via overland flow (c.f. conceptual model, Figure 19). If so, incorrect conclusions might be drawn.

The aforementioned seems to be the case for spring 48. A tracer test verified the connection between spring 48 and a small lake on top of the moraine ridge (Czarnowsky, 2016). This lake is fed by a stream flowing along the back of the ridge. The streams origin, in turn, is not confirmed but the water may be related to upstream permafrost areas which have been modelled by Vehling (2016). A potential connection to the same stream was also hypothesized for

spring 45, the second spring characterized by an old icy signal on moraine section A. A second tracer test however failed to reveal a connection. Whether this could be ascribed to implementation issues, as considered by Czarnowsky (2016), cannot be assessed at this point. Accordingly, the possibility that spring 45 could indicate dead ice within the lateral moraine remains, but has to be approached with caution.

Springs which are fed by ice, but are unlikely to originate from old waters are traced back to subsurface ice other than dead ice. Ground ice may be formed seasonally out of modern waters within the tills. Their growth could be based on persisting dead ice bodies, which may represent an upward freezing front, or occur independent of those through the development of a downward freezing front near-surface (Woo, 2012). Combined results of the present study and previous investigations (Czarnowsky, 2016) indicate that seasonal ice growth is occurring on both sides of the valley and with different distances to the current glacier position (c.f. section 6.3).

Springs evolving from north facing moraine complex C have been shown to originate from ice (Czarnowsky, 2016). Those results are affirmed by field observations which revealed the presence of a large subsurface ice core with sediment cover of various thickness. Approximately 300 m long, 100 m wide and several metres thick, the position and extent of the ice core make it clear that the ice body is that of dead ice. However, a relative age assessment failed to indicate the presence of old dead ice. These springs are largely associated with comparably high ^{129}I levels indicating modern rather than pre-nuclear origin, which is unexpected. Even the dropwise sample derived directly from the melting ice body is most likely to be of modern age. Similar findings have been made in a comparable setting on the opposite valley side (moraine complex E), where another dropwise sample was collected from the buried dead-ice.

From the distinct setting of moraine complex E, contributions of waters from upstream areas mixing with melt waters of dead ice may offer a possible explanation for the young age of the springs, despite the presence of old dead ice. Input from upstream areas is evidenced by fluvial channels present at the top of the moraine. Due to large concentration difference between modern and pre-nuclear waters, comparatively small amounts of modern waters are sufficient to distort the pre-nuclear signal. In order to demonstrate the issue of mixed sources, the following scenario is assumed: A spring is fed in equal parts by modern and pre-nuclear waters. The pre-nuclear water concentration is presumed as the lowest concentration measured in a glacial sample, while the modern water concentration is stated as the highest concentration reported for precipitation of Kaunertal Valley. The resulting ^{129}I concentration of the mixed water would be calculated at $1.64 \cdot 10^8$ at $^{129}I\ L^{-1}$. Such a high concentration could not be recognized as to be of old origin. However, waters entering from upstream areas do not necessarily explain the observed discrepancy of the dropwise sample collected from the bottom of the dead ice. Indicators of overland flow at moraine site C are also missing as well as other signs of distorting impacts as most springs were flowing directly above ice and rainfalls had not occurred for several hours prior to sampling. Therefore there must be another connection between anthropogenic levels of ^{129}I and the ice core, which explains the high ^{129}I concentrations in springs evolving from old dead ice.

Considering the minor thickness of overburdening sediments and at some places even exposed ice faces, the influence of anthropogenic ^{129}I on the ice core's surface seems plausible. Dead ice is constantly exposed to an atmosphere of anthropogenic enriched ^{129}I concentrations as well as dry and wet deposition. This may have altered the ^{129}I concentrations of the ice bodies surface areas sufficiently to cover up the old signal of buried glacier ice and would explain high ^{129}I concentrations observed. Alternatively, the formation of seasonal ice layers on top of the existing dead-ice core during winter offers a second possibility, as high amounts of the resulting summer melt waters could dilute pre-nuclear ^{129}I signals of melt waters from old dead ice. More details on the formation of seasonal ice based upon the local thermal regime on site are given in section 6.3.

Springs of moraine C which were sampled in September are concluded to relate to modern ice, while comparative records for moraine E could not be gathered due to safety concerns. If it is assumed that the reported modern spring signal is attributed to the melt out of segregated ice, it would consequently also mean that segregated ice growth of the previous winter season must have built up considerable quantities of modern ice that have not dissipated by September. Melt rates of the dead ice core of moraine C have been assessed via ablation stake measures during several time periods between late July and early October 2015 and allow approximate quantification of melted ice volumes. For the respective period of time, thermal erosion of roughly 2.5 ± 1.2 cm d^{-1} or 850 ± 407 $m^3 d^{-1}$ has been stated (Kraushaar et al., 2016). Simply extrapolating these numbers for the period between July and September sampling (54 days), approximately 135 ± 64.8 cm or 45,900 ± 21,978 $m^3 d^{-1}$ of ice would have been melted. If it is assumed that modern or mixed ^{129}I concentrations measured on site originate from modern melt waters, the formation of segregated ice seems to be of large volume. Certainly, the simple extrapolation has to be treated with caution and only gives a rough idea of volumes melted on site. Woo (2012) states that segregated ice growth of particular thickness will develop if a source of external water is available and a suction gradient is present as unfrozen water flows to the freezing front. The formation of modern ice to this extent seems unlikely to have taken place in the course of one winter. The ice core has seemingly not been exposed before 2015 (Morche, 2017). Simulations have shown that ground temperatures of ice-rich landforms covered by thick, coarse-blocky material react slower to warming surface conditions (Staub et al., 2015). The ice body might not have been exposed to melting to great extent before 2015 and segregated ice, originating from more than one winter season, might have been able to preserve and build up to this point. However, if it is not clarified that the contribution of melt water from modern segregated ice alters the age of springs evolving from the dead-ice cored moraine C, it must also be taken into account that alterations may be caused by the continuous exposition of the ice surface to dry and wet precipitation.

Whilte the majority of springs are influenced by ice, twelve springs within the proglacial area have been shown to be fed predominantly by precipitation rather than by ice (Czarnowsky, 2016). These springs are found primarily in the lower parts of the study area, which has been

deglaciated first. Noteworthy, also the springs of moraine complex D, only tens of metres away from the 2015 glacier snout, are equally uninfluenced by ice. Further, not any of the precipitation fed springs are associated with old origin with high likelihood. This is seen to confirm the assumptions that old groundwater is not a source of evolving springs in the study area. Pertinent uncertainties are hence dropped, especially as this is also in accordance with results from hydrological studies performed just downstream of the study area (Strauhal et al., 2016).

6.2 Topographic and hydro-chemical characteristics of potential dead ice sites

Hydro-chemical characterisation (Czarnowsky, 2016) and relative age estimation of spring waters evolving in proglacial area of Gepatschferner glacier indicate potential dead ice occurrences within LIA lateral moraines. The potential presence of dead ice bodies has further been shown throughout the study area (c.f. Figure 38). Their existence seems at first glance to be neither restricted to exposition, altitude, slope, time since last glacial cover or to be indicated by temperature or electrical conductivity. Springs observed to be old and to originate from ice, which is the case for all old springs, have been found on north, north-east, south-west and west exposed slopes with inclinations between 17 and 45° on altitudes between 2170 and 2330 m. Old springs have been found in parts of the study area that have been recently deglaciated as well as in areas that have been free of ice for 93 years at the least. Furthermore, hydro-chemical parameters of these springs vary widely with temperatures ranging from 0 to 11.8 °C and electrical conductivity values of 0.2 up to 197.4 µS cm^{-1}. Statistical exploration of existing relationships between ^{129}I concentration and topographic or hydro-chemical parameters of springs only revealed significant negative correlations with slope, spring temperature and electrical conductivity of weak to medium strength.

Results of the present study suggest that springs fed by old waters have higher temperatures, are of high electrical conductivity and are found on steeper slopes. Temperature and electrical conductivity have already been found to correlate with $\delta^{18}O$ and $\delta^{2}H$ values of springs from Kaunertal Valley and have been used to differentiate ice-fed springs and springs of none-ice origin (Czarnowsky, 2016). Correlations found by Czarnowsky (2016) were positive and ice-fed springs were characterized by low temperatures and low EC. Not all ice-fed springs are of old age, but all springs of old origin are fed by ice, as the influence of old groundwater has been excluded (c.f. section 6.1.3). Correlations in the opposite direction are implausible. Results of Czarnowsky (2016) hence challenge correlations found in the present study.

Deviating results of correlations may be ascribed to undedected dead ice bodies within moraine C and E. While isotopic measures clearly recognized ice origin of concerned springs, ^{129}I concentrations measures failed to detect old waters. This error concerns twelve springs. Given a total of 39 springs included in the correlation analysis, roughly 30 % of the data does not reflect the actual presence of old dead ice in the study area. Further at least one out of two springs on moraine site A, which have been characterized by very low ^{129}I concentrations, is associated with waters from upstream areas rather than from meltwaters from dead ice buried

inside the sediment matrix. Whether this also affects the second spring on site has not been fully clarified (Czarnowsky, 2016). This introduces further uncertainties into the underlying data set. The validity of significant correlations, their strength and direction are likely to have been distorted due to the aforementioned issues and are hence called into question. That a conclusion on the spatial distribution pattern of dead ice bodies can be made based on ^{129}I concentration is in this particular case doubtful. Conditions favouring dead ice formation and preservation in the proglacial of Gepatschferner glacier can consequently not be established based on the present data. This also means that the general understanding of ice-cored moraines wastage driven by topographic parameters rather than climate (Schomacker, 2008; Schomacker and Kjær, 2008; Tonkin et al., 2016) cannot be specified.

6.3 Ground surface temperatures

Whether the local ground thermal regime allows for segregated ice growth has been assessed with ground temperature measures. Ground temperatures have been measured over a period of one year (July 2015 to July 2016) at one distinct location, close to spring 45, within moraine complex A. Temperature records of 20 and 40 cm depth revealed that ground temperatures dropped below zero on a limited number of days in December and January only. At 40 cm depth further, merely five days have been characterized by temperatures below zero. The low number of days with negative ground temperatures are partly justified by mainly positive autumn temperatures up to the end of November (c.f. mean air temperature at Gepatschalm in Figure 5 and air temperatures in Figure 35) as well as the development of a sufficient snow cover only later in the season. A cold snap at the end of November reduced air and ground temperatures noticeably, but the ground temperatures did not drop below zero. Between late November and early December ground temperatures did further stabilise, while air temperature continued to oscillate. The short decoupling of ground and air temperature may be ascribed to the intermediate development of a snow cover of sufficient depth (Gubler et al., 2011). The extremely low thermal conductivity of snow acts as very efficient insulator (Zhang, 2005), if exaggerating a critical snow depth (Staub et al., 2015). The depth of snow at the location of the ground temperature measurements is not known and precipitation records of Gepatschalm only revealed minor precipitation events during that time. Observations of others have shown that a snow depth of > 80 cm thickness is sufficient to thermally decouple ground temperatures from air temperatures (Staub et al., 2015). Nevertheless, the snow cover is not expected to have been constant throughout the year as indicated by further oscillating ground temperatures during December and early January. In the interim ground temperatures dropped below zero. A few positive degree days recorded at Gepatschalm, may have been sufficient to reduce the thickness of covering snow. Simultaneously, precipitation events of quantity have been absent and failed to greatly restore a snow cover of sufficient thickness. Re-deposition of snow by wind or gravitation may have additionally thinned out local snow cover (Bernhardt et al., 2012), inducing a reduced insulation effect of the remaining snow layer. If only a thin snow cover (5 to 20 cm) remained, ground cooling may have even been intensified (Staub et al., 2015). After the first week of January ground temperatures stabilised

once more to around 0 °C and were almost consistent up to April. During those three months ground temperatures were decoupled from air temperatures. It can hence be assumed that a snow cover of sufficient depth had developed. This assumption is supported by several recorded precipitation events of up to 20 mm each. Onset of snow melt seems to have happened early in April and was associated with increasing ground temperatures. During snow-melt itself, GST will remain at 0 °C as melt water percolates. The so called zero-curtain lasts until snow melt is completed (PermaNET, 2011). Nevertheless, a distinct zero-curtain was not apparent in the recorded data due to overall GST close to 0 °C prior the onset of snow melt.

"Water in the ground usually freezes at temperatures of a fraction of a degree or even several degrees below 0 °C"(Woo, 2012, p. 2). At the distinct location of the GST measures at moraine A, only a small number of days with mean daily sub-zero ground temperatures were recorded on site and the GFI is very low. Segregated ice growth in the upper decimetres of this moraine should have therefore been thermally restricted. That large and outlasting amounts of segregation ice could have been developed in the upper sediments during these days is not assumed. As negative GST had been limited to a time prior to the establishment of an insulating snow cover, any frozen ground may additionally have started to thaw after a snow cover of sufficient thickness had formed (Zhang, 2005). *"By the end of winter, there may be a very thin frozen layer or no frozen ground at all under the snow cover, especially when snow cover is relatively thick"* (Zhang, 2005, p. 15). Ground temperatures observed after the establishment of a sufficiently thick snow cover are positive and near-surface freezing should not have formed. However, it is noted that if the negative errors associated with the temperature measures are taken into account, GST could also have been slightly negative during the time of thick snow cover at both measuring depths. Theoretically, thermal conditions for seasonal could have allowed for ice growth. Yet, according to the Permafrost Monitoring Network, winter equilibrium temperatures (WEqT) close to 0 °C or moderately negative are still attributed to non-frozen soils (PermaNET, 2011). Further it is stated that snow cover prevents seasonal freezing in soils (Zhang, 2005). This supports the previous assumption that local thermal conditions for significant downward segregated ice growth have not been met at the specific site within the study area during the winter season of 2015/2016.

Gathered data only represents ground temperatures for one year at one distinct location. Results may vary from year to year depending on snow cover history (PermaNET, 2011) and cannot be simply transferred to other locations within the study area. However, results yield a first approximation and ground temperatures of other parts of the moraine characterized by comparable properties might also be similar. If so, formation of great amounts of segregated ice within the upper decimetres of the ground surface is just as unlikely in other parts of moraine A. This assumption is also underscored by the hydro-chemical signals of evolving springs, not indicating melt waters of modern ice. Seasonal ice either may not been formed or has already been melted by mid-July. Nevertheless, it is suggested that the local ground thermal situation might be different for other moraines in the study area. This is also indicated by evolving springs characterised by modern waters of ice origin.

In mountain areas ground temperature regimes vary locally (Apaloo et al., 2012) and show great spatial variability regarding surface and near-surface conditions (Gruber and Haeberli, 2009). Variations are influenced by topographic variables such as altitude, slope and aspect as to incoming solar radiation (Gubler et al., 2011) and by conditions of snow cover as well as substrate properties (Apaloo et al., 2012). Ground temperatures have been evidenced to be noticeably lower in coarse blocky material (Apaloo et al., 2012; Etzelmüller and Frauenfelder, 2009; Gruber and Hoelzle, 2008; Gubler et al., 2011; Harris and Pedersen, 1998; Kellerer-Pirklbauer, 2005; Staub et al., 2015). This may be a result of a number of various processes, e.g. ventilation of cold air, low thermal conductivity of coarse blocky layers or discontinuous snow cover due to high surface roughness which reduces snow cover insulation effects (Etzelmüller and Frauenfelder, 2009; Gruber and Hoelzle, 2008; Gubler et al., 2011). Mean annual ground surface temperatures in the Canadian Rocky Mountains were found to be 4 to 7 °C cooler in blocky material than in mineral soils (Harris and Pedersen, 1998). Smaller differences of 1.6 °C were reported from the eastern part of the Swiss Alps (Gubler et al., 2011). Investigations on supercooled taluses in the Austrian Alps further revealed seasonal as well as perennial ice occurrences (Wakonigg, 1998, 1996). Herz et al. (2003) has further shown that on coarse debris talus slopes in the periglacial area of Matter valley, the penetration depth of summer heat is shallower by four times than those of cool winter temperatures. Additionally, incoming solar radiation is crucial. North-facing slopes are subject to lower ground surface temperatures than south-facing slopes, showing greater differences with increasing slope angles. Differences are up to 5 °C for an angle of 40° (Gubler et al., 2011). Steep, north-facing slopes of the study area which are covered by coarse blocks are more likely to be characterized by lower ground surface temperatures than those measured at the finer-grained south-west facing moraine A. This may be especially true if the insulating effect of snow cover, which prohibits sub-zero ground temperatures during the vast majority of freezing period, is not fully developed due to protruding blocks.

The aforementionen characteristics can be found on the ice-cored moraine of site C. Lower, sub-zero ground temperatures at the specific site are therefore likely and a freezing front near-surface may develop. Moreover, the massive dead ice core on site can, it itself, represent a freezing front and could simultaneously enable up-freezing. The thermal requirement for downward, upward, or two-sided segregated ice growth could therewith be fulfilled. This would support the hypothesized growth of segregated ice raised earlier as one out of two posed options explaining modern ^{129}I concentrations observed in areas where dead ice is buried by shallow tills (c.f. section 6.1.3).

Contrary to findings at moraine site C, similar modern ice signatures are not present where dead ice is believed to be located deeper. Spring signals of moraine B, where dead ice is believed to be buried by thick tills, clearly indicate the presence of old dead ice as early as in July. This either means that upward segregation ice growth based on existing dead ice did not occur during the previous winter season or any ice formed has already been degraded by July.

At the same time, near-surface frozen layers, if they were present at all, were likely not significantly thick and may have already melted by July as the thawing of seasonal frost may take place over the course of a few days (Zhang, 2005).

Regardless of whether local temperatures allow for downward-, upward- or two-sided freezing processes to occur, the availability of moisture is a necessary requirement and soil texture needs to allow for moisture migration (Woo, 2012). Moisture for ice lense formation may originate from waters present within the frozen fringe, waters from adjacent unfrozen sediments that are subject to suction or waters from surrounding areas (Woo, 2012). Hydraulic conductivity, further describes the ability of water to pass through porous media. For glacial till hydraulic conductivity is stated as the wide range of 10^{-4} to 10^{-12} m s^{-1}. The conductivity of the silty fractions within glacial till is good and allows water movement towards the freezing front. However, both fine- and course-grained extremes prohibit water transmission (Woo, 2012). Formation of segregated ice lenses within the study area is hence not only thermally restricted but also likely limited to areas where silty till fractions are present.

6.4 Implication of dead ice presence for sediment dynamics and sediment budget studies

Remote sensing, GIS and DEMs are part of the major methodological and conceptual progress made in examining sediment budgets during the last two decades. Applied in studies on sediment budgets, LiDAR computed DEMs and DoDs are state-of-the-art methods used to survey sediment fluxes as well as sediment volumes (Hinderer, 2012). A catchment-scale sediment budget for the proglacial area of Gepatschferner glacier was established, in the context of the PROSA project. In order to quantify present hillslope and channel processes, multi-temporal high resolution LiDAR data were gained and DoDs were computed (Heckmann et al., 2012). Several parts of the right LIA lateral moraine were identified as subjected to erosion (Dusik et al., 2015a). Detailed results of a surface change detection analysis focusing on a 0.04 km² large section of this lateral moraine revealed a net erosion of -1357.2 m³ (overall balance: -444 m³) and -926.2 m³ (overall balance: -307.5 m³) between July 2010 and September 2011 as well as July 2012 and July 2013 respectively (Dusik et al., 2014). Measured net volume losses have been attributed to debris flows, fluvial erosion, slope wash, gullying and other mass movements with main erosion taking place early on in the year (Dusik et al., 2014; Hilger et al., 2014). Taking the results of the present study into account, melt out of remaining dead ice bodies has to be considered as an ongoing process of potential significance, at the 1850 lateral moraine on the right valley side as well as on other moraine sites pointed out in the study area (c.f. section 6.1.3). At the moraine surface, de-icing is expressed as topographic lowering (Tonkin et al., 2016) (c.f. Figure 1B) and appears as an erosional signal in DoD calculations. The net volume loss caused by buried dead ice degradation may additionally be enhanced by the release of fine sediments by melt waters and any processes triggered by evolving melt waters.

Degradation of any remaining ice cores will delay the stabilisation of the moraine's surface (Lukas, 2011). Melt waters released by dead ice provide an additional source of water on the slopes. Supplemental water availability increases ground saturation and pore water pressure which hence reduces shear strength (Ahnert, 2009; Rickenmann, 2002; Schomacker, 2008). Observations from Upper Kaunertal Valley have shown that single rockfalls, small-scale debris flows and undercutting of moraines due to differential melting processes at clear ice surfaces occur frequently at heavily ice-cored moraines covered by shallow tills. Similar processes have also been observed at other dead-ice sites (Chiarle and Mortara, 2008; Diolaiuti and Smiraglia, 2010; Johnson, 1971; Lukas et al., 2005). Where dead ice is believed to be buried by sediments of greater thickness, ongoing processes have been observed to be less dynamic. Nevertheless, melt waters, if evolving at the surface, may leach nutrients and solutes in the subsurface and induce fluvial erosion, altering the moraines morphology. In addition to fluvial processes, dead ice degradation may be preconditioning gravity driven geomorphic processes such as debris flows. Mortara and Chiarle (2005) report examples where the melting of ice-cores in two lateral moraines was involved in large landslides at the Ortler Alps and the Grand Paradiso Group. In sum, processes triggered by ice core degradation will enhance sediment output and sediment delivery ratios, and material may be moved to the next temporary sediment sink within the sediment cascade or beyond, which will increase landscape coupling (Hinderer, 2012). These paraglacial activities may largely influence sediment yield of meltwater streams (Etzelmüller, 2000). They bear the potential to trigger surface elevation changes additionally to the volume losses caused by dead ice degradation itself.

The undetected degradation of buried dead ice bodies hence yields a definite but unquantified source of uncertainty when working on sediment budgets and using DoDs in recently deglaciated proglacial areas. Given the indications present for dead-ice occurrences, the causes of volume loss considered thus far and their ability to transport sediments on site have to be critically examined and revaluated. So too calculated masses of eroded material. Not to forget, the formation of segregation ice may also alter surface elevation. Yet, as segregation ice is believed to form during frost season but also to fully thaw again in the ablation period, no net volume change is triggered. Calculated DoDs might not necessarily be affected by surface alterations created by segregated ice growth. Nonetheless, it seems favourable to undertake DEM surveys in late summer, when potential segregation ice from last winter has already melted completely and new segregation ice has not yet been formed.

Estimating the volume of dead ice melting and the subsequently triggered volume reductions as actively operating processes of geomorphological significance goes beyond the present study, despite the attempt in the following paragraphs to give an idea of possible volume losses due to dead ice degradation itself. Glacial retreat since LIA maximum and the progress in multi-temporal surface imaging techniques allowed for the recording of increased data on melting ice-cored moraines in recent years (Schomacker and Kjær, 2008). Existing studies mainly focus on proglacial areas at higher latitudes rather than an alpine environment. Reported melt rates vary highly based on climatic and topographic conditions as well as controls of debris

cover. Rates of moraine wastage measured in high-arctic Svalbard range between -0.3 to -1.8 m a^{-1} (Ewertowski and Tomczyk, 2015; Schomacker and Kjær, 2008; Tonkin et al., 2016). Measurements from a humid and subpolar area of Iceland reveal similar melt rates of -0.3 to -1.4 m a^{-1} (Krüger and Kjær, 2000). Lukas et al. (2005) suggest melt rates beneath debris greater than 40 cm of less than 0.005 m d^{-1} and highlights the importance of debris cover (Everest and Bradwell, 2003). However, once the ice core is exposed, melt rates accelerate. Disintegration may then be tenfold (Lukas et al., 2005). Reports from increased wastage of exposed ice bodies state an annual subsidence of 22 m at Tsho Rolpa (Central Nepal) or a weekly decrease of 0.6 m witnessed at Donjek Glacier (Yukon, Canada) (Richardson and Reynolds, 2000). Further, annual material mobilisation due to thermal erosion can be in a similar range to those of annual suspended sediments (Etzelmüller, 2000).

Melt rates derived from the ice-cored moraine in the glacier forefield of Gepatschferner glacier during July and October 2015 total 2.5 ± 1.2 cm d^{-1}. Roughly interpolated to the estimated extent of the ice core, this is an ice volume of 850 ± 407 m^3 d^{-1} (Kraushaar et al., 2016). These numbers suggest that at least for this part of the study area, de-icing during ablation season is a substantial process driving geomorphological change. Comparable, or more likely even greater melt rates, are to be expected at the similarly ice-cored moraine E, where solar radiation should be higher due to a more southerly orientation. Certainly, dead ice masses shielded from direct solar radiation and insulated by sediments of greater depth are expected to degrade at a lower rate. Potential volume losses due to dead ice degradation at moraine site A and B are hence assumed to stay clearly lower than those estimated for moraine C. Yet, both sides are contrary to the north oriented site C expected to be subject to increased solar radiation due to their exposition to the south-west and north-east. Czarnowsky (2016) assessed potential volume losses due to ice degradation based on discharge measures of two springs. Spring 45 at moraine A as well as one spring at moraine C were shown to be of ice origin. Waters of spring 45 have further been shown to be old, while relative age estimation is missing for the second spring as the sample has not been selected for ^{129}I concentration determination. Volume losses during the ablation season were calculated to be as high as 86.7 ± 36.8 m^3 d^{-1} if spring 45 was fed 100 % by melt water. This has been translanted to melting rates of 2.56 ± 1.09 cm d^{-1}. It has been assumed that the waters are fed by at least 50 % from ice based on the negative isotopic signal (Czarnowsky, 2016). Due to the high influence of modern waters, this is also true for the estimated relative age of the waters. If a dead-ice melt water proportion of minimum 50 % is assumed, volume losses during ablation season would still total 43.4 ± 18.4 m^3 d^{-1} or melt rates of 1.28 ± 0.54 cm d^{-1}. Further studies would be needed in order to clarify to what amount spring 45 is fed by melt water (Czarnowsky, 2016). Moreover, assessments to distinctly exclude an existing connection between the spring and the stream on top of the moraine ridge are necessary (c.f. section 6.1.3). Nonetheless, consideration of potential volume losses due to melt out of dead ice show, especially when being compared with the overall net erosion measured (Dusik et al., 2014), that they are of potential significance and not to be neglected.

Emphasized uncertainties for the establishment of a proglacial sediment budget may remain for the foreseeable future. The presence of dead ice or ice-cored moraines implies, by definition, that the deglaciation of a proglacial area has not been completed (Lukas, 2011). In a proglacial environment dead ice may survive long after the glacier itself has retreated (Everest and Bradwell, 2003). Despite these observations, the preservation potential of ice-cored moraines is unclear (Tonkin et al., 2016). This applies even more to alpine settings, as studies on ice wastage are primarily focused on higher latitudes (e.g. Svalbard, Iceland). Investigations have shown that buried glacier ice in Virkisjökull persisted for 50 years (Everest and Bradwell, 2003). Similar survival rates are estimated for the proglacial of Kötlujökul under present climate conditions (Krüger and Kjær, 2000). Elsewhere in southern Iceland, dead ice has probably remained for 200 years (Everest and Bradwell, 2003). Climate conditions in the Alpine environment are different, yet results from Kaunertal Valley suggest that dead ice may have survived since ~ 1922 in a lateral moraine of Gepatschferner glacier. The prominent ice core within the lateral moraine of site C is detached from the glacier for at least 44 years. Despite being known to have preserved for several decades, dead ice occurrences are not associated with a permafrost domain (Haeberli cited in Harris and Murton, 2005). If permafrost conditions or even near permafrost conditions exist (Etzelmüller and Frauenfelder, 2009), buried dead ice may preserve over a long-time if the thickness of covering tills is greater than the thickness of the active layer (Etzelmüller and Frauenfelder, 2009; Harris and Murton, 2005; Tonkin et al., 2016; Waller et al., 2012). Active layer depths of mountain permafrost typically vary between 0.5 and 8 m (Gruber and Haeberli, 2009). When being in equilibrium with its environment an ice-cored moraine may fully stabilise (Tonkin et al., 2016) and would not play a role for surface elevation changes on site. In the central Austrian Alps discontinuous permafrost areas can generally be expected above 2500 to 2600 m a.s.l. (Kellerer-Pirklbauer, 2005) and altitude limits are expected to increase due to predicted temperature increases (APCC, 2014). Moraines of the study area do not reach these elevations. Hence, surface and geothermal heat fluxes will eventually cause the decay of any ice bodies within the moraines (Harris and Murton, 2005). High total ice losses observed at moraine C during the 2015 ablation period (Kraushaar et al., 2016) and evolving ice-fed waters of old origin emphasize this prospect. Lateral moraine complexes free of ice are hence the most likely end point for the moraines of Kaunertal valley. If the ice content of an ice-cored moraine has been large, the resulting geomorphic feature will likely be diffuse and of low topography (Tonkin et al., 2016). Even though little is known on the time frame in which de-icing takes place in an alpine setting (Schomacker, 2008), uncertainties for applied surface elevation measures arising from dead ice presence can only be excluded after final degradation.

Given the long periods of dead ice survival and potentially relevant rates of surface lowering once degradation has begun, users of DoDs in recently deglaciated proglacial areas need to be well aware of the melt out of dead ice. Its potential role as driver for geomorphological changes needs to be considered even if the existence of buried dead ice is not clearly evident from the surface. This is especially important considering that areas of dead-ice are going to occur more abundantly in the future (Schomacker, 2008).

7 Summary

In the face of present climate warming and its associated consequences for glacial and periglacial mountain environments, the origin of ice-fed springs evolving from lateral moraines of Gepatschferner glacier (Kaunertal Valley, Austria) has been clarified using ^{129}I relative age dating. Specific springs have been attributed to dead ice, which remained from former glacial extents and to seasonally forming ground ice. The applicability of the anthropogenic nuclide ^{129}I for relative age determination has been tested successfully. A further goal was to assess whether the indicated spatial pattern of dead ice is related to present topographic and/or hydro-chemical characteristics. The local ground thermal regime has been monitored over the course of one year in order to assess the possibility of seasonal ice formation. Outcomes gained are summarized based on raised hypotheses and briefly put into context in the following.

Anthropogenic ^{129}I mainly released by nuclear reprocessing facilities has significantly altered the natural inventory of this nuclide since the 1950s. The present study aims to use these definite enhancements in order to test the ability of ^{129}I concentration to distinguish modern waters from waters of pre-nuclear origin that have not had contact with anthropogenic ^{129}I. Determination of ^{129}I yield of 56 waters sampled from the proglacial area of Upper Kaunertal Valley revealed significant differences between glacial waters, spring waters and precipitation. Ice sampled at the front of Gepatschferner glacier which is generally assumed to have formed prior to any nuclear activities, yielded concentrations up to $3.50 \cdot 10^6$ at $^{129}I\ L^{-1}$. Glacial run off was further characterized by ^{129}I concentrations of $6.29 \cdot 10^6$ at L^{-1}. Clearly influenced by modern ^{129}I emissions, precipitation samples collected from Vergötschen (1263 m a.s.l.) and the study area (2152 m a.s.l.) between May and October 2015 show significantly higher values with a mean concentration of $1.77 \cdot 10^8$ at $^{129}I\ L^{-1}$. Evolving spring waters of unknown origin span the entire range of ^{129}I concentrations found in glacier and precipitation samples and even partially exceed the spectrum in both directions. Both ^{129}I concentrations of glacier ice as well as precipitation are rather low compared to measurements reported elsewhere in Europe. Thus far, comparable references are scarce.

Knowledge of natural ^{129}I concentrations is lacking. Defining a threshold to distinguish waters of pre-nuclear and modern concentration is consequently challenging. A threshold set up based upon ^{129}I measures of an ice core from a glacier in the Bernese Alps dated to the early 1950s has turned out to strongly overestimate the number of waters characterized by pre-nuclear origin in the setting of Kaunertal Valley. Guidelines based upon glacier and precipitation measures from the study area itself were applied in order to assess the likelihood of spring waters to be of old or modern origin. Following this classification nine springs are most likely fed by waters formed prior to nuclear age, four springs are very likely to be influenced by modern waters. The remaining 26 springs are likely to be mixtures of old and modern waters to varying proportions.

Combining the results of hydro-chemical monitoring (Czarnowsky, 2016) and the relative age assessment carried out, it can be excluded that groundwater formed prior to the 1950s is feeding springs on site, since all waters that have been classified to be of pre-nuclear origin are also fed by ice. At the same time, all ice-fed springs originating from old waters indicate the presence of dead ice, provided that infiltration from upstream areas is improbable. In contrast, ice-fed springs influenced by modern waters imply the presence of seasonal ice, which seems to be frequently appearing in the study area.

It has been proven that melt waters of ice-fed springs, evolving from the LIA lateral moraines, can be ascribed to modern seasonal ice and old dead ice, which has remained from former glacial extent, based on ^{129}I concentrations. Hypothesis 1 (H_1) has been verified. Yet, in case of visible, shallow buried dead ice bodies, either the constant exposure of the ice body or the formation of modern segregation ice based upon the dead ice body, conditioned ^{129}I concentration signals far off the assumed pre-nuclear level. The applied melt water analysis hence failed to identify the presence of old dead ice in these specific cases.

Ice-fed springs of pre-nuclear origin can be found throughout the study area. Their existence seems neither to be limited to exposition, altitude, slope, time since last glacial cover nor be indicated by temperature or electrical conductivity of evolving springs. In order to exam the hypothesis that spatial patterns of ice-fed springs low in ^{129}I, as surrogate for present dead ice, can be explained by topographic characteristics and/or indicated by hydro-chemical spring characteristics, a statistical analysis of existing correlations was undertaken. Even though significant correlations of medium strength were found between ^{129}I concentration and independent topographic and hydro-chemical parameters, roughly 30 % of the data does not reflect the actual presence of old dead ice in the study area as measured ^{129}I concentrations failed to indicate visible dead ice bodies. The validity of significant correlations, their strength and direction are likely to have been distorted and are in question. That a conclusion on the spatial distribution pattern of dead ice bodies and any indicating spring characteristics can be made based on ^{129}I concentration is, in this particular case, doubted, especially as identified correlations also contradict earlier findings (Czarnowsky, 2016). Hence, the second hypothesis (H_2) cannot be answered given the present data.

Three iButtons were used to measure ground surface temperature at one distinct location within the study area, at different depths (20, 40, 60 cm depth) and over the course of one year. Results indicate ground temperatures of over 20 °C and that temperatures oscillate as a function of air temperatures. In winter time, however, ground temperatures seem to have been decoupled from air temperatures over a long periods and remain just above 0 °C. This is likely ascribed to the development of a snow cover of significant thickness. Negative ground temperatures were only recorded for a limited number of days. The possibility of segregated ice growth in the moraine matrix is suggested to have been limited. That the local ground temperature regime did allow for extensive seasonal ice growth during the winter 2015/2016 is hence unlikely (H_3). It is however recognized, that the situation in other years or at other locations within the study area may possible be very different, especially as it has been shown

that ground temperatures below coarse blocky material, on steep slopes or in north exposed areas are likely to be lower (Etzelmüller and Frauenfelder, 2009; Gruber and Hoelzle, 2008; Gubler et al., 2011).

Results presented herein, give insights into the (sub)surface dynamics of recently deglaciated proglacial areas. Based upon springs characteristics and their relative age, it was possible to specify geomorphological processes on site. Further it has been shown that the degradation of present dead ice is capable of causing large volume losses on site. Thermal erosion has to be considered in applied surface elevation measurements and the resultant sediment budgets in proglacial areas. In addition, results may be of interest for the local hydrological situation, water resource management and natural hazard assessment.

8 Limitations and outlook

The present study has verified the basic applicability of ^{129}I for relative age determination. Yet, the method is in need of future research in order to handle issues emerged herein. Accordingly, the implementation of suitable thresholds used to distinguish pre-nuclear and modern ^{129}I concentrations in different matters is fundamental. Expanding the knowledge on natural concentration levels thereby seems indispensable. In the specific setting of the present study as well as in general terms, ice core records, sufficiently deep to include signals of pre-nuclear times, may yield required information. Simultaneously, the spatial and temporal variability of modern precipitation, especially in areas of high-altitudes, needs to be explored further. In doing so, the question of altitudinal gradients should be pursued. Focussing on the issue of mixed waters, the conduction of a dilution series may yield valuable insights and may facilitate the assessment of medium ^{129}I concentrations. When working with ice and anthropogenic enriched nuclides, rather than sampling melt water evolving from the ice it may be better to remove ice that is directly exposed to the atmosphere before sampling the ice in solid form. This approach may help to reduce the distorting impact of modern ^{129}I accumulation on the ice surface. Further, sampling may be timed best at the end of summer, when potentially seasonal ice is likely to have fully disipated. Nevertheless, it is desirable to clarify whether ^{129}I concentration of waters evolving from exposed dead ice bodies have been enriched due to seasonal ice growth or due to continuous exposure to the modern atmosphere and wet and dry deposition of anthropogenic iodine. Addressing a general assumption that has been made within the present study, it is essential that future studies focus on the migration and adsorption of ^{129}I in and onto sediments in order to assess to what extent ^{129}I concentrations of waters are altered during subsurface transportation. Furthermore, the validation of ^{129}I dating with an independent dating method, such as tritium dating, should be undertaken in the future.

Relative age assessment of springs in Upper Kaunertal Valley together with their hydro-chemical characterization successfully revealed the presence of ice-fed waters of pre-nuclear origin within the study area. Nonetheless, the analysis of the complete sample set, including the months thereafter is desirable. An increased number of analysed samples would allow the reinforcement of results gained and improve conclusions drawn based upon them, especially concerning the establishment of suitable thresholds. Since all waters of pre-nuclear age are derived from ice, old groundwater is not believed to feed any springs and old, icy waters within the proglacial most likely indicate the existence of dead ice within lateral moraines of Gepatschferner glacier. Indeed, the possibility of those waters being influenced by neighbouring catchments cannot be entirely excluded, as long as no hydro-geological model of the study area is established. Several tools of geophysical subsurface investigations, such as electrical resistivity tomography, ground penetrating radar or seismic refraction, would allow for an independent validation of main results presented here. Application of these tools would further facilitate the location of present dead ice bodies on slope, quantify their extent and assess the thickness of superimposed tills.

Whether the spatial distribution of ice-fed springs of pre-nuclear origin within the study area, as surrogate for dead ice, is following any topographical pattern could not be sufficiently assessed given the mentioned issues with the present data. In order to generate reasonable evidence, the issue of high ^{129}I concentration of waters emerging from visible dead ice bodies must be addressed. To circumvent this problem, information from stable isotopes, ^{129}I concentrations and from the field could be combined to generate a dichotomous variable with characteristic values of "no ice" and "dead ice". Testing any relationships between the dichotomous variable and topographic indicators may yield more plausible results. Furthermore, a data set containing more individual cases would enhance the validity of any results.

Measurements of ground surface temperatures presented here were restricted to one single location, due to financial limitations. The validity of the results gained and any conclusion on possible seasonal ice growth are consequently highly constrained. The expansion of ground temperature measures into several locations within the proglacial area would allow a broader characterization of prevailing ground thermal regimes. Presumed differences between specific moraine sites, especially concerning exposition and grain size of covering sediments, could thereby be assessed. In addition to near surface temperature measurements of different depths, information on bottom temperature of snow cover as well as height of snow cover may further assist to validate whether the thermal regime on site allows for seasonal ice formation within the proglacial area.

Uncertainties introduced into calculated erosion volumes and established sediment budgets due to dead ice degradation need quantification in order to address them appropriately. Further research concerning the degradation of dead ice bodies is necessary, as melt rates and melting volumes are largely missing for alpine areas. The quantification of sediments mobilised by thermal erosion is additionally required and needs to be incorporated into sediment dynamic- and sediment budget studies.

Dead ice presence is of interest for future hydrological studies as groundwater sourced from moraines is of concern for both quantity and timing of water discharge. Internal structures such as buried dead ice are further expected to exercise control on groundwater flow and storage. Lowlands critically depend on waters from snow, ice and permafrost of mountain areas during summer in a number of ways, when other water sources are limited (Huss et al., 2017). Annual glacier runoff has reached its maximum or may have even passed its peak by now. The Austrian reservoir of glacier ice could be largely exhausted by 2060 (APCC, 2014) and seasonal runoff regimes will experience major shifts due to reduced ice and snow cover (Huss et al., 2017). Water scarcity may follow thereafter, causing issues of water security for downstream communities (Knight and Harrison, 2014). Dead ice bodies could represent fresh water reserves that may outlast glacial resources. Similar to water systems of permafrost and rock glaciers (Knight and Harrison, 2014), further research is needed. Finally, the presence of dead ice and its degradation as well as secondary processes caused by it may have implication for the assessment of any (multi-) hazard potential emanating from the moraine deposits and should be recognized in any future investigations

References

Abdel-Moati, M.A., 1999. Iodine speciation in the Nile River estuary. Marine Chemistry 65, 211–225.

Abermann, J., Lambrecht, A., Fischer, A., Kuhn, M., 2009. Quantifying changes and trends in glacier area and volume in the Austrian Ötztal Alps (1969-1997-2006). The Cryosphere 3, 205–215.

Abermann, J.M., Kuhn, M., Lambrecht, A., Hartl, L., 2013. Gletscher in Tirol, ihre Verteilung und jüngsten Veränderungen, in: Koch, E.-M. (Ed.), Klima, Wetter, Gletscher Im Wandel, Alpine Forschungsstelle Obergurgl. Innsbruck University Press, Innsbruck, 49–67.

Ackert, R.P., 1984. Ice-Cored Lateral Moraines in Tarfala Valley, Swedish Lapland. Geografiska Annaler Series A Physical Geography 66, 79–88.

Ahnert, F., 2009. Einführung in die Geomorphologie, 4. ed. Verlag Eugen Ulmer, Stuttgart.

Aldahan, A., Alfimov, V., Possnert, G., 2007. 129I anthropogenic budget: Major sources and sinks. Applied Geochemistry 22, 606–618.

Aldahan, A., Persson, S., Possnert, G., Hou, X.L., 2009. Distribution of 127I and 129I in precipitation at high European latitudes. Geophysical Research Letters 36.

Apaloo, J., Brenning, A., Bodin, X., 2012. Interactions between Seasonal Snow Cover, Ground Surface Temperature and Topography (Andes of Santiago, Chile, 33.5°S). Permafrost and Periglacial Processes, 277–291.

APCC, 2014. Österreichischer Sachstandsbericht Klimawandel 2014: Austrian Panel on Climate Change (APCC). Austrian Assessment Report 2014 (AAR14). Vienna.

Atarashi-Andoh, M., Schnabel, C., Cook, G., MacKenzie, A.B., Dougans, A., Ellam, R.M., Freeman, S., Maden, C., Olive, V., Synal, H.-A., Xu, S., 2007. 129I/127I ratios in surface waters of the English Lake District. Applied Geochemistry 22, 628–636.

Baewert, H., Morche, D., 2014. Coarse sediment dynamics in a proglacial fluvial system (Fagge River, Tyrol). Geomorphology 218, 88–97.

Barsch, H., Billwitz, K., Bork, H.-R. (Eds.), 2000. Arbeitsmethoden in Physiogeographie und Geoökologie, 1st ed. Klett-Perthes, Gotha, Stuttgart.

Benesch, T., 2013. Schlüsselkonzepte zur Statistik. Die wichtigsten Methoden, Verteilungen, Tests anschaulich erklärt, 1st ed. Spektrum, Berlin, Heidelberg.

Bennett, M.R., Glasser, N.F., 2009. Glacial Geology. Ice Sheets and Landforms., 2nd ed. Wiley-Blackwell, Chichester.

Bernhardt, M., Schulz, K., Liston, G.E., Zängl, G., 2012. The influence of lateral snow redistribution processes on snow melt and sublimation in alpine regions. Journal of Hydrology 424–425, 196–206.

Brown, C.F., Geiszler, K.N., Lindberg, M.J., 2007. Analysis of 129I in groundwater samples: Direct and quantitative results below the drinking water standard. Applied Geochemistry 22, 648–655.

Brunner, K., 2006. Karten dokumentieren den Rückzug der Gletscher seit 1850. Wiener Schriften zur Geographie und Kartographie 17, 191–200.

Buraglio, N., Aldahan, A., Possnert, G., Vintersved, I., 2001. 129I from the Nuclear Reprocessing Facilities Traced in Precipitation and Runoff in Northern Europe. Environmental Science & Technology, 1579–1586.

Chiarle, M., Mortara, G., 2008. Geomorphological Impact of Climate Change on Alpine Glacial and Periglacial Areas, in: Mikos, M., Hübl, J., Koboltschnig, G. (Eds.), INTERPRAEVENT 2008 – Conference Proceedings, Vol. 2. Klagenfurt, 111–122.

Christl, M., Casacuberta, N., Lachner, J., Maxeiner, S., Vockenhuber, C., Synal, H.-A., Goroncy, I., Herrmann, J., Daraoui, A., Walther, C., Michel, R., 2015. Status of 236U analyses at ETH Zurich and the distribution of 236U and 129I in the North Sea in 2009. Nuclear Instruments and Methods in Physics Research B 361, 510–516.

Czarnowsky, V., 2016. Isotopenchemische und hydrologische Untersuchungen an perennierenden und episodischen Quellen zum Nachweis von Untergrundeis an den Seitenmoränen im Gletschervor-feld des Gepatschferners (Tirol, Österreich). Universität Leipzig, Leipzig.

Daraoui, A., 2010. Migration von Iod-129 und Retrospektive Dosimetrie. Universität Hannover, Hannover.

Diolaiuti, G., Smiraglia, C., 2010. Changing glaciers in a changing climate: how vanishing geomorphosites have been driving deep changes in mountain landscapes and environments. Géomorphologie: Relief, Processus, Environnement 16 (2), 131–152.

Dobhal, D.P., 2011. Dead Ice, in: Singh, V.P., Singh, P., Haritashya, U.K. (Eds.), Encyclopedia of Snow, Ice and Glaciers. Springer Netherlands, Dordrecht, p. 186.

Dusik, J.-M., Heckmann, T., Hilger, L., Haas, F., Becht, M., 2015a. Long- and shortterm sediment yield by fluvial reworking of proglacial slopes in the upper Kaunertal, in: Geophysical Research Abstracts - EGU2015-9799. Presented at the EGU General Assembly, Vienna.

Dusik, J.-M., Heckmann, T., Neugirg, F., Hilger, L., Haas, F., Becht, M., 2014. The effect of rainfall events with changing frequency and magnitude on reworking conditions of proglacial moraines, in: Geophysical Research Abstracts - EGU2014-9781. Presented at the EGU General Assembly, Vienna.

Dusik, J.-M., Leopold, M., Heckmann, T., Haas, F., Hilger, L., Morche, D., Neugirg, F., Becht, M., 2015b. Influence of glacier advance on the d evelopment of the multipart Riffeltal rock glacier, Central Austrian Alps. Earth Surface Processes and Landforms 40 (7), 965–980.

Egger, K., Hesse, A., 2014. Strategische Umweltprüfung - Umweltbericht. Wasserwirtschaftlicher Rahmenplan Großwasserkraftwerksvorhaben Tiroler Oberland. Speicherkraftwerke. Ausleitungskraftwerke am Inn. (Strategische Umweltprüfung - Umweltbericht). freiland Umweltconsulting ZT GmbH, Wien.

Ehlers, J., Gibbard, P., 2011. Quaternary Glaciation, in: Singh, V.P., Singh, P., Haritashya, U.K. (Eds.), Encyclopedia of Snow, Ice and Glaciers. Springer Netherlands, Dordrecht, 873–882.

Embleton-Hamann, C., 2007. Geomorphologie in Stichwörtern III. Exogene Morphodynamik. Karstmorphologie - Glazialer Formenschatz - Küstenformen., 6. neubearbeitet Auflage. ed. Gebrüder Borntraeger Verlagsbuchhandlung, Berlin.

Etzelmüller, B., 2000. Quantification of thermo-erosion in pro-glacial areas - examples from Svalbard. Zeitschrift für Geomorphologie 44, 343–361.

Etzelmüller, B., Frauenfelder, R., 2009. Factors Controlling the Distribution of Mountain Permafrost in the Northern Hemisphere and Their Influence on Sediment Transfer. Arctic, Antarctic, and Alpine Research 41, 48–58.

Everest, J., Bradwell, T., 2003. Buried glacier ice in southern Iceland and its wider significance. Geomorphology 52, 347–358.

Ewertowski, M.W., Tomczyk, A.M., 2015. Quantification of the ice-cored moraines' short-term dynamics in the high-Arctic glaciers Ebbabreen and Ragnarbreen, Petuniabukta, Svalbard. Geomorphology 234, 211–227.

Fabryka-Martin, J., Davis, S.N., Elmore, D., 1987. Applications of 129I and 36Cl in hydrology. Nuclear Instruments and Methods in Physics Research B 29, 361–371.

Fabryka-Martin, J.T., 1984. Natural iodine-129 as a ground-water tracer. University of Arizona, Tucson, Arizona.

Fan, Y., Hou, X., Zhou, W., 2013. Progress on 129I analysis and its application in environmental and geological researches. Desalination 321, 32–46.

Fehn, U., 2012. Tracing Crustal Fluids: Applications of Natural 129I and 36Cl. Annual Review of Earth and Planetary Sciences 40, 45–67.

Fehn, U., Moran, J.E., Snyder, G.T., Muramatsu, Y., 2007a. The initial 129I/I ratio and the presence of 'old' iodine in continental margins. Nuclear Instruments and Methods in Physics Research B 259, 496–502.

Fehn, U., Snyder, G.T., Muramatsu, Y., 2007b. Iodine as a tracer of organic material: 129I results from gas hydrate systems and fore arc fluids. Journal of Geochemical Exploration 95, 66–80.

Fischer, A., 2017. Gletscherbericht 2015/2016. Sammelbericht über die Gletschermessungen des Österreichischen Alpenvereins im Jahre 2016. Bergauf, 18–25.

Fischer, A., 2016. Gletscherbericht 2014/2015.Sammelbericht über die Gletschermessungen des Österreichischen Alpenvereins im Jahre 2015. Bergauf, 6–13.

Fischer, A., 2015. Gletscherbericht 2013/2014. Sammelbericht über die Gletschermessungen des Österreichischen Alpenvereins im Jahre 2014. Bergauf, 26–33.

Fischer, A., 2014. Gletscherbericht 2012/2013. Sammelbericht über die Gletschermessungen des Oesterreichischen Alpenvereins im Jahre 2013. Bergauf, 34–40.

Fischer, A., 2013. Gletscherbericht 2011/2012. Sammelbericht über die Gletschermessungen des Oesterreichischen Alpenvereins im Jahre 2012. Bergauf, 22–28.

Fischer, A., 2012. Gletscherbericht 2010/2011. Sammelbericht über die Gletschermessungen des Oesterreichischen Alpenvereins im Jahr 2011. Bergauf, 30–36.

Fischer, A., 2011. Gletscherbericht 2009/2010. Sammelbericht über die Gletschermessungen des Oesterreichischen Alpenvereins im Jahre 2010. Bergauf, 34–40.

Fischer, A., 2010. Gletscherbericht 2008/2009. Sammelbericht über die Gletschermessungen des Oesterreichischen Alpenvereins im Jahre 2009. Bergauf, 24–31.

Freidlin, B., Gastwirth, J.L., 2000. Should the Median Test be Retired from General Use? The American Statistican 54 (3), 161–164.

French, H.M., 2007. The periglacial environment, 3. ed. ed. Wiley, Chichester.

Frezzotti, M., Orombelli, G., 2014. Glaciers and ice sheets: current status and trends. Rendiconti Lincei 25, 59–70.

Gabay, J.J., Paperiello, C.J., Goodyear, S., Daly, J.C., Matuszek, J.M., 1974. A Method for Determining Iodine-129 in Milk and Water. Health Physics 26 (1), 89–96.

Geboy, N.J., Engle, M.A., 2011. Quality assurance and quality control of geochemical data—A primer for the research scientist (U.S. Geological Survey Open File Report No. 2011–1187). USGS, Reston, Virginia.

Gilfedder, B.S., Petri, M., Biester, H., 2007. Iodine and bromine speciation in snow and the effect of orographically induced precipitation. Atmospheric Chemistry and Physics 7, 2661–2669.

Gröning, M., Lutz, H.O., Roller-Lutz, Z., Kralik, M., Gourcy, L., Pöltenstein, L., 2012. A simple rain collector preventing water re-evaporation dedicated for δ18O and δ2H analysis of cumulative precipitation samples. Journal of Hydrology 448–449, 195–200.

Groß, J., 2010. Grundlegende Statistik mit R. Eine anwendungsorientierte Einführung in die Verwendung der Statistik Software R, 1st ed. Vieweg+Teubner Verlag, Wiesbaden.

Gruber, S., Haeberli, W., 2009. Mountain Permafrost, in: Margesin (Ed.): Permafrost Soils, Soil Biology. Springer, Berlin, Heidelberg, pp. 33–44.

Gruber, S., Hoelzle, M., 2008. The cooling effect of coarse blocks revisited: a modeling study of a purely conductive mechanism, in: 9th International Conference on Permafrost, Fairbanks, Alaska, 29 Juni 2008 - 3 Juli 2008. Presented at the 9th International Conference on Permafrost, Fairbanks, pp. 557–561.

Gubler, S., Fiddes, J., Keller, M., Gruber, S., 2011. Scale-dependent measurement and analysis of ground surface temperature variability in alpine terrain. The Cryosphere 5, 431–443.

Haeberli, W., Hoelzle, M., Paul, M., Zemp, M., 2007. Integrated monitoring of mountain glaciers as key indicators of global climate change: the European Alps. Annals of Glaciology 46 (1), 150–160.

Harris, C., Murton, J.B., 2005. Interactions between glaciers and permafrost: an introduction, in: Harris & Murton (Eds.): Cryospheric Systems: Glaciers and Permafrost, Geological Society Special Publication. The Geological Society, London, p. 162.

Harris, S.A., Pedersen, D.E., 1998. Thermal regimes beneath coarse blocky materials. Permafrost and Periglacial Processes 9, 107–120.

Hartl, L., 2010. The Gepatschferner from 1850 - 2006. Changes in Length, Area and Volume in Relation to Climate (Diploma Thesis). Universität Innsbruck, Innsbruck.

Hartl, L., Fischer, A., 2014. The Gepatschferner from 1850 - 2006, with links to digital elevation models and glacier margins. PANGAEA.

Heckmann, T., Haas, F., Morche, D., Schmidt, K.H., Rohn, J., Moser, M., Leopold, M., Kuhn, M., Briese, C., Pfeifer, N., Becht, M., 2012. Investigating an Alpine proglacial sediment budget using field measurements, airborne and terrestrial LiDAR data, in: Erosion and Sediment Yields in the Changing Environment (Proceedings of a Symposium Held at the Institute of Mountain Hazards and Environment, CAS-Chengdu, China, 11–15 October 2012). Chengdu, 438–447.

Heckmann, T., Hilger, L., Vehling, L., Becht, M., 2016. Integrating field measurements, a geomorphological map and stochastic modelling to estimate the spatially distributed rockfall sediment budget of the Upper Kaunertal, Austrian Central Alps. Geomorphology 260, 16–31.

Heckmann, T., McColl, S., Morche, D., 2016. Retreating ice: research in pro-glacial areas matters. Earth Surface Processes and Landforms, 271–276.

Hedderich, J., Sachs, L., 2016. Angewandte Statistik, 15th ed. Springer, Berlin, Heidelberg.

Heideman, M., 1993. The Global Carbon Cycle, Series I, Global envrionmental change; vol. 15. NATO ASI series, Berlin, Heidelberg.

Herod, M.N., Li, T., Pellerin, A., Kieser, W.E., Clark, I.D., 2016. The seasonal fluctuations and accumulation of iodine-129 in relation to the hydrogeochemistry of the Wolf Creek Research Basin, a discontinuous permafrost watershed. Science of the Total Environment 569–570, 1212–1223.

Herz, T., King, L., Gubler, H., 2003. Thermal regime within coarse debris of talus slopes in the alpine periglacial belt and its effect on permafrost. Presented at the 8th International Permafrost Conference, Zürich.

Hilger, L., Becht, M., Heckmann, T., 2014. Investigating sediment budgets and pathways using LiDAR DEMs of difference and a geomorphological map, in: Geophysical Research Abstracts - EGU2014-4306. Presented at the EGU General Assembly, Vienna.

Hinderer, M., 2012. From gullies to mountain belts: A review of sediment budgets at various scales. Sedimentary Geology 280, 21–59.

Hippe, K., Ivy-Ochs, S., Kober, F., Zasadni, J., Wieler, R., Wacker, L., Kubik, P.W., Schlüchter, C., 2014. Chronology of Lateglacial ice flow reorganization and deglaciation in the Gotthard Pass area, Central Swiss Alps, based on cosmogenic 10Be and in situ 14C. Quaternary Geochronology 19, 14–26.

Hoehn, E., Oktay, S., Santschi, P.H., 1999. 129Iodine: a new tracer for surface water/groundwater interaction. Presented at the International Symposium on Isotope Techniques in Water Resources Development and Management, UNT Digital Library, Livermore, California.

Hohenberg, C.M., Pravdivtseva, O.V., 2008. I–Xe dating: From adolescence to maturity. Chemie der Erde 68, 339–351.

Hou, X., Aldahan, A., Nielsen, S.P., Possnert, G., 2009a. Time Series of I-129 and I-127 Speciation in Precipitation from Denmark. Environmental Science & Technolology 43, 6522–6528.

Hou, X., Dahlgaard, H., Rietz, B., Jacobsen, U., P. Nielsen, S., Aarkrog, A., 1999. Determination of 129I in seawater and some environmental materials by neutron activation analysis. Analyst 124, 1109–1114.

Hou, X., Hansen, V., Aldahan, A., Possnert, G., Lind, O.C., Lujaniene, G., 2009b. A review on speciation of iodine-129 in the environmental and biological samples. Analytica Chimica Acta 632, 181–196.

Hou, X., Zhou, W., Chen, N., Zhang, L., Liu, Q., Luo, M., Fan, Y., Liang, W., Fu, Y., 2010. Determination of Ultralow Level 129I/127I in Natural Samples by Separation of Microgram Carrier Free Iodine and Accelerator Mass Spectrometry Detection. Analytical Chemistry 82, 7713–7721.

Hu, Q.-H., Weng, J.-Q., Wang, J.-S., 2010. Sources of anthropogenic radionuclides in the environment: a review. Journal of Environmental Radioactivity 101, 426–437.

Huss, M., Bookhagen, B., Huggel, C., Jacobsen, D., Bradley, R.S., Clague, J.J., Vuille, M., Buytaert, W., Cayan, D.R., Greenwood, G., Mark, B.G., Milner, A.M., Weingartner, R., Winder, M., 2017. Toward mountains without permanent snow and ice. Earths Future 5, 418–435.

Iturrizaga, L., 2011. Paraglacial Landscape Transformations, in: Singh, V.P., Singh, P., Haritashya, U.K. (Eds.), Encyclopedia of Snow, Ice and Glaciers. Springer Netherlands, Dordrecht, 817–823.

Ivy-Ochs, S., 2015. Glacier Variations in the European Alps at the End of the Last Glaciation. Cuadernos Investigacion Geográfica 41 (2), 295–315.

Ivy-Ochs, S., Kerschner, H., Maisch, M., Christl, M., Kubik, P.W., Schlüchter, C., 2009. Latest Pleistocene and Holocene glacier variations in the European Alps. Quaternary Science Reviews 28, 2137–2149.

Ivy-Ochs, S., Kerschner, H., Reuther, A., Preusser, F., Heine, K., Maisch, M., Kubik, P.W., Schlüchter, C., 2008. Chronology of the last glacial cycle in the European Alps. Journal of Quaternary Science 23 (6-7), 559–573.

Izmer, A.V., Boulyga, S.F., Zoriy, M.V., Becker, J.S., 2004. Improvement of the detection limit for determination of 129I in sediments by quadrupole inductively coupled plasma mass spectrometer with collision cell. Journal of Analytical Atomic Spectrometry 19, 1278–1280.

Jabbar, T., Steier, P., Wallner, G., Cichocki, O., Sterba, J.H., 2013a. Investigation of the isotopic ratio 129I/I in petrified wood. Journal of Environmental Radioactivity 120, 33–38.

Jabbar, T., Steier, P., Wallner, G., Kandler, N., Katzlberger, C., 2011. AMS analysis of iodine-129 in aerosols from Austria. Nuclear Instruments and Methods in Physics Research B 269, 3183–3187.

Jabbar, T., Steier, P., Wallner, G., Priller, A., Kandler, N., Kaiser, A., 2012a. Iodine Isotopes (127I and 129I) in Aerosols at High Altitude Alp Stations. Environmental Science & Technology 46, 8637–8644.

Jabbar, T., Wallner, G., Steier, P., 2013b. A review on 129I analysis in air. Journal of Environmental Radioactivity 126, 45–54.

Jabbar, T., Wallner, G., Steier, P., Katzlberger, C., Kandler, N., 2012b. Retrospective measurements of airborne 129Iodine in Austria. Journal of Environmental Radioactivity 112, 90–95.

Johnson, P.G., 1971. Ice Cored Moraine Formation and Degradation, Donjek Glacier, Yukon Territory, Canada. Geografiska Annaler Series A Physical Geography 53 (3), 198–202.

Kääb, A., Chiarle, M., Raup, B., Schneider, C., 2007. Climate change impacts on mountain glaciers and permafrost. Global and Planetary Change 56, vii–ix.

Kellerer-Pirklbauer, A., 2005. Alpine permafrost occurrence at its spatial limits: First results from the eastern margin of the European Alps. Norsk Geografisk Tidsskrift - Norwegian Journal of Geography 59, 184–193.

Kendall, C., McDonnell, J.J., 2006. Isotope Tracers in Catchment Hydrology. Elsevier, Amsterdam.

Kendall, C., Snyder, D., Caldwell, E., 2004. Isotope Tracers Project. Resources on Isotopes. USGS.

Kerschner, H., 2009. Gletscher und Klima im Alpinen Spätglazial und frühen Holozän, in: Schmidt, R., Matulla, C., Psenner, R. (Eds.), Klimawandel in Österreich. Die Letzten 20.000 Jahre Und Ein Blick Voraus, Alpine Space - Man & Environment. Innsbruck Univ. Press, Innsbruck.

Kerschner, H., Ivy-Ochs, S., 2008. Palaeoclimate from glaciers: Examples from the Eastern Alps during the Alpine Lateglacial and early Holocene. Global and Planetary Change 60, 58–71.

Keutterling, A., Thomas, A., 2006. Monitoring glacier elevation and volume changes with digital photogrammetry and GIS at Gepatschferner glacier, Austria. International Journal of Remote Sensing 27, 4371–4380.

Kieser, E.W., Zhao, L.X., Soto, Y.C., Tracy, B., 2005. Accelerator mass spectrometry of 129I: Technique and applications. Journal of Radioanalytical and Nuclear Chemistry 263, 375–379.

Klipsch, K., 2005. Bestimmung von 129I und 127I in Umweltproben zwecks der Ermittlung radioökologischer Parameter des 129I auf seinem Weg von Quellen durch die Nahrungskette bis zum Menschen. Universität Hannover, Hannover.

Knight, J., Harrison, S., 2014. Mountain glacial and paraglacial environments under global climate change: lessons from the past, future directions and policy implications. Geografiska Annaler Series A Physical Geography 96, 245–264.

Knight, J., Harrison, S., 2009. Sediments and future climate. Nature Geoscience 2, 230–230.

Kocher, D.C., 1981. A dynamic model of the global iodine cycle and estimation of dose to the world population from releases of iodine-129 to the environment. Environment International 5, 15–31.

Kraushaar, S., Blöthe, J., Baewert, H., Dubberke, K., Culha, C., Knöller, K., Morche, D., 2014. Supportive methods for sediment budgeting: Stable isotope measurements of perrenial springs in the Kaunertal Valley. Presented at the 8th. I.A.G./A.I.G. working group SEDIBUD (Sediment Budgets in Cold Environments) Sediment Cascades in Cold Climate Geosystems, Zugspitze/Reintal, Bavaria/Germany.

Kraushaar, S., Kamleitner, S., Czarnowsky, V., Morche, D., Knöller, K., Lachner, J., 2016. Is there still ice in the lateral moraines? Hydro-chemical analyses of episodic springs from lateral moraines and their implications for the interpretation of geomorphological process studies. Presented at the Jahrestagung von geomorph.at und der Schweizerischen Geomorphologischen Gesellschaft (SGmG), Innsbruck.

Krieger, H., 2012. Grundlagen der Strahlungsphysik und des Strahlenschutzes. Wiesbaden.

Kronthaler, F., 2016. Statistik angewandt. Datenanalyse ist (k)eine Kunst, Springer-Lehrbuch. Springer, Berlin, Heidelberg.

Krüger, J., Kjær, K.H., 2000. De-icing progression of ice-cored moraines in a humid, subpolar climate, Kötlujökull, Iceland. The Holocene 10, 737–747.

Krupp, G., Aumann, D.C., 1999. Iodine-129 in rainfall over Germany. Journal of Environmental Radioactivity 46, 287–299.

Langston, G., Bentley, L.R., Hayashi, M., McClymont, A., Pidlisecky, A., 2011. Internal structure and hydrological functions of an alpineproglacial moraine. Hydrological Processes 25, 2967–2982.

Leeuwen, C.J. van, 1995. Risk assessment of chemicals : an introduction. Kulwer Acadamic Publishers, Dordrecht.

Lewkowicz, A., 2008. Evaluation of miniature temperature-loggers to monitor snowpack evolution at mountain permafrost sites, northwestern Canada. Permafrost and Periglacial Processes 19, 323–331.

Liu, Q., Hou, X., Zhou, W., Fu, Y., 2015. Accelerator Mass Spectrometry Analysis of Ultra-Low-Level 129I in Carrier-Free AgI-AgCl Sputter Targets. Journal of the American Society for Mass Spectrometry 26, 725–733.

Liu, Y., v. Gunten, H.R., 1988. Migration Chemistry and Behaviour of Iodine Relevant to Geological Disposal of Radioactive Wastes: A Literature Review with a Compilation of Sorption Data. Paul-Scherrer-Institut, Nagra.

López-Gutiérrez, J.M., García-León, M., García-Tenorio, R., Schnabel, C., Suter, M., Synal, H.-A., Szidat, S., 2000a. 129I/127I ratios and 129I concentrations in a recent sea sediment core and in rainwater from Sevilla (Spain) by AMS. Nuclear Instruments and Methods in Physics Research B 172, 574–578.

López-Gutiérrez, J.M., Synal, H.-A., Suter, M., Schnabel, C., García-León, M., 2000b. Accelerator mass spectrometry as a powerful tool for the determination of 129I in rainwater. Applied Radiation and Isotopes 53, 81–85.

Lu, Z., Fehn, U., Tomaru, H., Elmore, D., Ma, X., 2007. Reliability of 129I/I ratios produced from small sample masses. Nuclear Instruments and Methods in Physics Research B 259, 359–364.

Lukas, S., 2011. Ice-Cored Moraines, in: Singh, V.P., Singh, P., Haritashya, U.K. (Eds.), Encyclopedia of Snow, Ice and Glaciers. Springer Netherlands, Dordrecht, 616–619.

Lukas, S., Graf, A., Coray, S., Schlüchter, C., 2012. Genesis, stability and preservation potential of large lateral moraines of Alpine valley glaciers – towards a unifying theory based on Findelengletscher, Switzerland. Quaternary Science Reviews 38, 27–48.

Lukas, S., Nicholson, L.I., Ross, F.H., Humlum, O., 2005. Formation, Meltout Processes and Landscape Alteration of High-Arctic Ice-Cored Moraines—Examples From Nordenskiold Land, Central Spitsbergen. Polar Geography 29, 157–187.

Lysså, A., Lønne, I., 2001. Moraine development at a small High-Arctic valley glacier: Rieperbreen, Svalbard. Journal of Quaternary Science 16, 519–529.

Maro, D., Hebert, D., Gandon, R., Solier, L., 1999. Iodine 129 measurements by gamma spectrometrie in biological samples Résults in seaweeds (fucus serratus et laminaria digitata) from the English Channel. Radioprotection 34, 13–24.

Maxim Integrated Products, 2015. DS1922L/DS1922T. iButton Temperature Loggers with 8KB Datalog Memory.

Michel, R., Daraoui, A., Gorny, M., Jakob, D., Sachse, R., Tosch, L., Nies, H., Goroncy, I., Herrmann, J., Synal, H.-A., Stocker, M., Alfimov, V., 2012. Iodine-129 and iodine-127 in European seawaters and in precipitation from Northern Germany. Science of the Total Environment 419, 151–169.

Mook, W.G. (Ed.), 2000. Environmental isotopes in the hydrological cycle. Principles and applications. Volume i. Introduction: Theory, Methods, Review., UNESCO/IAEA Series on Environmental isotopes in the hydrological cycle. Prinicples and Applications. Paris.

Morche, D., 2017. Oral information - Vienna, 26.4.2017.

Mortara, G., Chiarle, M., 2005. Instability of recent moraines in the Italian Alps. Effects of natural processes and human intervention having environmental and hazard implications. Giornale di Geologia Applicata1, 139–146.

Müller, J., Gärtner-Roer, I., Kenner, R., Thee, P., Morche, D., 2014. Sediment storage and transfer on a periglacial mountain slope (Corvatsch, Switzerland). Geomorphology 218, 35–44.

Muramatsu, Y., Yoshida, S., Fehn, U., Amachi, S., Ohmomo, Y., 2004. Studies with natural and anthropogenic iodine isotopes: iodine distribution and cycling in the global environment. Journal of Environmental Radioactivity 74, 221–232.

Murawski, H., Meyer, W., 2010. Geologisches Wörterbuch, 12. überarbeitete und erweiterte Auflage. ed. Spektrum Akademischer Verlag, Heidelberg.

Neugirg, F., Haas, F., Heckmann, T., Hilger, L., Dusik, J.-M., Becht, M., 2014. Different rates of reworking of Little Ice Age lateral moraines in the Kaunertal valley, Austrian Alps: A morphometric and morphodynamic case study using multi-epoch LiDAR surveys, in: Geophysical Research Abstracts - EGU2014-7563. Presented at the EGU General Assembly, Vienna.

Nicolussi, K., Kaufmann, M., Patzelt, G., Plicht van der, J., Thurner, A., 2005. Holocene tree-line variability in the Kauner Valley, Central Eastern Alps, indicated by dendrochronological analysis of living trees and subfossil logs. Vegetation History amd Archaeobotany 14, 221–234.

Nicolussi, K., Patzelt, G., 2000. Untersuchungen zur holozänen Gletscherentwicklung von Pasterze und Gepatschferner (Ostalpen). Zeitschrift für Gletscherkunde und Glaziogeologie 36, 1–87.

Ohta, T., Mahara, Y., Kubota, T., Abe, T., Matsueda, H., Tokunaga, T., Sekimoto, S., Takamiya, K., Fukutani, S., Matsuzaki, H., 2013. Separation and measurement of 129I and 127I in pre-nuclear-era marine algae with ultra-low 129I/127I isotopic ratios. Nuclear Instruments and Methods in Physics Research B 294, 559–562.

Østrem, G., 1971. Rock Glaciers and Ice-Cored Moraines, a Reply to D. Barsch. Geografiska Annaler Series A Physical Geography 53, 207–213.

Patzelt, G., 2009. Gletscherbericht 2007/2008. Sammelbericht über die Gletschermessungen des Oesterreichischen Alpenvereins im Jahre 2008. Bergauf, 18–25.

Patzelt, G., 2008. Gletscherbericht 2006/2007. Sammelbericht über die Gletschermessungen des Oesterreichischen Alpenvereins im Jahr 2007. Bergauf, 26–32.

Patzelt, G., 2007. Gletscherbericht 2005/2006. Sammelbericht über die Gletschermessungen des OeAV im Jahre 2006. Bergauf, 20–25.

Penck, A., Brückner, E., 1909. Die Alpen im Eiszeitalter: in drei Bänden. Leipzig: Tauchnitz.

PermaNET, 2011. Guide lines for monitoring. GST Ground surface temperature, Alpine Space permafrost monitoring network. PermaNET.

Persson, S., Aldahan, A., Possnert, G., Alfimov, V., Hou, X., 2007. 129I Variability in precipitation over Europe. Nuclear Instruments and Methods in Physics Research B 259, 508–512.

Povinec, P.P., Aoyama, M., Biddulph, D., Breier, R., Buesseler, K., Chang, C.C., Golser, R., Hou, X.L., Ješkovský, M., Jull, A.J.T., Kaizer, J., Nakano, M., Nies, H., Palcsu, L., Papp, L., Pham, M.K., Steier, P., Zhang, L.Y., 2013. Cesium, iodine and tritium in NW Pacific waters – a comparison of the Fukushima impact with global fallout. Biogeosciences 10, 5481–5496.

Reithmeier, H., 2005. 129I in Umweltproben als Tracer für die atmosphärischen 131I-Freisetzungen in Majak. Technische Universität München, München.

Reithmeier, H., Lazarev, V., Kubo, F., Rühm, W., Nolte, E., 2005. 129I in precipitation using a new TOF system for AMS measurements. Nuclear Instruments and Methods in Physics Research B 239, 273–280.

Reithmeier, H., Lazarev, V., Rühm, W., Nolte, E., 2010. Anthropogenic 129I in the atmosphere: Overview over major sources, transport processes and deposition pattern. Science of the Total Environment 408, 5052–5064.

Reithmeier, H., Lazarev, V., Rühm, W., Nolte, E., 2007. 129I measurements in lake water for an estimate of regional 129I depositions. Science of the Total Environment 376, 285–293.

Reithmeier, H., Lazarev, V., Rühm, W., Schwikowski, M., Gäggeler, H.W., Nolte, E., 2006. Estimate of European 129I Releases Supported by 129I Analysis in an Alpine Ice Core. Environmental Science & Technology 5891–5896.

Richardson, S.D., Reynolds, J.M., 2000. Degradation of ice-cored moraine dams: implications for hazard development. Debris Covered Glaciers Proceedings of a Workshop Held in Seattle Washington USA Sept. 2000, 187–197.

Rickenmann, D., 2002. Über Murgänge in den Alpen. Wasser Boden 54 (4), 23–26.

Roy, J.W., Hayashi, M., 2009. Multiple, distinct groundwater flow systems of a single moraine–talus feature in an alpine watershed. Journal of Hydrology 373, 139–150.

Schmidt, A., Schnabel, C., Handl, J., Jakob, D., Michel, R., Synal, H.-A., Lopez, J.., Suter, M., 1998. On the analysis of iodine-129 and iodine-127 in environmental materials by accelerator mass spectrometry and ion chromatography. Science of the Total Environment 223, 131–156.

Schnabel, C., López-Gutiérrez, J.M., Szidat, S., 2001. On the origin of 129I in rain water near Zürich. Radiochimica Acta 89, 815–822.

Schomacker, A., 2011. Moraine, in: Singh, V.P., Singh, P., Haritashya, U.K. (Eds.), Encyclopedia of Snow, Ice and Glaciers. Springer Netherlands, Dordrecht, pp. 747–756.

Schomacker, A., 2008. What controls dead-ice melting under different climate conditions? A discussion. Earth-Science Reviews 90, 103–113.

Schomacker, A., Kjær, K.H., 2008. Quantification of dead-ice melting in ice-cored moraines at the high-Arctic glacier Holmströmbreen, Svalbard. Boreas 211–225.

Sharp, R.P., 1988. Living Ice. Understanding Glaciers and Glaciation. Cambridge University Press, Cambridge.

Slaymaker, O., 2011. Criteria to Distinguish Between Periglacial, Proglacial and Paraglacial Environments. Quaestiones Geographicae 30, 85-94.

Smith, M.W., Carrivick, J.L., Hooke, J., Kirkby, M.J., 2014. Reconstructing flash flood magnitudes using 'Structure-from-Motion': A rapid assessment tool. Journal of Hydrology 519, Part B, 1914–1927.

Snyder, G., Aldahan, A., Possnert, G., 2010. Global distribution and long-term fate of anthropogenic 129I in marine and surface water reservoirs. Geochemistry Geophysics Geosystems 11.

Snyder, G., Fehn, U., 2004. Global distribution of 129I in rivers and lakes: implications for iodine cycling in surface reservoirs. Nuclear Instruments and Methods in Physics Research B 223–224, 579–586.

Staub, B., Marmy, A., Hauck, C., Hilbich, C., Delaloye, R., 2015. Ground temperature variations in a talus slope influenced by permafrost: a comparison of field observations and model simulations. Geographica Helvetica 70, 45–62.

Steland, A., 2016. Basiswissen Statistik. Kompaktkurs für Anwender aus Wirtschaft, Informatik und Technik, 4th ed, Springer-Lehrbuch. Springer, Berlin, Heidelberg.

Strauhal, T., Prager, C., Millen, B., Spötl, C., Brandner, R., 2016. Aquifer geochemistry of crystalline rocks and Quaternary deposits in a high altitude alpine environment (Kauner Valley, Austria). Austrian Journal of Earth Sciences 109, 29-44.

Sturges, H.A., 1926. The Choice of a Class Interval. Journal of the American Statistical Association 21, 65–66.

Suárez, J.A., Espartero, A.G., Rodríguez, M., 1996. Radiochemical analysis of 129I in radioactive waste streams. Nuclear Instruments and Methods in Physics Research Section A 369, 407–410.

Suzuki, T., Kitamura, T., Kabuto, S., Togawa, O., Amano, H., 2006. High Sensitivity Measurement of Iodine-129/Iodine-127 Ratio by Accelerator Mass Spectrometry. Journal of Nuclear Science and Technology 43, 1431–1435.

Szidat, S., 2000. Iod-129: Probenvorbereitung, Qualitätssicherung und Analyse von Umweltmaterialien. Universität Hannover, Hannover.

Szidat, S., Schmidt, A., Handl, J., Jakob, D., Botsch, W., Michel, R., Synal, H.-A., Schnabel, C., Suter, M., López-Gutiérrez, J., Städe, W., 2000. Iodine-129: Sample preparation, quality control and analyses of pre-nuclear materials and of natural waters from Lower Saxony, Germany. Nuclear Instruments and Methods in Physics Research B 172, 699–710.

Temme, A.J.A.M., Heckmann, T., Harlaar, P., 2016. Silent play in a loud theatre — Dominantly time-dependent soil development in the geomorphically active proglacial area of the Gepatsch glacier, Austria. Catena 147, 40–50.

Tirol Atlas, 2013. Institut für Geographie, Universität Innsbruck. Thematische Karten. Klima. Niederschlag. Kaunertal – Feichten.

TIWAG (Tiroler Wasserkraft AG), 2016. Niederschlag und Lufttemperatur 2015 – Station Gepatschalm (1_302).

Tonkin, T.N., Midgley, N.G., Cook, S.J., Graham, D.J., 2016. Ice-cored moraine degradation mapped and quantified using an unmanned aerial vehicle: A case study from a polythermal glacier in Svalbard. Geomorphology 258, 1–10.

Tschada, H., Hofer, B., 1990. Total solids load from the catchment area of the Kaunertal hydroelectric power station: the results of 25 years of operation, in: Sinniger R.O., Monbarron M. (Eds.): Hydrology in mountainous regions II: artificial reservoirs, water and slopes. IAHS publications, 121–128.

Umweltbundesamt (Ed.), 1993. Gletscherschigebiete Österreichs. Bestandsaufnahme und chemischanalytische Untersuchungen. Wien.

van Husen, D., 1997. LGM and late-glacial fluctuations in the Eastern Alps. Quaternary International 38, 109–118.

Vehling, L., 2016. Gravitative Massenbewegungen an alpinen Felshängen - Quantitative Bedeutung in der Sedimentkaskade proglazialer Geosysteme (Dissertation). Friedrich-Alexander-Universität Erlangen-Nürnberg (FAU), Erlangen - Nürnberg.

Vehling, L., Rohn, J., Moser, M., 2016. Quantification of small magnitude rockfall processes at a proglacial high mountain site, Gepatsch glacier (Tyrol, Austria). Zeitschrift für Geomorphologie 60, 93–108.

Veit, H., 2002. Die Alpen: Geoökologie und Landschaftsentwicklung. Ulmer, Stuttgart.

Vockenhuber, C., Casacuberta, N., Christl, M., Synal, H.-A., 2015. Nuclear Instruments and Methods in Physics Research B 361, 445–449.

Vosselman, G., Maas, H.-G., 2010. Airborne and Terrestrial Laser Scanning. Whittles Publishing, Dunbeath.

Wagner, M.J.M., 1995. Mittelschwere Radionuklide. Neue Nachweismethode und Anwendungen von Nickel-59, Zinn-126 und Iod-129. ETH Zürich, Zürich.

Wagner, M.J.M., Dittrich-Hannen, B., Synal, H.-A., Suter, M., Schotterer, U., 1996. Increase of 129I in the environment. Nuclear Instruments and Methods in Physics Research B 113, 490–494.

Wakonigg, H., 1998. Neue Beobachtungen an unterkühlten Schutthalden, in: Mitteilungen der Österreichischen Geographischen Gesellschaft. Wien, 115–130.

Wakonigg, H., 1996. Unterkühlte Schutthalden, in: Lieb G.K. (Hrsg.): Beiträge zur Permafrostforschung in Österreich, Arbeiten aus dem Institut für Geographie der Karl-Franzens-Universität Grau. Graz, 209–223.

Waller, R.I., Murton, J.B., Kristensen, L., 2012. Glacier–permafrost interactions: Processes, products and glaciological implications. Sedimentary Geology 255–256, 1–28.

Wallner, G., Steier, P., Brandl, T., Friesacher, M.E., Hille, P., Kutschera, W., Tatzber, M., Ayromlou, S., 2007. Developments toward the measurement of I-129 in lignite. Nuclear Instruments and Methods in Physics Research B 259, 714–720.

Williams, R., Brasington, J., Vericat, D., Hicks, M., Labrosse, F., Neal, M., 2011. Chapter Twenty - Monitoring Braided River Change Using Terrestrial Laser Scanning and Optical Bathymetric Mapping, in: Mike J. Smith, P.P. and J.S.G. (Ed.), Developments in Earth Surface Processes. Elsevier, 507–532.

Woo, M., 2012. Permafrost Hydrology. Springer, Berlin, Heidelberg.

Zasadni, J., 2007. The Little Ice Age in the Alps: its Record in Glacial Deposits and Rock Glacier Formation. Studia Geomorphologica Carpatho-Balcanica 41, 117–137.

Zemp, M., Paul, F., Hoelzle, M., Haeberli, W., 2008. Glacier fluctuations in the European Alps, 1850–2000: an overview and spatio-temporal analysis of available data, in: Orlove, B., Wiegandt, E., Luckman, B.H. (Eds.), Darkening Peaks: Glacier Retreat, Science, and Society. University of California Press, Berkeley, 152–167.

Zepp, H., 2014. Geomorphologie. Eine Einführung., 6th ed. UTB, Stuttgart.

Zhang, T., 2005. Influence of the seasonal snow cover on the ground thermal regime: An overview. Reviews of Geophysics 43.

Zhou, W., Chen, N., Hou, X., Zhang, L., Liu, Q., He, C., Fan, Y., Luo, M., Zhao, Y., Wang, Z., 2013. Analysis and environmental application of 129I at the Xi'an Accelerator Mass Spectrometry Center. Nuclear Instruments and Methods in Physics Research B 294, 147–151.

Zöfel, P., 2008. Statistik verstehen. Ein Begleitbuch zur computergestützten Anwendung., 10th ed. Addison-Wesley, München.

Eidesstattliche Erklärung

Hiermit versichere ich.

- dass die ich die vorliegende Masterarbeit selbstständig verfasst, andere als die angegebenen Quellen und Hilfsmittel nicht benutzt und mich auch sonst keiner unerlaubter Hilfe bedient habe.
- dass ich dieses Masterarbeitsthema bisher weder im In- noch im Ausland in irgendeiner Form als Prüfungsarbeit vorgelegt habe
- und dass diese Arbeit mit der vom Begutachter beurteilten Arbeit vollständig übereinstimmt.

Wien, 11.10.2017

Appendix

Sample sheet

Sample	Month	Description	Date [dd.mm.yy]	Time [hh.mm]	Temperature [°C]	EC [µS cm^{-1}]	Weather Conditions	Discharge	Exposition	Slope [°]	Altitdue [m a.s.l.]	Min. deglaciated since
KT-I 04	July	Fagge River	25.07.15	11:45	1.2	24.4	sunny, scattered clouds, no rain, 15.7 °C	medium, clear	n/a	n/a	2207	2015
KT-I 05	July	Spring	19.07.15	16:15	17.8	181.2	sunny, scattered clouds, no rain, 24.3 °C	very low, clear	SE	39.2	2234	2012
KT-I 06	July	Spring	19.07.15	17:00	15.8	186.3	overcast, windy, 14.0 °C	low, turbid	S	36.4	2224	2015
KT-I 08	July	Spring	19.07.15	16:45	15.0	193.3	sunny, scattered clouds, light breeze, 19.8 °C	low, clear	SE	42.2	2229	2015
KT-I 20	July	Spring	19.07.15	15:30	9.2	12.5	sunny, windy, 22 °C	low, turbid	S	27.4	2268	2012
KT-I 26	July	Spring	19.07.15	15:00	3.8	37.1	sunny, scattered clouds, 23.6 °C	low, clear	S	30.2	2292	2006
KT-I 27	July	Spring	19.07.15	14:30	3.8	17.0	sunny, scattered clouds, light breeze, 20.0 °C	low, turbid	SE	32.1	2296	2006
KT-I 29	July	Spring	19.07.15	14:00	8.1	30.4	sunny, scattered clouds, light breeze, 14.7 °C	medium, clear	NW	45.2	2286	2012
KT-I 32	July	Dead Ice	19.07.15	15:45	3.1	6.9	sunny, scattered clouds, light breeze, 21.9 °C	low, turbid	S	33.1	2245	2012
KT-I 40	July	Spring	18.07.15	10:00	12.0	58.6	sunny, 18.0 °C	ver low, clear	SW	32.7	2171	1971
KT-I 41	July	Spring	18.07.15	09:00	10.5	75.6	sunny, 19.0 °C	medium, clear	W	12.1	2131	1971
KT-I 42	July	Spring	18.07.15	09:15	9.9	54	sunny, 10.5 °C	low, clear	W	23.9	2157	1971
KT-I 43	July	Spring	18.07.15	09:30	10.2	54.6	sunny, 12.5 °C	low, clear	SW	29.7	2168	1971
KT-I 45	July	Spring	18.07.15	10:30	6.5	52.4	sunny, 18.0 °C	medium, clear	SW	35.5	2170	1971
KT-I 45 (2)	July	Spring	18.07.15	10:30	6.5	52.4	sunny, 18.0 °C	medium, clear	SW	35.5	2170	1971
KT-I 46	July	Spring	18.07.15	11:00	12.8	37.9	sunny, 12.4 °C	low, clear	W	43.7	2169	1971
KT-I 47	July	Spring	18.07.15	11:30	14.8	38.6	sunny, scattered clouds, 32.0 °C	very low, clear	SW	36.5	2162	1971
KT-I 48	July	Spring	18.07.15	12:15	11.8	33.6	sunny, scattered clouds, 30.0 °C	medium, clear	W	35.9	2125	1971
KT-I 49	July	Spring	18.07.15	12:30	14.4	38.5	sunny, scattered clouds, 30.0 °C	low, clear	SW	34.5	2126	1971
KT-I 50	July	Pool	18.07.15	14:15	23.6	24.5	sunny, windy, 34.0 °C	n/a	n/a	n/a	2183	2006
KT-I 51	July	Spring	18.07.15	14:45	18.4	85.4	overcast, windy, 20.3 °C	low, clear	SW	49.45	2185	2006
KT-I 52	July	Spring	18.07.15	15:30	16.5	61.1	overcast, windy, 20.3 °C	medium, clear	E	22.12	2123	1971
KT-I 61	July	Spring	17.07.15	13:30	1.2	6.5	sunny, scattered clouds, 28.7 °C	medium - high, turbid	SW	16.31	2236	2015
KT-I 65	July	Spring	17.07.15	13:00	1.6	62.1	sunny, 28.0 °C	medium, clear	NW	15.63	2239	1971
KT-I 66	July	Spring	17.07.15	11:45	1.5	22.3	sunny, 27.0 °C	very low, clear	N	25.24	2247	1971
KT-I 67	July	Spring	17.07.15	11:15	0.1	6.2	sunny, 26.0 °C	low, clear	NW	28.81	2247	1971
KT-I 68	July	Spring	17.07.15	13:45	0.6	7.1	sunny, 16.9 °C	low, turbid	NW	26.57	2254	1971

Sample	Month	Description	Date [dd.mm.yy]	Time [hh.mm]	Temperature [°C]	EC [µS cm^{-1}]	Weather Conditions	Discharge	Exposition	Slope [°]	Altitdue [m a.s.l.]	Min. deglaciated since
KT-I 74	July	Spring	20.07.15	15:30	n/a	n/a	sunny, scattered clouds, 25.0 °C	medium, clear	N	17.3	2184	1971
KT-I 76	July	Spring	18.07.15	08:30	16.4	39.1	overcast, windy, 20.3 °C	medium, clear	NE	22.0	2124	1971
KT-I 77	July	Spring	19.07.15	09:00	9.2	86	sunny, windy, scattered clouds, 16.3 °C	low, clear	NE	33.7	2276	1971
KT-I 78	July	Spring	19.07.15	09:45	8.2	197.4	sunny, windy, 17.1 °C	low, clear	NE	36.4	2329	1922
KT-I 79	July	Spring	19.07.15	15:00	4.6	96.2	sunny, scattered clouds, 16.8 °C	high, clear	N	18.9	2304	1971
KT-I 80	July	Glacier Ice	17.07.15	10:00	0.0	1.4	overcast, 18.0 °C	dropwise	n/a	n/a	2305	2016
KT-I 90	July	Spring	19.07.15	10:45	7.5	38.8	sunny, scattered clouds, 22.0 °C	low, clear	NW	34.4	2303	1922
KT-I 91	July	Dead Ice	19.07.15	11:15	0.0	3.8	sunny, scattered clouds, 23.4 °C	dropwise, turbid	S	27.0	2259	1971
KT-I 92	July	Spring	19.07.15	12:15	3.5	11.2	sunny, scattered clouds, 27.5 °C	low, clear	NW	18.4	2237	1971
KT-I 93	July	Glacial Run-off	19.07.15	12:45	0.1	0.2	sunny, cold wind, 10.7 °C	medium, clear	n/a	n/a	2257	2016
KT-I 94	July	Glacier Ice	19.07.15	13:15	3.2	23.4	sunny, cold wind, 8.7 °C	medium, turbid	N	23.0	2285	2015
KT-I 95	July	Glacier Ice	19.07.15	18:00	0.0	4.8	sunny, cold wind, 10.3 °C	dropwise, clear	n/a	n/a	2292	2016
KT-I 68	August	Spring	17.08.15	13:15	2.4	6.2	overcast, drizzling rain, 9.4 °C	high, turbid	NW	26.6	2254	1971
KT-I 45	September	Spring	10.09.15	14:30	6.9	51.6	unsettled, no rain, 12.4 °C	medium - high, clear	SW	35.5	2170	1971
KT-I 48	September	Spring	10.09.15	13:00	6.6	33.0	overcast, no rain, 12.2 °C	medium - high, clear	W	35.9	2125	1971
KT-I 49	September	Spring	10.09.15	12:30	7.1	26.9	unsettled, no rain, 10.5 °C	low, clear	SW	34.5	2126	1971
KT-I 65	September	Spring	11.09.15	16:15	1.9	78.7	overcast, no rain, 10.5 °C	low - medium, clear	NW	15.6	2239	1971
KT-I 67	September	Spring	11.09.15	15:45	2.4	12.6	overcast, drizzling rain, 12.5 °C	very low - low, clear	NW	28.8	2247	1971
KT-I 77	September	Spring	11.09.15	12:45	6.8	195	sunny, scattered clouds, no rain, 14.6 °C	low - medium, clear	NE	33.7	2276	1971
KT-I HR	20.05 - 12.06	Precipitation	12.06.15	n/a	n/a	n/a	n/a	n/a	n/a	n/a	1263	n/a
KT-I HR	20.05 - 12.06	Precipitation	12.06.15	n/a	n/a	n/a	n/a	n/a	n/a	n/a	1263	n/a
KT-I HR	12.06 - 29.07	Precipitation	29.07.15	n/a	n/a	n/a	n/a	n/a	n/a	n/a	1263	n/a
KT-I HR	22.07 - 07.08	Precipitation	07.08.15	n/a	n/a	43.1	n/a	n/a	n/a	n/a	1263	n/a
KT-I HR	22.07 - 07.08	Precipitation	07.08.15	n/a	n/a	43.1	n/a	n/a	n/a	n/a	1263	n/a
KT-I HR	20.08 - 13.09	Precipitation	13.09.15	n/a	n/a	57.5	n/a	n/a	n/a	n/a	1263	n/a
KT-I RS	09.06 - 20.07	Precipitation	20.07.15	n/a	n/a	n/a	n/a	n/a	n/a	n/a	2152	n/a
KT-I RS	20.07 - 20.08	Precipitation	20.08.15	n/a	n/a	5.7	n/a	n/a	n/a	n/a	2152	n/a
RS	20.08 - 13.09	Precipitation	13.09.15	n/a	n/a	4.7	n/a	n/a	n/a	n/a	2152	n/a
RS	13.09 - 08.10	Precipitation	08.10.15	n/a	n/a	3.9	n/a	n/a	n/a	n/a	2152	n/a

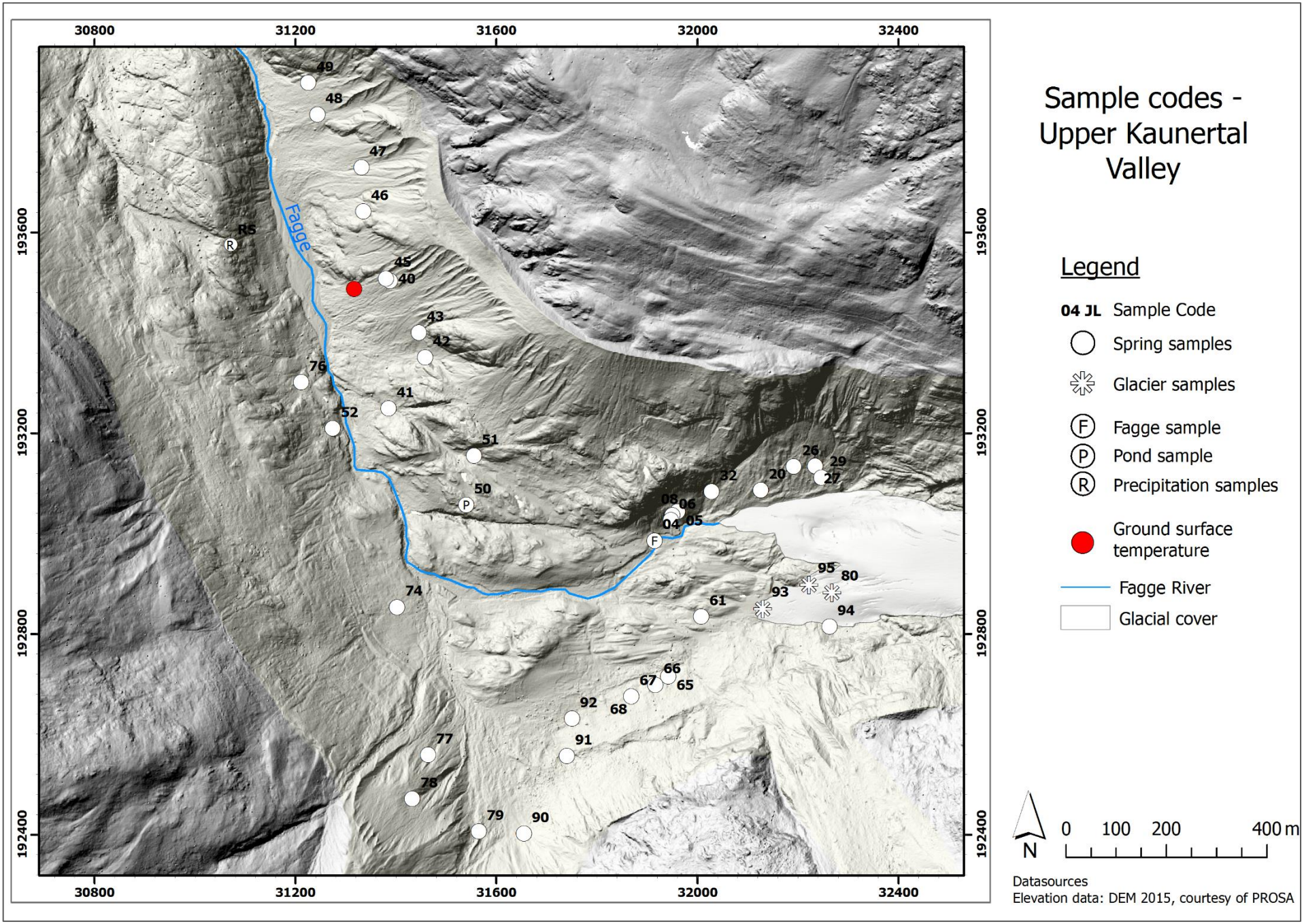
Sample codes - Upper Kaunertal Valley
Legend
04 JL Sample Code
Spring samples
Glacier samples
Fagge sample
Pond sample
Precipitation samples
Ground surface temperature
Fagge River
Glacial cover
Fagge
RS
30800
31200
31600
32000
32400
193600
193200
192800
192400
N
0 100 200 400 m
Datasources
Elevation data: DEM 2015, courtesy of PROSA